IDŐJÁRÁS

QUARTERLY JOURNAL
OF THE HUNGARIAN METEOROLOGICAL SERVICE

CONTENTS

IDŐJÁRÁS

Estimation of rainfall erosivity in Piedmont (Northwestern Italy) by using 10-minute fixed-interval rainfall data

Fiorella Acquaotta [1,2], **Alice Baronetti** [1], **Mario Bentivenga** [3], **Simona Fratianni** [1,2],*, and **Marco Piccarreta** [4]

[1] *Dipartimento di Scienze della Terra, Università di Torino, Via Valperga Clauso 35, 10125Torino, Italia*

[2] *NatRisk Centro interdipartimentale sui rischi naturali in ambiente montano e collinare, Largo Paolo Braccini, 2, 10095, Grugliasco (TO), Italia*

[3] *Dipartimento di Scienze, Università della Basilicata, Viale dell'Ateneo Lucano, 10 - 85100 Potenza, Italia*

[4] *Ministero dell'Istruzione, dell'Università e della Ricerca, Via Giustino Fortunato 8/M, 70125 Bari, Italia*

* Corresponding author E-mail: simona.fratianni@unito.it

(Manuscript received in final form April 19, 2018)

Abstract— Rainfall erosivity index (EI_{30}) is widely used in soil erosion models for predicting soil loss. This index consists in the product between the maximum intensity of 30-min rainfall and the total kinetic energy of a precipitation event. The main goal of this study was to characterize the soil erosion in Piedmont (Northwestern Italy), studying the magnitude, frequency, and trends of rainfall erosivity. Rainfall erosivity for twelve stations well distributed over the whole region were firstly computed on the basis of 10-min time-resolution rainfall data using a continuous 17-year series of daily rainfall events. For each station the equation to predict EI_{30} from daily rainfall data was calculated, and, using the *Nash* and *Sutcliffe* (1970) model-efficiency, the relationships between real EI_{30} and modeled EI_{30} was validated. The rainfall erosivity model was applied to the long term daily rainfall series of the selected stations, to create annual and seasonal erosivity time series for the climate normal period 1986–2015. Afterwards, the Mann–Kendall non-parametric test statistic to detect time trends in the rainfall erosivity time series was applied. The results have led to the conclusion that the annual rainfall erosivity should have experienced mixed trends in most of the study area, although more than half of the stations did not show a statistical trend.

Key-words: rainfall erosivity, time trend, soil erosion, Piedmont, Northwestern Italy

1. Introduction

The concept of soil erosion caused by high energy rainfall was introduced by *Hudson* (1971) and *Wischmeier* and *Smith* (1978) where they describe the erosivity (*R*) like the interaction between the total kinetic energy of a storm and the soil surface *(EI$_{30}$)*. Rainfall erosivity is one of the six factors in the Universal Soil Loss Equation, developed to predict the soil erosion (*Renard et al.,* 1997). This equation permits to quantify the ability of rainfall to cause soil loss and is largely used in two of the main prediction models (USLE and RUSLE). The calculation of the erosivity *R* factor uses breakpoint rainfall intensity data derived from recording rain gauges. Because the limited availability of sub-hourly rainfall data, several study (*Ateshian*, 1974; *Arnoldus*, 1977; *Richardson et al.*, 1983; *Bagarello* and *D'Asaro,* 1994; *Ferro et al.,* 1991; *Renard* and *Freimund,* 1994; *Yu* and *Rosewell,* 1996a, 1996b, 1996c; *Loureiro* and *Couthino,* 2001; *Yu et al.*, 2001; *Capolongo et al.,* 2008; *Joon-Hak* and *Jun-Haeng,* 2011) developed methods for the estimation of the *EI$_{30}$* using yearly, monthly and daily rainfall data. *Yin et al.* (2007) highlighted that the computed *R* factor will be more accurate with detailed rainfall data. *Richardson et al.* (1983), *Bagarello et al.* (1994), and *Petkovsek* and *Mikoš* (2004) tried to predict rainfall erosivity from daily rainfall (*P*) using the following exponential relationships:

$$EI_{30} = aP^b,$$ (1)

where the two Richardson's coefficients (*Richardson et al.,* 1983) are:

- *a*, which is considered like the scale factor, and represents the temporal and spatial variability (*Richardson et al.,* 1983);
- *b*, which is considered as a process parameter and is relatively more constant. The value of the exponent *b*, obtained by means of theoretically based approach approximates 2.0 (*Brown* and *Foster,* 1987), whereas empirical approaches gave values ranging from 1.5 to 2.2 (reference in *Bagarello* and *D'Asoro,* 1994; *Capolongo et al.,* 2008).

In recent times, *Borrelli et al.* (2016) investigated the spatiotemporal distribution of rainfall erosivity in Italy by using both 30- and 60-min time-step data. They have found high variability in erosivity within the country, with a 97% difference between the lowest and highest values. At regional scale relevant studies have been realised especially for such central-southern regions as Basilicata, Calabry, Sicily and Tuscany (*D'Asaro et al.,* 2007; *Capolongo et al.,* 2008; *Vallebona et al.,* 2014; *Capra et al.,* 2017).

For Piedmont (Northwestern Italy), 10-min rainfall records are available from 1989 to 2007. By using data from 12 rain gauges well distributed over the regional territory we tested the *Richardson et al.* (1983) power relationship between rainfall erosivity (EI_{30}) and daily precipitation > 10 mm (P) to create a newly derived daily erosivity index for each of the investigated stations. It is considered really important due to the lack of a similar study for the region. It has to be stressed that Piedmont is largely devoted to agriculture, in particular to grapevine cultivation, with the production of different top-quality Italian wines. More than 53,000 hectares of the region have been covered by vineyards. According to the agricultural statistical database of the Piedmont Regional Administration, almost 90% of the vineyard surface of the region is on hilly areas and near 2% on mountain areas, which are characterized by large estimates of soil loss due to the high erodibility of the soils and the climate (*Tropeano,* 1984; *Luino,* 2005; *Corti et al.,* 2011). On the basis of a recent study of *Acquaotta* and *Fratianni* (2013), both the general decreasing trend of precipitation amounts and the weak increasing trend of rainfall intensity occurred in Piedmont from 1971 to 2000 are giving the idea that the erosive power of daily rainfall events in the region should have increased in recent years.

The objective of this study is:

− to quantify principally the rainfall erosivity temporal pattern in the Piedmont region by applying the newly derived daily erosivity rainfall indexes to the climatologic normal 1989–2015 daily record series of the investigated 12 rainfall gauging stations;

− to generate and evaluate extended historical time series of annual rainfall erosivity for the whole region;

− to detect and explain possible time trends in rainfall erosivity.

2. Study area

Piedmont is a region in the northwestern part of Italy (*Fig. 1*). It borders France and Switzerland, and in Italy it borders the Aosta Valley region, Lombardy, Emilia Romagna, and Liguria. It has an area of 25,402 km^2 and is characterized by a complex territory (*Fazzini et al.,* 2004). In fact, the geography is 43% mountainous, along with extensive areas of hills (30%) and plains (27%). The hills area is composed by Torino, Langhe, and Monferrato. The plain characterized, at East, by the Po Plain crossed by the longest river in Italy, the Po, and its many tributaries. The alpine mountain area is located on the northwestern Italian border with France and Switzerland (*Terzago et al.,* 2012; *Giaccone et al.*, 2015).

According to the orientation of the Alps and Apennines in Piedmont, there is a strong geographical differentiation in the rainfall distribution, in fact, the annual rainfalls are more abundant along the Alps, in particular at the north, with peaks above 2000 mm/year (*Fratianni et al.,* 2015). While the drier area is the central sector, the Po Plain, with amounts of even less than 600 mm/year in Alessandria plains and Susa valley with the presence of a great number of foehn days (*Fratianni et al.,* 2009).

Acquaotta and *Fratianni* (2013) have subdivided Piedmont into three different climatic regions on the basis of the Bagnouls and Gaussen's method: sub-Mediterranean, temperate and cool-temperate.

The sub-Mediterranean region is located in the Piedmont plain. The region has a subalpine pluviometric regime with a maximum in autumn and spring and a main minimum in winter. The temperate region is characterized by the Piedmont hill, and this area has a prealpine pluviometric regime with a principal maximum in spring and a principal minimum in winter. The cool-temperate region concern the mountain area and has a prealpine pluviometric regime.

Several study developed by the Earth Science Department of Turin show a decrease of consecutive rainy days in the Piedmont plain and hills, a general increase of the annual precipitation, and a positive tendency in the density of precipitation and in the numbers of days. These positive trends make the region particularly prone to severe erosion, with serious consequences on agriculture and grapevine cultivation (*Baronetti et al.,* 2018).

3. Materials and methods

3.1. Database

Rainfall data recorded with a temporal resolution of 10-minute were obtained from twelve electronic rain-gauge stations of the Agenzia Regionale per la Protezione Ambientale (ARPA) operating in Piedmont. The twelve stations (Boves, Bra, Casale Monferrato, Lanzo, Luserna, Mondovì, Oropa, Piamprato, Susa, Torino, Varallo Sesia, and Vercelli) were selected on the basis of their location in order to cover the whole region (*Fig. 1*) as well as of the quality of the data records, i.e., no missing data (*Venema et al.,* 2013). The system of observation, started in 1986, and we used data until 2015 (*Table 1*). The rainfall series passed a quality control (*Acquaotta et al.,* 2016; *Zandonadi et al.,* 2016), and for each station an erosive events database has been created (*Acquaotta et al.*, 2018a). The erosive events were determined by the RUSLE criterion (*Foster et al.,* 1981; *Renard et al.,* 1997). A threshold of 1.27 mm (0,05 inch) of precipitation in six hours was selected to represent breaks in rainstorms. Afterwards, rainstorms with less than 12.7 mm (0.5 inch) of precipitation were omitted from the EI_{30} calculation. *Foster et al.* (1981) made an exception for rainstorm events of 15 min duration with at least one peak greater than 6.5 mm.

Recorded rainfall intensities showed different behavior for all the investigated stations confirming the observations made by *Acquaotta* and *Fratianni* (2013). On the whole, 4626 detected storms recorded on a 10-min interval basis were used in the analysis.
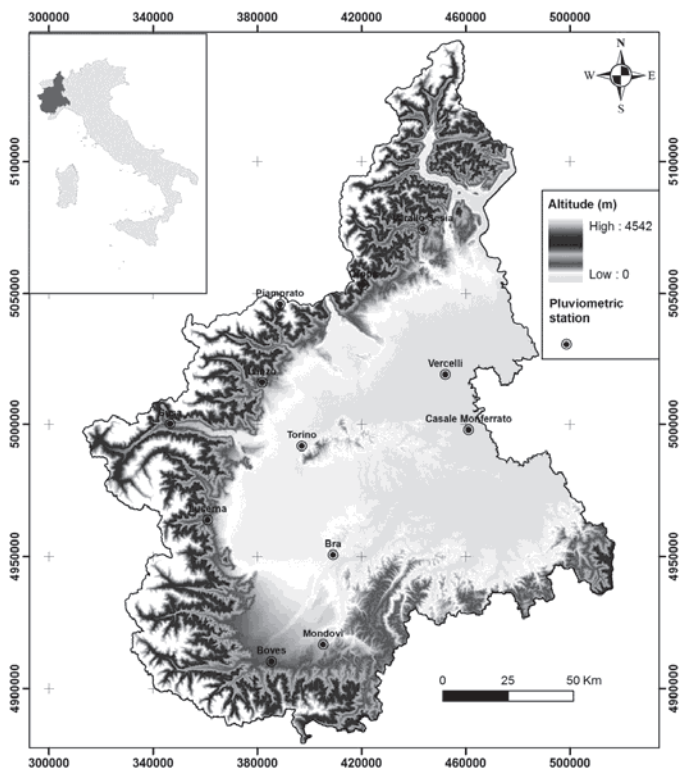
Fig. 1. Geographic, location of the meteorological stations in Piedmont, Italy.

Table 1. Characteristics of the meteorological stations analyzed in this study (Latitude North, longitude East, elevation (m ASL))

Stations	Latitude N	Longitode E	Elevation (m)	Period
Boves	44° 20' 06"	7° 33' 43"	575	1989–2005
Bra	44° 04' 18"	7° 51' 09"	285	1993–2007
Casale Monferrato	45° 07' 56"	8° 30' 15"	136	1990–2006
Lanzo	45° 17' 23"	7° 29' 38"	580	1990–2007
Luserna	44° 48' 46"	7° 14' 28"	475	1990–2007
Mondovì	44° 23' 44"	7° 48' 38"	422	1993–2007
Oropa	45° 37' 40"	7° 58' 56"	1186	1990–2007
Piamprato	45° 33' 02"	7° 34' 07"	1550	1993–2007
Susa	45° 08' 31"	7° 03' 14"	520	1990–2007
Torino	45° 17' 23"	7° 41' 23"	239	1990–2007
Varallo Sesia	45° 49' 14"	8°16' 30"	470	1990–2007
Vercelli	45° 19' 32"	8° 23' 26"	132	1990–2006

3.2. Rainfall erosivity index

The rainfall erosivity has been calculated by applying the RUSLE *R* (*Renard et al.,* 1997) equation as proposed by *Brown* and *Foster* (1987):

$$R = \frac{1}{n}\sum_{j=1}^{n}\sum_{k=1}^{m_j}(EI_{30})_k \,, \qquad (2)$$

where n is the number of years of records, m_j is the number of erosive events of a given year j, and EI_{30} is the rainfall erosivity index of a singular event k. Thus, the R factor is the average value of the annual cumulative EI_{30} over a given period. Quantitative evaluation of rainstorm erosivity (EI_{30}) requires rainfall kinetic energy and intensity values associated to 30-minute observation time intervals.

The kinetic energies of all the rainfall events have been evaluated as:

$$E = 0.29[1 - 0.72 e^{(-0.05/r^2)}], \qquad (3)$$

where E denotes the rainfall kinetic energy in MJ ha^{-1} mm^{-1} and Ir is the rainfall intensity in mm h^{-1}. This equation type was tested and found adequate for Mediterranean and Southern European conditions by several authors (*Coutinho* and *Tomas*, 1995; *Cerro et al.*, 1998).

The maximum 30 min (0.5 h) intensity, I_{30} (mm·h^{-1}), was calculated as:

$$I_{30} = \frac{(P_{30})}{0.5h} \, , \tag{4}$$

where P_{30} (mm) was the maximum accumulated rainfall depth in three contiguous 10 min intervals.

The average EI_{30}, as the mean erosivity of all rainfall events, is calculated.

Event rainfall erosivity values (EI) were fitted to the event precipitation amount (P) by the *Richardson et al.* (1983) exponential relationship in Eq (1). The parameters a and b have been adjusted month-by-month to take account of intra-annual variations in rainfall characteristics.

The performance of the relations was assessed by computing the Nash-Sutcliffe coefficient of efficiency (ME), which was calculated as follows (*Nash* and *Sutcliffe*, 1970):

$$ME = 1 - \frac{\sum \left(R_i - \hat{R}_i\right)^2}{\sum \left(R_i - \overline{R}_i\right)^2} \, , \tag{5}$$

where $\overline{R}_i$ is the mean of observed erosivity values, and R_i and $\hat{R}_i$ are the observed and predicted erosivity values for the ith pair of observations.

ME indicates how close scatters of predicted values are to the line of best fit; this is similar to the coefficient of determination R^2, without being markedly affected by outlier data. This validation statistic is commonly used in rainfall erosivity studies (*Yu et al.*, 2001; *Petkovsek* and *Mikoš*, 2004; *Capolongo et al.*, 2008; *Angulo-Martínez* and *Beguería*, 2009). The *ME* has a range between $-\infty$ and 1.0 (perfect fit). *ME* value of 0 indicates that the model predictions are as accurate as the mean of the observed data. Generally acceptable levels of performance are between 0.0 and 1.0, whereas values <0.0 indicate that the simulated value is not a good predictor and the performance is unacceptable, while the mean observed value is a better predictor.

In agreement with *Willmott* and *Matsuura* (2005) and *Angulo-Martínez* and *Beguería* (2009), we did not use the root mean square error (*RMSE*) because it is highly biased by outlier data, and it is difficult to discern whether it reflects the average error or the variability of the squared errors.

The monthly exponential relationships derived for each of the twelve stations have been then applied to the daily rainfall series from 1986 to 2015 to create long-time erosivity series of Piedmont.

3.3. Trend analysis

Annual and seasonal time series were obtained by adding the daily erosivity values to the appropriate aggregation periods. Natural years (from January 1 to December 31) were used for the annual series, and the usual convention (winter = December to February, spring = March to May, summer = June to August, autumn = September to November) was used for the seasonal series.

The trends were computed using the Mann-Kendall (MK) test (*Hirsch et al.,* 1992; *Acquaotta et al.,* 2018b), and the significance of the coefficients *Z* was checked for four different levels of probability ($p \leq 0.001$, 0.01, 0.05, and 0.10).

4. Results and discussion

In this study the exponential relationship of Richardson coefficient (*Richardson et al.,* 1983) in Eq. (1) above was employed to obtain the *a* and *b* parameters calibrated monthly.

The values of these coefficients for each station are reported in *Table 2*. Then, this regression equation, for each station, was used to developed erosivity series starting from daily data. The erosivity data have been plotted versus the real erosivity founding a strong relationship (*Fig. 2*). The Nash-Sutcliffe efficiency model results (*Table 2*) are always higher than 0.39 showing a good performance of the twelve derived equations.

Table 2. List of monthly *a* and *b* Richardson coefficients

|	Richard coeff.	Boves	Brn	Casale Monferrato	Lauzo	Luserna	Mondovi	Oropa	Pianoprato	Susa	Torino	Varallo Sesia	Vercelli
Emissivity number		449	209	269	481	424	295	387	344	246	371	626	315
January	a	0.038	0.000	0.147	0.020	0.038	0.088	0.092	0.270	0.203	0.106	0.075	0.016
	b	1.720	3.086	1.332	1.917	1.706	1.499	1.548	1.097	1.184	1.421	1.546	2.020
February	a	0.033	0.120	0.035	0.084	0.035	0.170	0.053	0.066	0.089	0.033	0.020	0.053
	b	1.810	1.393	1.781	1.540	1.760	1.356	1.669	1.634	1.523	1.780	1.911	1.641
March	a	0.213	0.016	0.005	0.079	0.147	0.065	0.138	0.019	0.504	0.094	0.071	0.006
	b	1.324	2.129	2.699	1.639	1.457	1.692	1.512	2.074	1.017	1.531	1.672	2.525
April	a	0.345	0.092	0.521	0.174	0.076	0.237	0.129	0.044	0.156	0.165	0.152	0.115
	b	1.238	1.584	1.084	1.489	1.673	1.289	1.579	1.763	1.350	1.462	1.492	1.591
May	a	0.742	0.031	0.144	0.171	0.376	2.149	0.211	0.088	0.097	0.088	0.268	0.324
	b	1.181	3.173	1.770	1.663	1.410	0.861	1.630	1.663	1.597	1.911	1.481	1.434
June	a	0.110	1.027	2.893	0.131	0.088	0.227	0.227	0.190	2.692	0.068	0.127	1.811
	b	1.855	1.239	0.975	1.960	1.986	1.715	1.729	1.622	0.845	2.212	1.873	1.088
July	a	0.347	0.054	2.546	0.213	0.153	0.028	0.271	2.730	0.099	0.205	0.433	1.512
	b	1.782	2.369	1.137	1.892	1.926	2.499	1.863	0.954	1.847	1.972	1.635	1.346
August	a	1.376	0.165	2.509	1.470	0.098	0.819	0.346	0.238	0.007	0.297	0.448	0.330
	b	1.268	2.032	1.188	1.283	2.095	1.566	1.773	1.640	2.803	1.866	1.623	1.837
September	a	0.110	0.067	0.060	0.181	0.247	0.481	0.247	0.029	0.301	0.291	0.196	0.103
	b	1.762	1.823	2.022	1.722	1.522	1.281	1.605	2.008	1.326	1.533	1.671	1.902
October	a	0.072	0.039	0.079	0.055	0.041	0.065	0.198	0.021	0.050	0.099	0.102	0.070
	b	1.739	1.869	1.740	1.823	1.912	1.755	1.535	2.013	1.806	1.651	1.703	1.850
November	a	0.080	0.076	0.055	0.043	0.039	0.070	0.095	0.012	0.025	0.052	0.050	0.067
	b	1.620	1.677	1.862	1.815	1.790	1.680	1.639	2.081	1.924	1.755	1.777	1.706
December	a	0.023	0.144	0.055	0.042	0.019	0.025	0.038	0.024	0.115	0.101	0.032	0.047
	b	1.930	1.336	1.786	1.684	1.983	1.926	1.804	1.862	1.342	1.442	1.813	1.689
Nash-Sutcliff Model efficiency		0.44	0.53	0.43	0.74	0.6	0.57	0.68	0.87	0.39	0.72	0.56	0.45
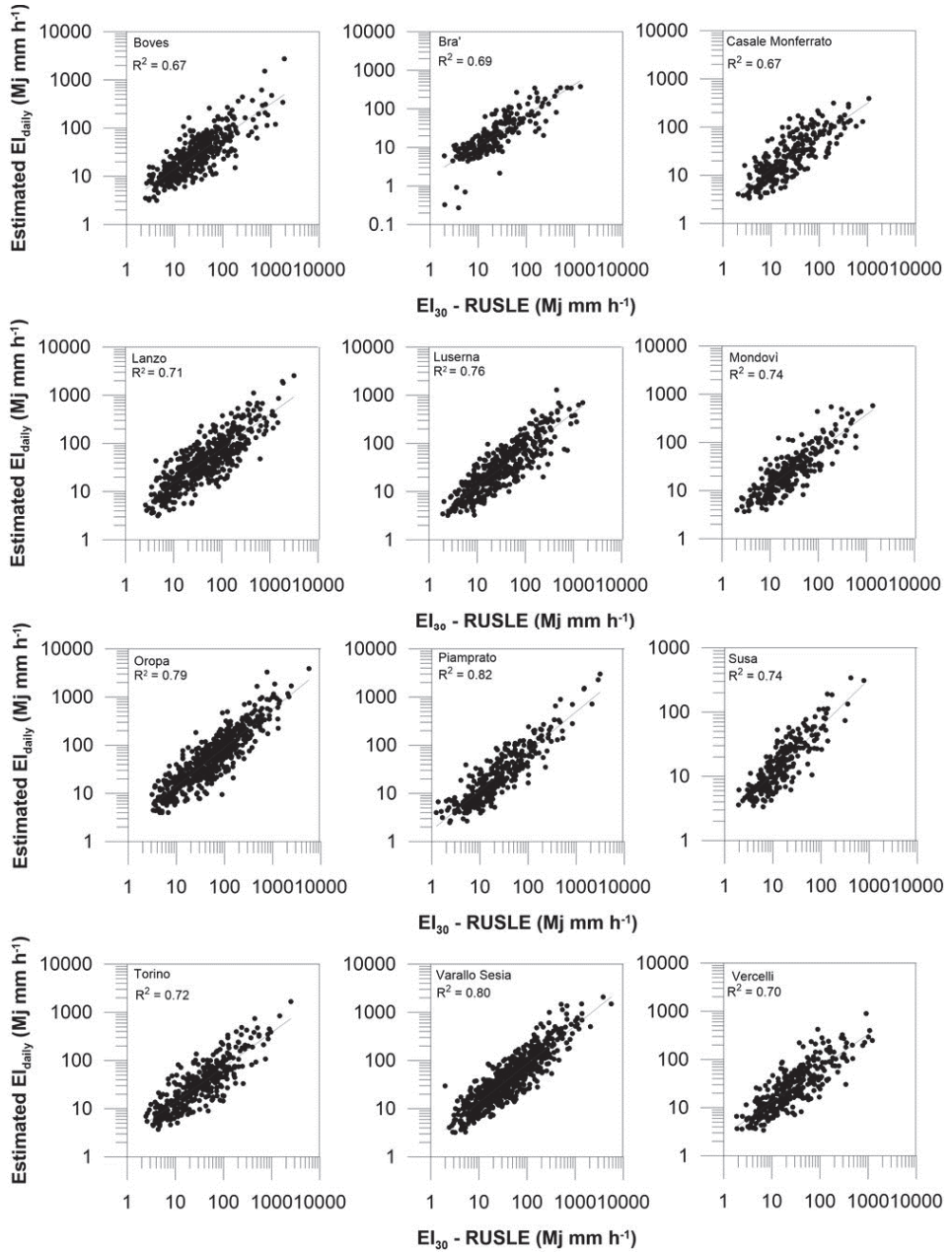
Fig. 2. Scatterplots between estimated (*EI_{daily}*) and measured rainfall erosivity (*EI₃₀*-RULSE) values for the calibration and fitted values.

Afterwards, starting from the daily rainfall series from 1986 to 2015, the daily erosivity equation of each month was applied to create annual, seasonal, and monthly series of rainfall erosivity.

Thereafter, using the MK test, annual, seasonal, and monthly time trends during the observation period were verified, and the MK test statistics are shown in *Table 3*.

Table 3. Mann-Kendall trend test of rainfall erosivity using annual, seasonal, and monthly datasets of all Piedmont stations. The significance of the coefficients Z was checked for different levels of probability, p≤ ***0.001, **0.01,**0.05, and +0.10.

	Bovès	Brn	Casale Monferrato	Lauzo	Luserna	Mondovì	Oropa	Piamprato	Susa	Torino	Varallo Sesia	Vercelli
January	-0.76	-2.050 *	-0.940	-0.910	-1.120	0.310	-1.010	-0.020	-1.380	-0.770	-0.760	0.070
February	0.07	-0.470	0.470	0.100	-0.360	0.920	-1.400	0.450	-1.320	0.890	0.380	0.460
March	1.23	0.600	1.360	0.620	1.620	1.380	0.720	0.890	0.040	1.380	1.420	1.300
April	-2.59 **	-2.250 *	-1.780 -	-0.180	-1.110	-2.000 *	-1.860 -	0.040	-0.670	-1.110	-1.110	-1.210
May	-1.57	-0.640	0.610	2.210 *	0.800	-0.210	-0.040	2.250 *	1.320	0.370	1.000	0.890
June	-0.02	-0.410	0.400	1.770 -	1.360	1.370	-0.640	0.480	0.000	1.040	0.480	0.070
July	-0.09	-0.650	-0.460	1.930 -	0.750	1.590	-0.230	1.930 -	0.790	0.050	0.980	-0.490
August	0.00	1.300	-0.410	2.270 +	-1.240	-0.450	0.790	2.530 *	0.330	-0.860	0.500	1.790 -
September	-0.66	-0.940	-0.320	0.290	0.590	-0.640	0.000	0.460	-0.220	0.430	0.290	0.360
October	-1.14	-1.480	-0.950	0.020	-1.060	-0.820	-1.940 -	-0.820	-1.310	-1.780 -	-0.950	-1.130
November	1.11	1.740 +	1.880 -	2.560 *	2.810 **	1.810 -	1.360	1.670 -	2.280 *	2.140 *	1.540	1.900 -
December	-0.60	-0.790	-0.120	0.230	0.500	0.670	-1.450	0.470	-0.270	0.170	0.050	0.860
Annual	-1.71 -	-1.000	-0.360	2.460 *	0.210	0.820	-2.140 *	0.890	-0.390	-0.390	0.360	1.850 -
Winter	-0.11 -	-0.950	-0.950	-0.770	-0.480	1.090	-2.070 *	0.000	-1.660 -	0.320	-0.370	0.520
Spring	-1.89	-1.390	0.290	1.460	0.140	-0.860	-2.180 *	0.820	0.430	-0.040	-0.360	-0.230
Summer	-0.36	0.450	-0.390	2.640 **	0.360	1.120	-0.040	2.390 *	-0.200	0.000	1.610	1.460
Autumn	-0.54	-0.860	-0.460	0.500	0.790	0.210	-1.070	0.110	0.380	0.500	-0.320	0.390

The annual rainfall erosivity experienced increasing trends in six series (Lanzo, Luserna, Mondovì, Piamprato, Varallo Sesia, and Vercelli), whereas a decreasing trend characterizes the other series (Boves, Bra, Casale Monferrato, Oropa, Susa, and Torino) (*Fig. 3*). Only four stations (Boves, Lanzo, Oropa, and Vercelli) show statistically significant trend in rainfall erosivity. To verify the environmental/economic impact of erosivity on agriculture, the mean annual erosivity of Piedmont has been plotted versus the wine grapes productivity from 1981 to 2015 (*Fig. 4*, ISTAT source). The graph shows how an increase in annual erosivity often corresponds to a clear decrease in annual wine grapes productivity. Thus, the main important economic activities of the region are strongly affected by the soil loss caused by rainfall.

At seasonal and monthly levels, a different behaviour of rainfall erosivity emerges (*Figs. 5* and *6*). During winter only three stations (Mondovì, Torino, and Vercelli) show an upward statistically not significant trend. The remaining stations experienced a decrease in rainfall erosivity, which is statistically significant for Oropa and Susa. The trend signal seems to be controlled by the decrease in rainfall erosivity during the months of December and January (downward, statistically significant trend for Bra), whereas during February a general increase is recorded (*Table 3*). A downward trend is recorded during spring at seven stations, which is statistically significant for Boves and Oropa. From the monthly analysis it appears, that the main responsible for the overall spring trend is April, when many stations are characterized by a downward, statistically significant trend (Boves, Bra, Casale Monferrato, Mondovì, and Oropa). During March and May, many stations show an upward trend. In summer, an increase in rainfall erosivity is detected with the exception of the stations of Boves, Casale Monferrato, and Susa (Oropa and Torino show a stationary trend). It seems that no month is mainly responsible for the summer trend. A similar trend is recorded during autumn, without any statistically significant values. The monthly analysis shows that the autumn trend is mainly influenced by the rainfall erosivity behavior during November (upward, statistically significant trend for Bra, Casale Monferrato, Lanzo, Luserna, Mondovì, Piamprato, Susa, Torino, and Vercelli).
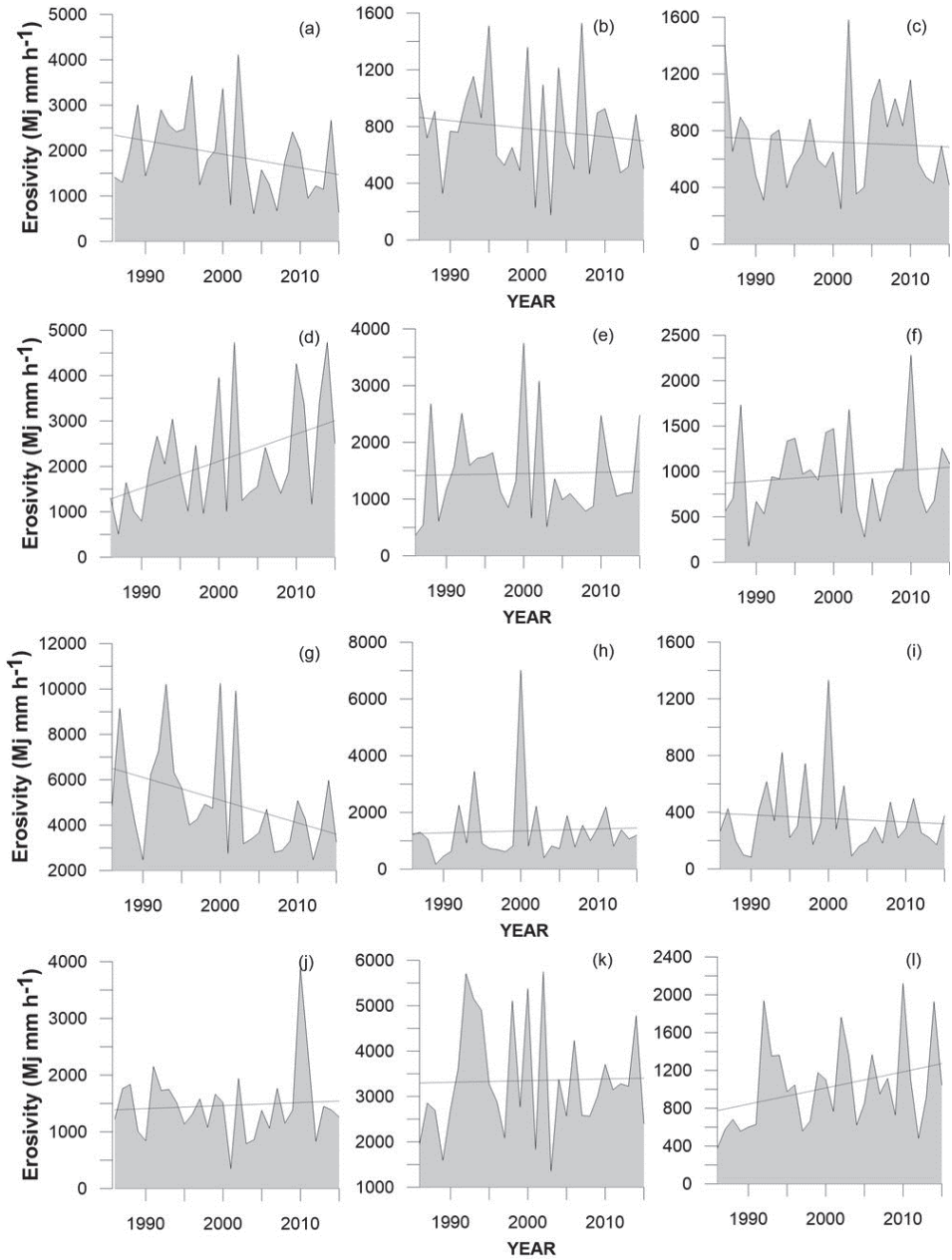
Fig. 3. Total annual rainfall erosivity from 1986 to 2015 for (a) Boves, (b) Bra, (c) Casale Monferrato, (d) Lanzo, (e) Luserna, (f) Mondovì, (g) Oropa, (h) Piamprato, (i) Susa, (l) Torino, (m) Varallo Sesia, and (n) Vercelli.
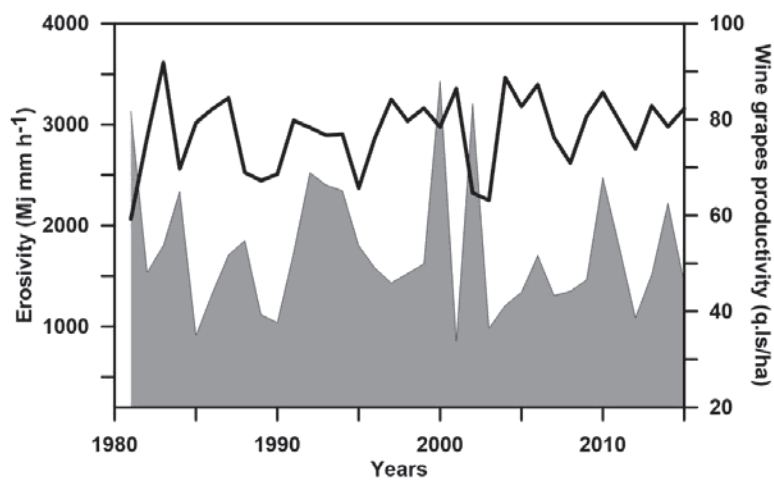
Fig. 4. Mean annual erosivity versus annual wine grape productivity (from ISTAT) in Piedmont for the period 1981–2015.
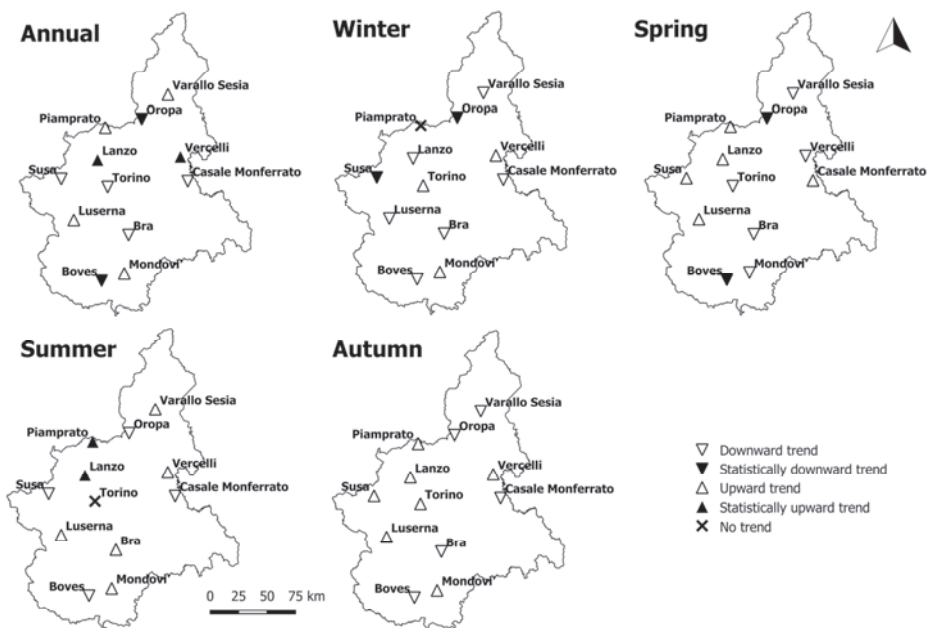
Fig. 5. Trends in seasonal rainfall erosivity in Piedmont for the period 1986–2015.

Fig. 6. Trends in annual rainfall erosivity in Piedmont for the period 1986–2015.

5. Conclusions

In Piedmont, (Northwestrn Italy), viticulture is strongly affected by soil erosion caused by rainfall events. In this regards, the RUSLE rainfall erosion index or R-factor for twelve pluviometric stations spread in the whole region was applied to obtain a set of daily rainfall time series from a 10-minute precipitation series. Those equations were applied to obtain the erosivity of a single erosive event from daily rainfall events greater or equal to 12.7 mm. After the application of the daily rainfall erosion index equations to the daily series of precipitation, the long-term trends of annual, monthly, and seasonal rainfall erosivity for the Piedmont region have been generated and analyzed. The main obtained results are:

– The annual rainfall erosivity experienced increasing trends in six series (Lanzo, Luserna, Mondovì, Piamprato, Varallo Sesia, and Vercelli), whereas a decreasing trend characterizes the other series (Boves, Bra, Casale Monferrato, Oropa, Susa, and Torino). Only four stations (Boves, Lanzo, Oropa and Vercelli) show statistically significant trend in rainfall erosivity.

– A widespread a decrease in rainfall erosivity, which is statistically significant for Oropa and Susa, has been recorded in winter.

– A downward trend is recorded at more than half of the stations during spring (especially in April), which is statistically significant for Boves and Oropa.

– An increase in rainfall erosivity is detected both in summer (statistically significant for Lanzo and Piamprato) and in autumn, especially during the month of November.

References

Acquaotta, F., Fratianni, S., 2013: Analysis on Long Precipitation Series in Piedmont (North-West Italy). *Amer. J. Climate Change 2,* 14–24.https://doi.org/10.4236/ajcc.2013.21002

Acquaotta, F., Fratianni, S. and *Venema, V.,* 2016: Assessment of parallel precipitation measurements networks in Piedmont, Italy. *Int. J. Climatol. 36*, 3963–3974. https://doi.org/10.1002/joc.4606

Acquaotta F., Faccini F., Fratianni S., Paliaga G., Sacchini A., and *Vilimek V.,* 2018a: Increased flash flooding in Genoa Metropolitan Area: a combination of climate changes and soil consumption? *Meteorol. Atmos. Phys.* https://doi.org/10.1007/s00703-018-0623-4

Acquaotta F., Faccini F., Fratianni S., Paliaga G., Sacchini A., 2018b: Rainfall intensity in the Genoa Metropolitan Area (Northern Mediterranean): secular variations and consequences. *Weather 73*, 356–363. https://doi.org/10.1002/wea.3208

Angulo-Martínez, M., and *Beguería, S.,* 2009: Estimating rainfall erosivity from daily rainfall records: A comparison among methods using data from the Ebro Basin (NE Spain). *J. Hydrol. 379*, 111–121. https://doi.org/10.1016/j.jhydrol.2009.09.051

Angulo-Martínez, M., and Beguería, S., 2012: Trends in rainfall erosivity in NE Spain at annual, seasonal and daily scales, 1955–2006. *Hydrol. Earth Syst. Sci. 16*, 3551–3559. https://doi.org/10.5194/hess-16-3551-2012

Arnoldus, H.M.J., 1977: Methodology used to determine the maximum potential average annual soil loss due to sheet and rill erosion in Morocco. *FAO Soil Bull. 34,* 39–51.

Ateshian, J.K.H., 1974: Estimation of rainfall erosion index. *J. Irrig. Drain. Div. Am. Soc. Civ. Eng. 100*, 293–307.

Baronetti, A., Acquaotta F., and Fratianni, S., 2018. Rainfall variability from a dense rain gauge network in North -West Italy. *Climate Res. 75,* 201–213. https://doi.org/10.3354/cr01517

Bagarello, V. and D'Asaro, F., 1994: Estimating single storm erosion index. *Trans. Am. Soc. Agric. Eng. 37*, 785–791. https://doi.org/10.13031/2013.28141

Borrelli, P., Diodato, N., and Panagos, P., 2016: Rainfall erosivity in Italy: a national scale spatio-temporal assessment. *Int. J. Digit. Earth 9*, 835 – 850. https://doi.org/10.1080/17538947.2016.1148203

Brown, L.C. and Foster, G.R., 1987: Storm erosivity using idealized intensity distribution. *Trans ASAE 30*, 379–386. https://doi.org/10.13031/2013.31957

Capolongo, D., Diodato, N., Mannaerts, C.M., Piccarreta, M., and Strobl, R.O., 2008: Analyzing temporal changes in climate erosivity using a simplified rainfall erosivity model in Basilicata (southern Italy). *J. Hydrol. 356,* 119– 130. https://doi.org/10.1016/j.jhydrol.2008.04.002

Capra, A., Porto, P., and La Spada, C., 2017: Long-term variation of rainfall erosivity in Calabria (Southern Italy). *Theor. Appl. Climatol. 128,* 141–158. https://doi.org/10.1007/s00704-015-1697-2

Cerro, C., Bech, J., Codina, B., and Lorente, J., 1998. Modelling rain erosivity using distrometric techniques. *Soil Sci. Soc. Amer. J. 62*, 731–735. https://doi.org/10.2136/sssaj1998.03615995006200030027x

Corti, G., Cavallo, E., Cocco, S., Biddoccu, M., Brecciaroli, G., and Agnelli, A., 2011: Evaluation of erosion intensity and some of its consequences in vineyards from two hilly environments under a Mediterranean type of climate, Italy. Soil Eros. Issues Agric. In (Eds. *Godone D, Sanchi S*) 01/2011, ISBN: 978-953-307-435-1.

Coutinho, M.A. and Tomas P.P., 1995: Characterisation of raindrop size distributions at the Vale Formosa experimental Erosion Center. *Catena 25,*187–197. https://doi.org/10.1016/0341-8162(95)00009-H

D'Asaro, F., D'Agostino, L., and Bagarello, V., 2007: Assessing changes in rainfall erosivity in Sicily during the twentieth century. *Hydrol. Proc. 21*, 2862–2871. https://doi.org/10.1002/hyp.6502

Fazzini M., Fratianni S., Biancotti A., and Billi P., 2004: Skiability conditions in several skiing complexes on Piedmontese and Dolomitic Alps. *Meteorol. Zeit. 13,*253–258. https://doi.org/10.1127/0941-2948/2004/0013-0253

Ferro, V., Giordano, G., and Iovino, M., 1991: Isoerosivity and erosion risk map for Sicily. *J. Hydrol. Sci. 36*, 549–564. https://doi.org/10.1080/02626669109492543

Foster, G.R., McCool, D.K., Renard, K.G., and Moldenhauer, W.C., 1981: Conversion of the Universal Soil Loss Equation to SI Metric Units. *J. Soil Water Conserv. 36*, 355–359.

Fratianni, S., Cassardo, C., and Cremonini, R., 2009: Climatic characterization of foehn episodes in Piedmont, Italy. *Geografia Fisica e Dinamica Quaternaria 32,* 15–22.

Fratianni, S., Terzago, S., Acquaotta, F., Faletto, M., Garzena, D., Prola, M.C., and Barbero, S., 2015: How Snow and its Physical Properties Change in a Changing Climate Alpine Context? Engineering Geology for Society and Territory - Volume 1: *Clim. Change Engineer. Geol., 57-60*, https://doi.org/10.1007/978-3-319-09300-0_11

Giaccone, E., Colombo N., Acquaotta, F., Paro, L., Fratianni, S., 2015: Climate variations in a high altitude Alpine basin and their effects on a glacial environment (Italian Western Alps). *Atmosfera 28,* 117–128. https://doi.org/10.20937/ATM.2015.28.02.04

Hirsch, R.M., Slack, J.R., and Smith, R.A., 1982: Techniques of trend analysis for monthly water quality data. *Water Resour. Res. 18,* 107–121. https://doi.org/10.1029/WR018i001p00107

Hudson, N.W., 1971. Soil Conservation. Batsford Ltd, London.

Joon-Hak, L. and Jun-Haeng, H., 2011: Evaluation of estimation methods for rainfall erosivity based on annual precipitation in Korea. *J. Hydrol. 409,* 30–48. https://doi.org/10.1016/j.jhydrol.2011.07.031

Yu, B., Hashim, G. M., and Eusof, Z., 2001: Estimating the R-factor with limited rainfall data: A case study from Peninsular Malaysia. *J. Soil Water Conserv. 56,* 101–105.

Loureiro, N.S. and *Coutinho, M.A.,* 2001: A new procedure to estimate the RUSLE EI$_{30}$ index, based on monthly rainfall data and applied to the Algarve region, Portugal. *J. Hydrol. 250,* 12–18. https://doi.org/10.1016/S0022-1694(01)00387-0

Luino, F., 2005: Sequence of instability processes triggered by heavy rainfall in the northern Italy. *Geomorphology 66,* 13–39. https://doi.org/10.1016/j.geomorph.2004.09.010

Nash, J.E., and *Sutcliffe, J.V.,* 1970: River flow forecasting through conceptual models. Part I – a discussion of principles. *J. Hydrol. 10,* 282–290. https://doi.org/10.1016/0022-1694(70)90255-6

Petkovšek, G. and *Mikoš, M.,* 2004: Estimating the R factor from daily rainfall data in the sub-mediterranean climate of southwest Slovenia. *Hydrol. Sci. J. 49,* 869–877. https://doi.org/10.1623/hysj.49.5.869.55134

Renard, K.G., Foster, G.R., Weesies, G.A., McCool, D.K., and *Toder, D.C.,* 1997: Predicting soil erosion by water: a guide to conservation planning with the revised universal soil loss equation (RUSLE). *USDA Agric. Handb. 703,* U. S. Gov. Print Office Washington DC

Renard, K.G. and *Freimund, J.R.,* 1994: Using monthly precipitation data to estimate the R-factor in the revised USLE. *J. Hydrol. 157,* 287–306. https://doi.org/10.1016/0022-1694(94)90110-4

Richardson, C.W., Foster, G.R., and *Wright, D.A.,* 1983: Estimation of erosion index from daily rainfall amount. *Trans. ASAE 26,* 153–156. https://doi.org/10.13031/2013.33893

Terzago, S., Cremonini, R., Cassardo, C, and *Fratianni, S.,* 2012: Analysis of snow precipitation during the period 2000-09 and evaluation of a MSG/SEVIRI snow cover algorithm in SW Italian Alps. *Geografia Fisica e Dinamica Quaternaria 35, 91-99.*

Tropeano, D., 1984: Rate of soil erosion processes on vineyards in Central Piedmont (NW Italy). *Earth Surf. Process. Landf. 9,* 253–266. https://doi.org/10.1002/esp.3290090305

Vallebona, C., Pellegrino, E., Frumento, P., and *Bonari, P.,* 2015: Temporal trends in extreme rainfall intensity and erosivity in the Mediterranean region: a case study in southern Tuscany, Italy. *Clim. Change 128,* 139–151. https://doi.org/10.1007/s10584-014-1287-9

Venema, V.K.C., Mestre, O., Aguilar, E., Auer, I., Guijarro, J.A., Domonkos, P., Vertacnik, G., Szentimrey, T., Stepanek, P., Zahradnicek, P., Viarre, J., Müller-Westermeier, G., Lakatos, M., Williams, C.N., Menne, M.J., Lindau, R., Rasol, D., Rustemeier, E., Kolokythas, K., Marinova, T., Andresen, L., Acquaotta, F., Fratianni, S., Cheval, S., Klancar, M., Brunetti, M., Gruber, C., Prohom Duran, M., Likso, T., Esteban, P., Brandsma, T., and *Willett, K.,* 2013: AIP Conference Proceedings, 9th International Temperature Symposium on Temperature: Its Measurement and Control in Science and Industry, ITS 2012. Vol. 1552 8, 1060–1065, https://doi.org/10.1063/1.4819690

Willmott, C.J. and *Matsuura, K.,* 2005: Advantages of the mean absolute error (MAE) over the root mean square error (RMSE) in assessing average model performance. *Clim. Res. 30,* 79–82. https://doi.org/10.3354/cr030079

Wischmeier, W.H. and *Smith, D.D.,* 1978: Predicting rainfall erosion losses – a guide to conservation planning. *USDA Sci. Educ. Adm. Agric. Res. Agric. Handb. 537,* 58 pp.

Yin, S., Xie, Y., Nearing, M.A., and *Wang, C.,* 2007: Estimation of rainfall erosivity using 5- to 60-minute fixed-interval rainfall data from China. *Catena 70,* 306–312. https://doi.org/10.1016/j.catena.2006.10.011

Yu, B., Hashim, G.M., and *Eusof, Z.,* 2001: Estimating the R-factor with limited rainfall data: a case study from peninsular Malaysia. *J. Soil Water Conserv. 56,* 101–105.

Yu, B., and *Rosewell, C.J.,* 1996a: An assessment of daily rainfall erosivity model for New South Wales. *Aust. J. Soil Res. 34,* 139–152. https://doi.org/10.1071/SR9960139

Yu, B. and *Rosewell, C.J.,* 1996b: A robust estimator of the R factor for the Universal Soil Loss Equation. *Trans ASAE 39,* 559–561. https://doi.org/10.13031/2013.27535

Yu, B. and *Rosewell, C.J.,* 1996c: Rainfall erosivity estimation using daily rainfall amounts for South Australia. *Aust. J. Soil Res. 34,* 721–733. https://doi.org/10.1071/SR9960721

Zandonadi, L., Acquaotta, F., Fratianni, S., and *Zavattini, J.A.,* 2016: Changes in precipitation extremes in Brazil (Paraná River Basin). *Theor. Appl. Climatol. 123,* 741–756. https://doi.org/10.1007/s00704-015-1391-4

IDŐJÁRÁS

Synoptic-climatological analysis of high level air flow over the Carpathian Basin

Anna Zsilinszki[1], **Zsuzsanna Dezső**[1*], **Judit Bartholy**[1,2], and **Rita Pongrácz**[1,2]

[1]*Department of Meteorology, Eötvös Loránd University,*
Pázmány Péter st. 1/A, H-1117, Budapest, Hungary

[2] *Excellence Center, Faculty of Science, Eötvös Loránd University,*
Brunszvik u. 2, H-2462, Martonvásár, Hungary

Corresponding author E-mail: dezsozsuzsi@caesar.elte.hu

(Manuscript received in final form February 24, 2018)

Abstract— In recent years, several unusual (or at least very rare) weather events occurred in the Carpathian Basin, e.g., the severe snow in March 2013. We are assuming that this anomaly may be a part of the climate change-related macro-scale circulation changes, especially the changes in the characteristics of polar jetstream. For evaluating this hypothesis, we performed a detailed statistical analysis of the high level wind fields of the region for 22 vertical layers above the 500 hPa pressure level, including the detailed analysis of average wind speed and wind directions, trend analysis of daily wind speed values, and extreme wind speed values. The results show negative trends in the mean wind speed at the higher tropospheric levels, and positive trends at the very high stratospheric levels in the Carpathian Basin. Furthermore, statistically significant trends mostly occurred in westerly winds, which is the most frequent wind direction.

Key-words: wind speed, wind direction, jet stream, frequency distribution, trend analysis

1. Introduction

Global climate change includes several direct and indirect consequences within the climate system. Some of these consequences are associated with regional scale climatic conditions, others are more directly linked to large-scale processes, such as atmospheric circulation regimes (e.g.,, *Barnes* and *Polvani,* 2013; *Francis* and *Skific,* 2015). *Screen* and *Simmonds* (2010) showed that the warming of the Arctic polar region is much faster than the warming of any other

part of the world, which can be due to an Arctic amplification originating from the change in the net radiation balance causing a larger change in regional temperature compared to the global average. This is why temperature contrast between the lower and higher latitudes tends to decrease, which can result in the rearrangement of large-scale atmospheric circulation (e.g., in the behavior of the polar jet stream), and decreasing wind speeds, especially in the mid-latitudes (*Francis et al.*, 2009).

The Arctic amplification is discussed by *Hwang et al.* (2011) and *Screen and Simmonds* (2010) in details. Specifically, sea ice loss is considered the main trigger factor to contribute to this phenomenon through several strongly interrelated positive feedbacks: (i) decreasing albedo, (ii) enhanced surface fluxes (heat and moisture fluxes are anomalously larger during the period of below normal sea ice extent), (iii) more water vapor from the open sea, (iv) higher sea surface temperatures, (v) more frequent unstable boundary layer conditions, and (vi) stronger cloud formation. As a result, more clouds lead to more downward longwave radiation, and finally, these effects together lead to warmer climatic conditions. The analysis of *Francis et al.* (2009) concludes that large scale atmospheric circulation patterns in the years with less sea ice tend to resemble to the circulation patterns of the negative phase of the North Atlantic Oscillation (NAO) and Arctic Oscillation (AO), because warming results in higher sea level pressure (SLP) above the North Pole affecting the storm tracks as well.

On one hand, there are lots of studies (e.g., *Francis* and *Vavrus*, 2012; *Miller et al.*, 2010 ; *Zhang et al.*, 2012; *Knudsen et al.*, 2015) pointing out clear evidences of the Arctic amplification to affect atmospheric conditions and result in anomalous behavior not only in the polar region, but in the midlatitudes as well. Several analyses (*Overland et al.*, 2012; *Peings* and *Magnusdottir*, 2014) conclude that the increasing (at least in some seasons) amplitude in Rossby waves causes their slower eastward propagation, and consequently, more persistent weather conditions in the midlatitudes. Thus, longer anomalous weather patterns can lead to extreme meteorological events. On the other hand, several studies (e.g.,, *Screen* and *Simmonds*, 2013; *Barnes* and *Screen*, 2015) emphasize the uncertainties of such overall statements.

Small changes in global circulation may lead to significant changes regionally, so in this study we focus on the region of the Carpathian Basin, by performing general statistical analysis to identify the direct or indirect effects of large scale changes in regional circulation regimes. Large scale circulation changes can be recognized more easily at higher levels than near the surface due to the negligible role of surface from the mid-troposphere upward. Therefore, this analysis covers the high level wind characteristics and trends. After introducing the data and methods (Section 2) the analysis of average wind speed and wind directions is discussed in Section 3 followed by the trend analysis of

daily mean wind speed values, and extreme wind speed values. Finally, Section 4 summarizes the main conclusions of the paper.

2. Data and methods

For the present analysis we use ERA Interim Reanalysis data (*Dee et al.*, 2011) compiled by the European Centre for Medium-Range Weather Forecast (ECMWF), for the period 1979–2015, and for 240 grid points with 0.75° horizontal resolution covering Hungary and its vicinity (the geographical extent of the study domain is shown in *Fig. 1*). Daily 12:00 UTC wind speed and direction data of 22 levels from 500 hPa to 1 hPa pressure level are analyzed. The closest grid point to Budapest (47.25°N, 18.75°E) is selected among the 240 grid points to represent the Carpathian Basin, and the results are shown for this representative grid point throughout this paper, where the analysis are carried out for each grid point separately.
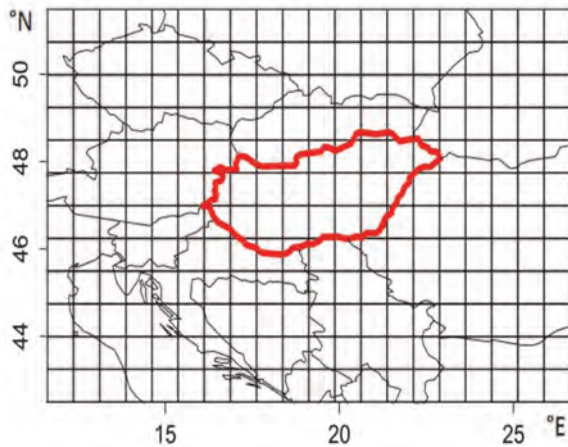
Fig. 1. The study area with 0.75° horizontal resolution. Red contour indicates the country border of Hungary.

3. Results and discussion

Our main motivation is associated with the winter of 2012–2013 and early spring of 2013 when an anomalously large number of Mediterranean cyclones

occurred in the Carpathian Basin (*Fig. 2*) resulting in significantly high amount of precipitation during this period (*Vincze*, 2013) compared to the usual precipitation conditions. These weather characteristics are related to a quasi-permanent synoptic pattern over Europe with a south-shifted location of jet stream (*Fig. 3*). For the detailed analysis of the high level circulation patterns, a general statistical analysis of the high level wind fields of the region is performed for 22 vertical levels above the 500 hPa pressure level.
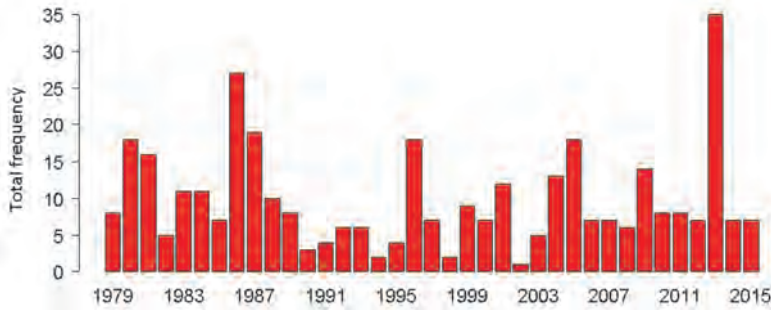
Fig. 2. The number of Mediterranean cyclones for January-February-March (JFM) in every year from 1979 to 2015 on the basis of *Péczely* (1961) classification types.
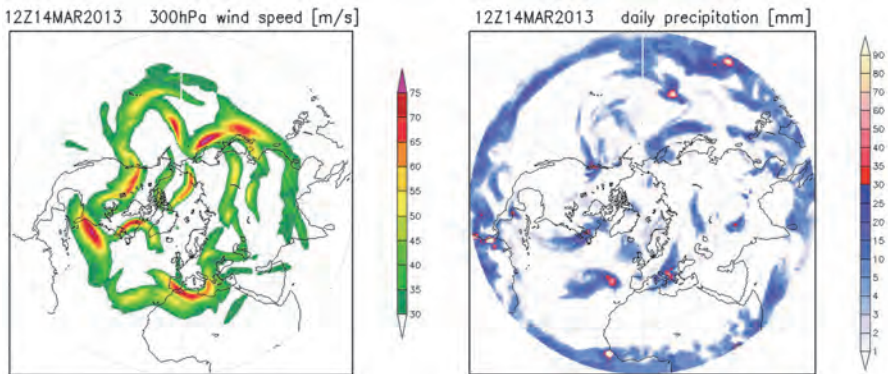
Fig. 3. Jet stream location derived from the 300 hPa level wind field (left) and precipitation pattern (right) on March 14, 2013.

3.1. High level wind climatology in the Carpathian Basin

3.1.1. Wind speed

As a very first statistical overview about the vertical structure of wind average, wind speed values are calculated for the target region for all the pressure levels taking into account the entire period. *Fig. 4* clearly shows that the greatest mean wind speed values can be found at the 250 hPa level within the upper troposphere. The large values of wind speed are associated with the atmospheric level where the polar jet stream is mostly located. Besides the mean, which is a very robust statistical feature of time series, the distribution of the actual values is also important, especially for meteorological variables with asymmetric distribution. Wind speed is one of these variables, and it is often modeled with Weibull distribution (e.g., *Péliné et al.,* 2016). The empirical distribution of the 250 hPa level wind speed values and the fitted Weibull probability density function are shown in *Fig. 5*. The Weibull parameters are estimated with the numerical gradient technique based on the maximum-likelihood method. For the scale and shape parameters the estimated values are 24.56 and 1.84, respectively. The most frequent wind speed values at 250 hPa level are between 10 m/s and 20 m/s wind speed (the average is 22 m/s). A comprehensive summary of distribution can be seen in Box-Whisker plot diagram where the maximum, minimum, upper and lower quartiles, and median values are separately indicated. The Box-Whisker plot diagrams in *Fig. 6* compare the distributions of the wind speed values at 18 analyzed levels. In addition to the full distribution, extreme values are especially analyzed by defining different thresholds (i.e., the median and the 99th percentile), and the Box-Whisker plot diagrams are prepared for the wind speed values above these thresholds. The intervals of wind speed range move to greater values with the height up to the 250 hPa level, then a decrease can be recognized up to the 50 hPa level where they start to increase again reaching the greatest values, overall, at the 1 hPa level.
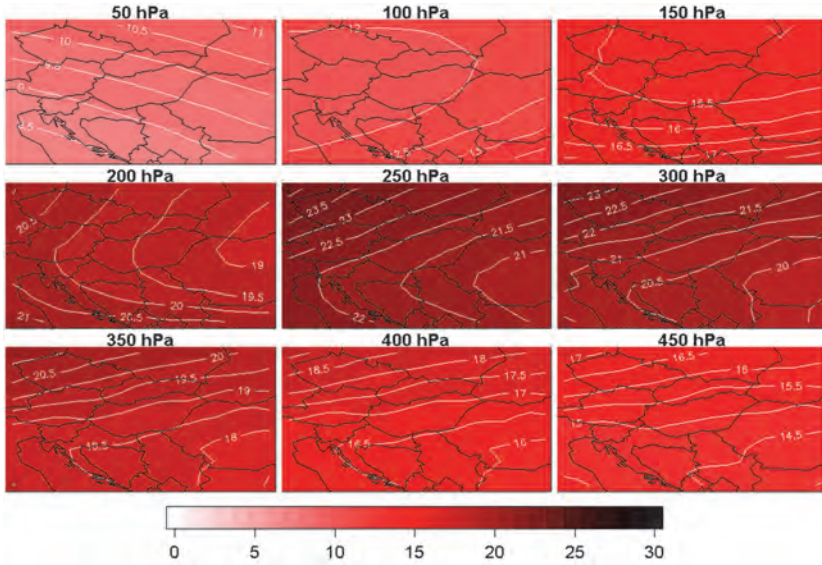
Fig. 4. Mean wind speed values [m/s] at different levels of the upper troposphere/lower stratosphere, in the period 1979–2015.
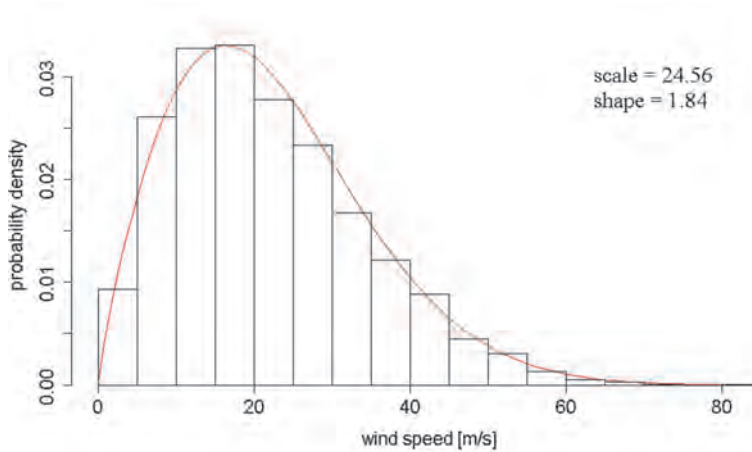
Fig. 5. Histogram of wind speed at the 250 hPa level in the closest grid point to Budapest (47.25°N, 18.75°E) and the estimated probability density function (indicated by the red curve) fitted to the empirical distribution. The scale and shape parameters of the fitted Weibull distribution are shown in the upper right corner of figure.
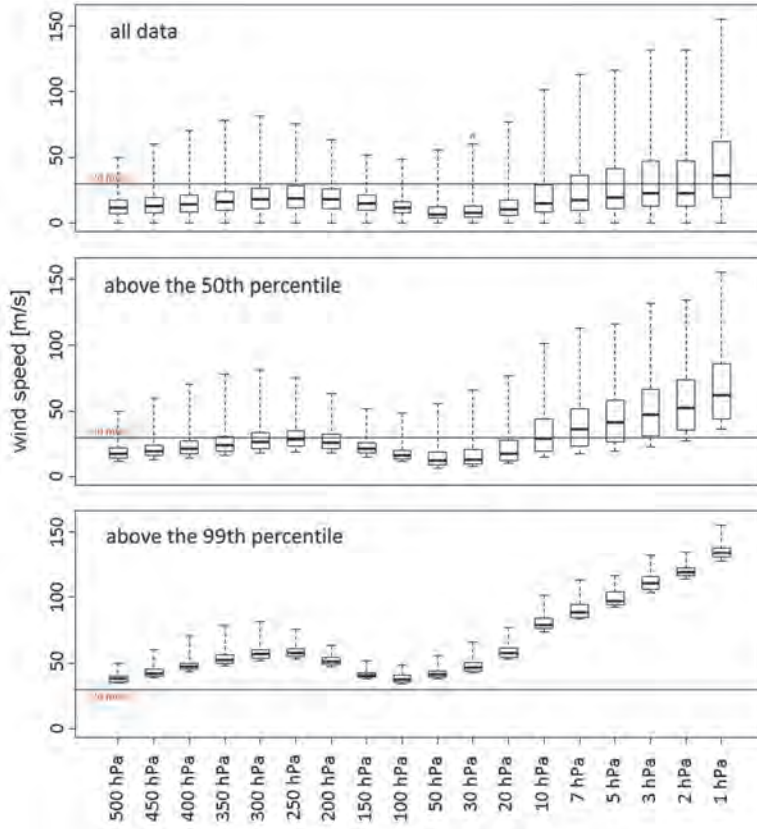
Fig. 6. Box-Whisker diagrams for wind speed distribution for the whole time series (top), wind speed values above the 50th percentile, i.e., median (middle), and the 99th percentile (bottom) in the closest grid point to Budapest (47.25°N, 18.75°E), 1979-2015. Dashed vertical lines indicate the ranges between the minimum and maximum wind speed, boxes are drawn between the lower and upper quartiles, and the medians are indicated by the thicker horizontal lines within the boxes. The long horizontal line highlights the wind speed value of 30 m/s (which is the threshold value commonly used for jet stream identification).

3.1.2. Wind direction

37-year daily averages of wind speed and direction are plotted together to represent the annual cycle of long-term mean wind at different levels. *Figs. 7* and *8* show the results for the 250 hPa and 50 hPa level, respectively. The mean wind directions were calculated with the method discussed by *Grange* (2014), i.e., by the arcus tangent function of mean wind components. Only a very weak

annual cycle can be recognized in both the wind directions and wind speed values at the 250 hPa level (*Fig, 7*). Above the 70 hPa level, a substantial annual cycle is clearly visible at the stratospheric levels (*Fig. 8*).
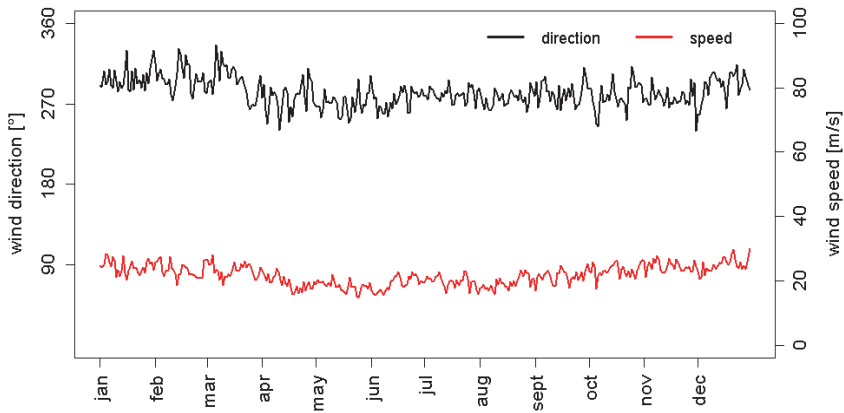
Fig. 7. Annual average wind direction [°] and wind speed [m/s] at the 250 hPa level in the closest grid point to Budapest (47.25°N, 18.75°E), in the period 1979–2015.
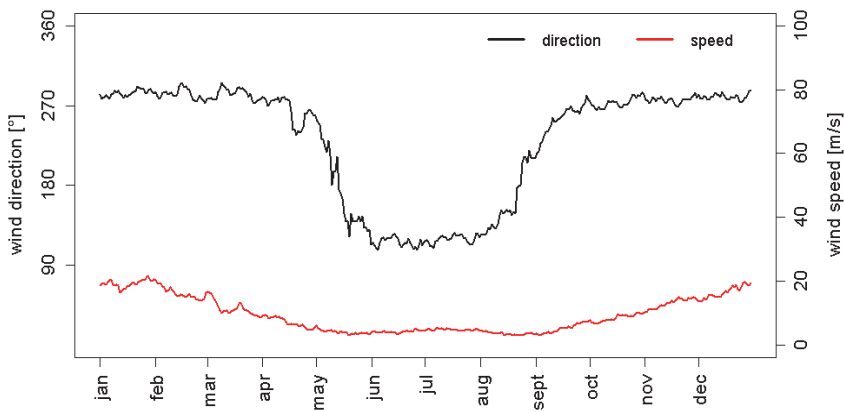
Fig. 8. Annual average wind direction [°] and wind speed [m/s] at the 50 hPa level in the closest grid point to Budapest (47.25°N, 18.75°E), in the period 1979–2015.

Besides the overall means, the annual cycle can be analyzed in more details when the actual time series are plotted for the entire period of 1979–2015. For this purpose, directions are divided into two main groups, westerly wind (between 180° and 360°) and easterly wind (between 0° and 180°). The full time series are shown for five selected levels, 10 hPa, 50 hPa, 150 hPa, 250 hPa, and 500 hPa (*Fig. 9*). At the higher levels (between 1 hPa and 70 hPa), the wind turns from westerly to easterly direction, and the wind speed becomes weaker around early May, and then, it turns back to westerly in late August, early September (*Fig. 9*). At the lower levels (from 100 hPa down to 500 hPa), this annual periodicity disappears, and easterlies become less frequent (below 25%) overall. The least frequency occurrence of easterlies can be detected at the 150 hPa level, where it is only 10% for the entire 37 years.

The total ratio of the westerly (W) and easterly (E) winds are shown above the upper right corners of the diagrams for each level.

For further analysis, the annual cycle of the relative frequency distributions of wind directions at each level is determined using four main classes (i.e., N: above 315° or below 45°, E: 45°–135°, S: 135°–225°, and W: 225°–315°). *Fig. 10* shows that below the100 hPa level, class W is clearly the dominant wind direction with about 50% occurrence. Class N, S, and E occurred with an average 25%, 15%, and 10% relative frequency, respectively, at the 250 hPa level, and no significant annual cycle can be identified. Substantially different results with a clear annual cycle can be recognized above 100 hPa. The 50 hPa level is shown among these high levels in *Fig. 11*. It can be seen that class W is still the most dominant wind direction on annual average (53% is the overall relative frequency), but the distribution changes throughout the year: 70–75% from October to mid-April, then decreases to <1% by July, and starts to increase again in August. The annual mean relative frequency of class N at the 50 hPa level is 12% – about the half of the relative frequency of class N at the 250 hPa level, which is due to the dominant occurrence of class E above 100 hPa in summer when both class W and class N disappear from the distribution. The relative frequency of class S also increases during April-May, reaches its maximum in June-July (~25%), and decreases in August-September together with class E. Overall, the annual mean relative frequency of class S and class E at the 50 hPa level is 15% and 20%, respectively. The dominant occurrence of class E in summer results in becoming the second most often appearing direction at this high level with the maximum relative frequency reaching 75% in July.
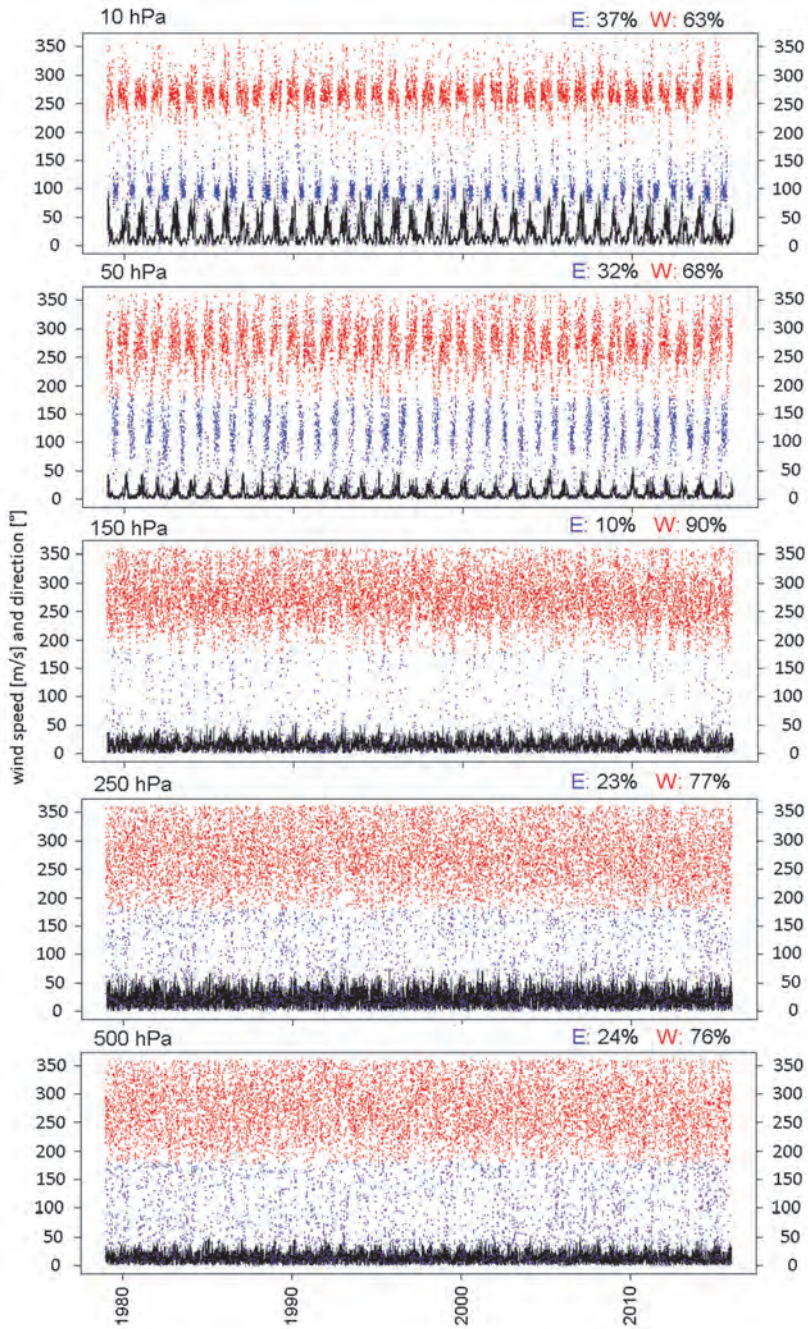
Fig. 9. Time series of wind speed (black lines) and directions (blue dots – easterly directions, red dots – westerly directions) at the closest grid point to Budapest (47.25°N, 18.75°E), in the period 1979–2015.

28
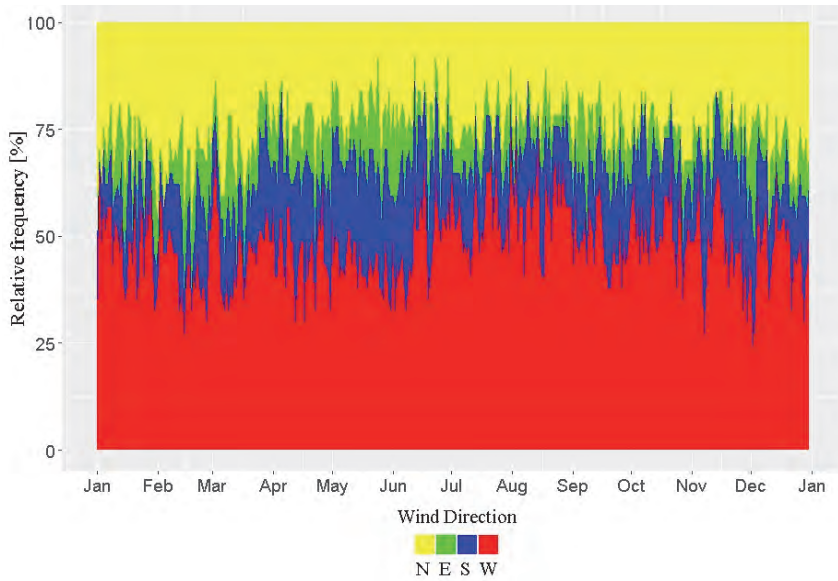
Fig. 10. Annual relative frequency of wind direction classes at the 250 hPa level in the closest grid point to Budapest (47.25°N, 18.75°E), in the period 1979-2015.
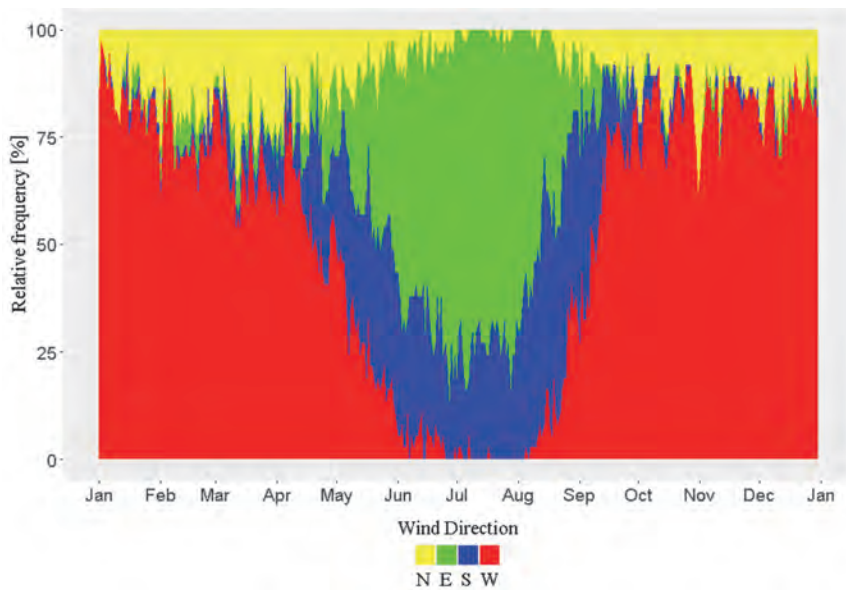
Fig. 11. Annual relative frequency of wind direction classes at the 50 hPa level in the closest grid point to Budapest (47.25°N, 18.75°E), in the period 1979–2015.

In order to analyze the distribution of wind direction in more details throughout the year, wind roses were determined on a monthly scale for every level. The wind roses indicate the total frequency in a given direction using 8 different subclasses of directions (*Table 1*) and the corresponding wind speed distributions.

Table 1. Defined subclasses of wind direction used in wind roses

subclass	interval
N	>337.5°, or <22.5°
NE	22.5°–67.5°
E	67.5°–112.5°
SE	112.5°–157.5°
S	157.5°–202.5°
SW	202.5°–247.5°
W	247.5°–292.5°
NW	292.5°–337.5°

Table 2 compares the total occurrences and relative frequencies of the subclasses at the two selected levels (i.e., 250 hPa and 50 hPa). In overall agreement with previous results shown in Figs. 7–11, subclass W is dominant at every level in the most part of the year. As an example, the monthly distributions at the 250 hPa level are shown in *Fig. 12*, since this is the general level of the polar jet in the region. At this level, 26% of the total data are in subclass W, and together with the adjacent subclasses (i.e., NW, SW) the relative frequency is 65%, while easterly subclasses (NE, E, SE) together add up to only 15% leaving 13% and 7% in subclasses N and S, respectively. At a monthly resolution, a small fluctuation can be seen in the frequency of direction subclasses during the year.

Table 2. Distribution of wind direction subclasses at 250 hPa (left) and 50 hPa (right), in the period 1979–2015, in the closest grid point to Budapest (47.25°N, 18.75°E). The most frequent subclass is highlighted by bold numbers

subclass	250 hPa level		50 hPa level	
	total frequency	relative frequency	total frequency	relative frequency
N	1722	13%	655	5%
NE	883	7%	420	3%
E	525	4%	1376	10%
SE	549	4%	1777	13%
S	998	7%	812	6%
SW	2491	18%	1565	12%
W	**3547**	**26%**	**4516**	**33%**
NW	2799	21%	2393	18%
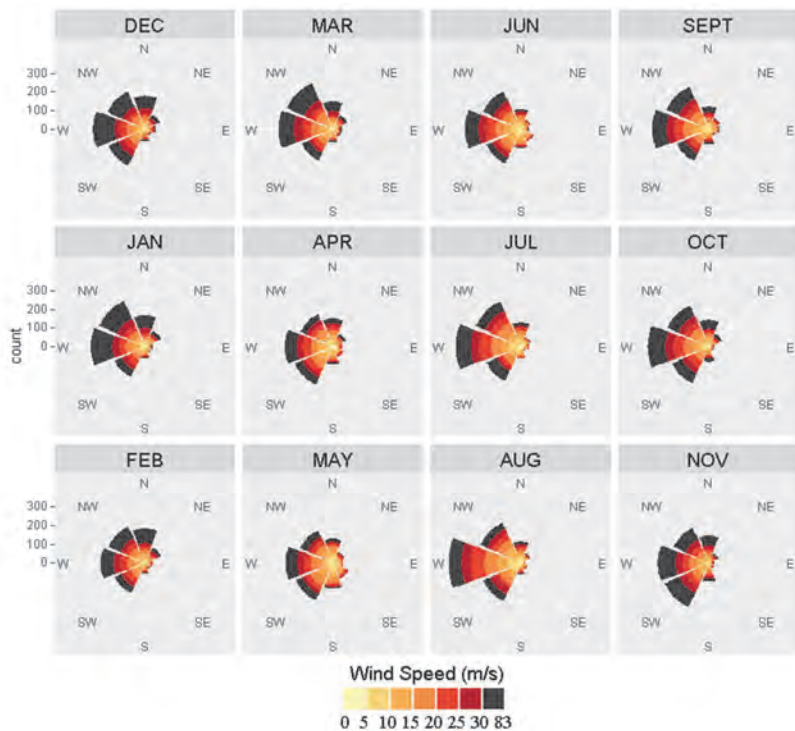
*Fig. 12. M*onthly distribution of wind direction subclasses at the 250 hPa level, the radius of an individual graph indicates the frequency, colors indicate the distribution of wind speed values within the direction subclasses. The total number of cases is 13149 (the number of wind calm conditions, i.e., below 0.1 m/s is 2) in the closest grid point to Budapest (47.25°N, 18.75°E), in the period 1979–2015.
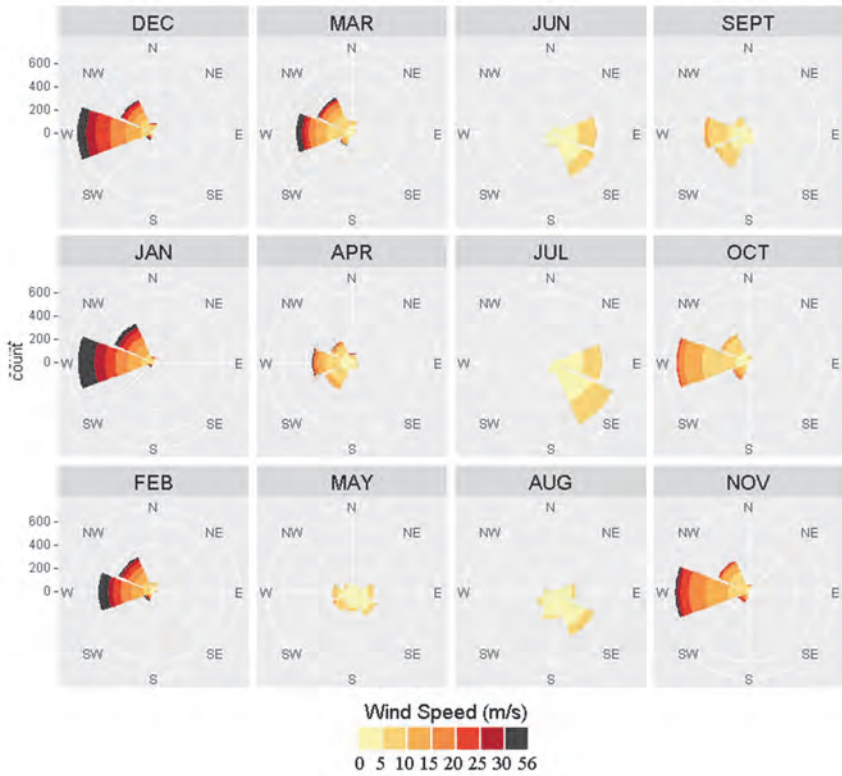
Fig. 13. Monthly distribution of wind direction subclasses at the 50 hPa level, the radius of an individual graph indicates the frequency, colors indicate the distribution of wind speed values within the direction subclasses. The total number of cases is 13149 (the number of wind calm conditions, i.e., below 0.1 m/s is 5), in the closest grid point to Budapest (47.25°N, 18.75°E), in the period 1979–2015.

Then, in the higher atmospheric levels, subclasses E and SE occur more frequently during summer with weaker wind speed values (e.g., at the 50 hPa level as shown in *Fig. 13*). Consequently, the annual frequency of easterly winds (subclasses NE, E, SE) add up to 26% at the 50 hPa level, which is about 1.5 times of the combined frequency of these at the 250 hPa level. Despite this increased frequency, westerlies (i.e., subclasses NW, W, SW) are still dominant on annual scale with 63% altogether. Finally, the meridional subclasses (N, S) almost disappear, with a relative frequency of 5% and 6%, respectively. Similar conclusions can be drawn at the high levels above 50 hPa.

3.2. Linear trend analysis

After the detailed frequency distribution analysis, we focused on the potentially systematic changes of wind by fitting linear trends to the entire database of wind time series (1979–2015) for the Carpathian Basin using the linear regression function, $y = a \cdot x + b$. First, annual mean wind speeds (calculated from the daily data of 12 UTC) are analyzed. The fitted linear trend coefficients (*Fig. 14*) are significant (at the p=0.05 level of significance) at very high levels, i.e., from 3 hPa upward (increasing trend) and at the tropospheric levels between 300 hPa and 500 hPa (decreasing trend). Besides the annual mean wind speed time series, the annual occurrences of strong wind, i.e., wind speed values above 30 m/s, are also analyzed (*Fig. 15*). In this case, statistically significant increasing and decreasing trends can be identified above the 5 hPa level and at the 350 hPa level, respectively.
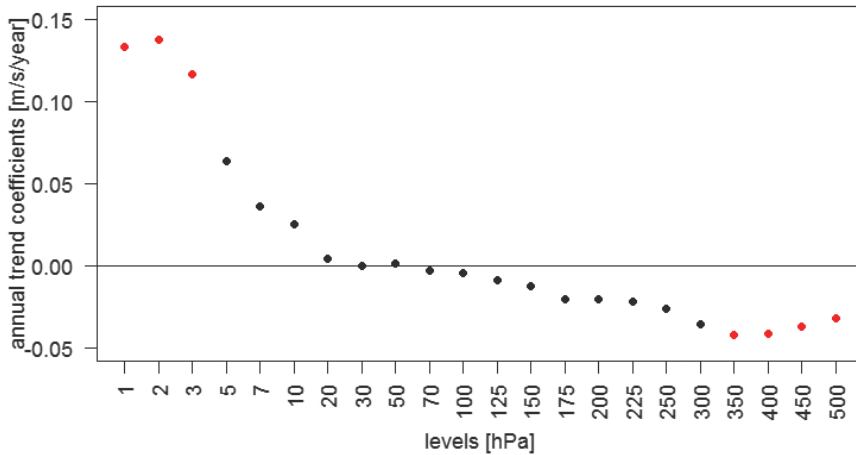
Fig. 14. Trend coefficients (steepness) of linear regression fitted to the annual mean wind time series for all the analyzed levels, for the period 1979-2015, in the closest grid point to Budapest (47.25°N, 18.75°E). Red symbols indicate the statistically significant (p=0.05) coefficient values.
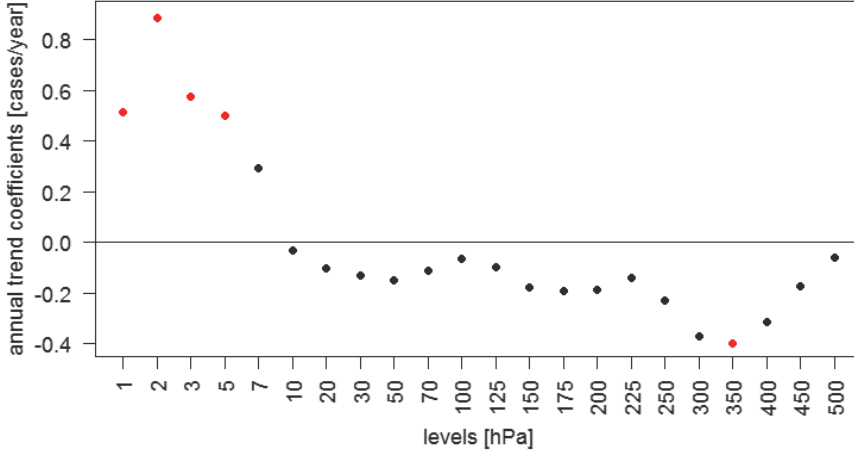
Fig. 15. Trend coefficients (steepness) of linear regression fitted to the annual frequency of wind speed above 30 m/s for all the analyzed levels, for the period 1979-2015, in the closest grid point to Budapest (47.25°N, 18.75°E). Red symbols indicate the statistically significant coefficient values.

The dataset of the 250 hPa level wind speed is divided into two parts (i.e., 1979–1997 and 1997–2015), and trend analysis is carried out on them separately. The fitted linear regression trend coefficients for the second period (1997–2015) are negative: –0.14 m/s/year and –1.12 cases/year for the annual mean wind speed and the annual frequency of wind speed above 30 m/s, respectively. According to the Mann-Kendall significance test, the corresponding p-values are 0.032 and 0.014, which show statistically significant decrease in the past few decades.

The trend analysis is also completed by the four wind direction classes (N, E, S, and W) both for the annual means and the annual frequencies of cases with wind speed above 30 m/s. The fitted linear regressions are shown in *Fig. 16* for the 250 hPa and 500 hPa levels.
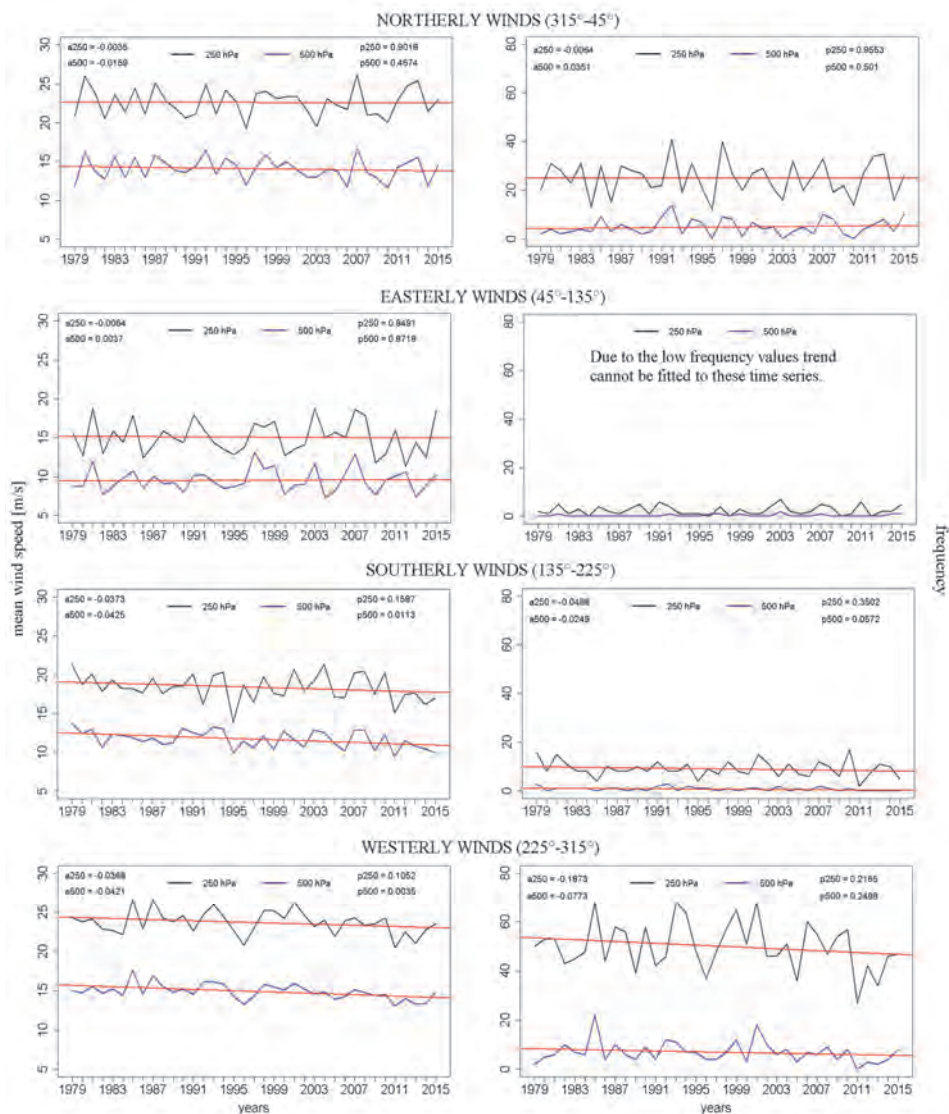
Fig. 16. Summary of the linear trend analysis of high level winds by the main wind direction classes at the 250 hPa (black line) and 500 hPa (blue line) levels at Budapest for the annual mean wind speed (left) and the annual number of cases with strong wind speed (> 30 m/s) (right). The steepness of the fitted trend lines are shown as a250 (expressed in m/s/year) and a500 (expressed in case/year), respectively. Furthermore, the corresponding p-values are also shown as p250 and p500, respectively.

The conclusions from all the 22 analyzed levels are summarized by the wind direction classes for the annual means as follows. (1) Slight decrease (negative trend coefficient) can be seen in the annual means of northerly winds in 18 levels out of the total 22 analyzed levels, but none of them is statistically significant. (2) The trend coefficients of the annual mean easterly winds are mostly positive (from 1 hPa to 225 hPa), which are significant only at the very high stratospheric levels: the 2 hPa, 3 hPa, 5 hPa, 20 hPa, 30 hPa, and 50 hPa levels. The fitted linear trend coefficients turns to negative at the tropospheric levels (from 250 hPa down to 500 hPa levels), but none of them is significant according to the Mann-Kendall significance test. (3) Significant decrease can be recognized in the southerly annual means in the upper tropospheric levels, i.e., between 300 hPa and 500 hPa levels, the fitted linear regression coefficients are –0.056 m/s/year (300 hPa level), –0.060 m/s/year (350 hPa level), –0.051 m/s/year (400 hPa level), –0.036 m/s/year (450 hPa level), –0.036 m/s/year (500 hPa level), with the corresponding p-values from Mann-Kendall test of 0.045, 0.027, 0.048, 0.043, 0.048, respectively. (4) Westerly mean winds significantly increase at three very high stratospheric levels (1 hPa, 2 hPa, 3 hPa with the trend coefficients of 0.249 m/s/year, 0.215 m/s/year and 0.164 m/s/year, and the corresponding p-values of 0.001, 0.009 and 0.012, respectively). The fitted trend coefficients become negative below the 20 hPa level, and the identified decrease is significant at the tropospheric levels of 350 hPa, 400 hPa, 450 hPa, and 500 hPa.

In the case of the annual frequency of extreme wind speeds (above 30 m/s), the fitted linear trend coefficients are mostly negative, however, they are not statistically significant in any given direction at any level. The occurrences of strong wind in the easterly, southerly, and northerly direction classes are quite rare at every analyzed level – the average annual frequencies are 3.7 (class E), 2.5 (class S), and 7.3 (class N) cases per year considering all the examined levels, whereas strong wind occurred 54.0 cases/year on average in class W.

Finally, the spatial differences of the above discussed linear trends are analyzed. For this purpose, we calculated the linear trend coefficients in every grid point along the longitude of 28.75°E. The results for the frequency of extreme winds above 30 m/s at the 250 hPa level are shown in *Fig. 17* for the second part of the period (1997–2015). The trend coefficients show southward increasing negative values, which become significant at the closest latitude to Budapest (47.25°N).
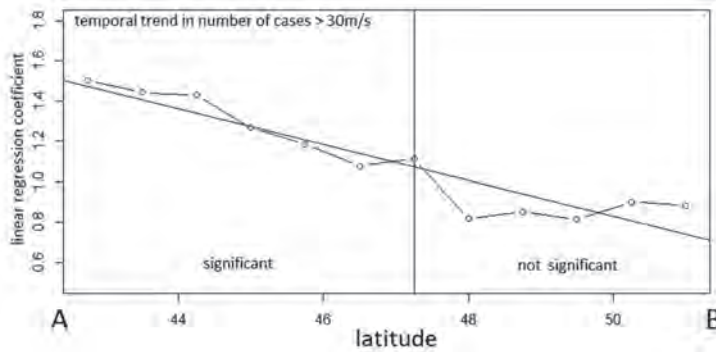
Fig. 17. The absolute value of the linear regression coefficients along the 18.75°E longitude (1997–2015) at the 250 hPa level for the frequency of strong wind (i.e., wind speed above 30 m/s).

4. Conclusions

From the synoptic meteorological practical experiences we know, that the jet stream has an important effect on daily weather in the midlatitudes. The international literature pays more and more attention to the changes in circulation regimes including jet stream at the midlatitudes (e.g., *Francis et al.,* 2009), as a result of substantial ice melting at the poles due to the detected and expected global warming. In this paper, we analyzed these changes from the specific point of view of the Carpathian Basin. For this purpose, first a general statistical climatological description of the high level wind characteristics was presented using reanalysis data (wind speed and direction) at 22 levels above the 500 hPa level pointing out the general dominance of westerly winds and highlighting the strongest winds at the 250 hPa and 300 hPa levels, which can be considered the vertical position of polar jet stream. Furthermore, we analyzed the temporal behavior of the time series by fitting linear trends on the data. In general, decreases of mean wind speed were found at the tropospheric levels (above 500 hPa), and increases at the very high stratospheric levels, which do not depend on the direction. Statistically significant trends mostly occurred in westerly winds, which is the most frequent wind direction of the Carpathian region as well, as the midlatitudes in general.

References

Barnes, E.A. and *Screen, J.A*, 2015: The impact of Arctic warming on the midlatitude jet-stream: Can it? Has it? Will it? *WIREs Clim Change 6*, 277–286. https://doi.org/10.1002/wcc.337

Barnes, E.A. and Polvani, L., 2013: Response of the midlatitude jets, and of their variability, to increased greenhouse gases in the CMIP5 models. *J. Climate*, *26*, 7117–7135. https://doi.org/10.1175/JCLI-D-12-00536.1

Dee, D.P., Uppala, S.M., Simmons, A.J., Berrisford, P., Poli, P., Kobayashi, S., Andrae, U., Balmaseda, M. A., Balsamo, G., Bauer, P., Bechtold, P., Beljaars, A. C. M., van de Berg, L., Bidlot, J., Bormann, N., Delsol, C., Dragani, R., Fuentes, M., Geer, A. J., Haimberger, L., Healy, S.B., Hersbach, H., Hólm, E. V., Isaksen, L., Kållberg, P., Köhler, M., Matricardi, M., McNally, A.P., Monge-Sanz, B. M., Morcrette, J.-J., Park, B.-K., Peubey, C., de Rosnay, P., Tavolato, C., Thépaut, J.-N., and *Vitart, F.,* 2011 For the case study we used the Péczely synoptic classification types (*Péczely*, 1983), which has been provided by Cs. Károssy (pers.comm.).: The ERA-Interim reanalysis: configuration and performance of the data assimilation system. *Q.J.R. Meteorol. Soc., 137*, 553–597. https://doi.org/10.1002/qj.828

Francis, J., and *Skific, N.*, 2015: Evidence linking rapid Arctic warming to mid-latitude weather patterns. *Phil.Trans.R. Soc. A*. 373: 20140170. https://doi.org/10.1098/rsta.2014.0170

Francis, J.A. and *Vavrus, S.J.*, 2012: Evidence linking Arctic amplification to extreme weather in mid-latitudes. *Geophys. Res.Letters 39*, L06801. https://doi.org/10.1029/2012GL051000

Francis, J.A., Chan, W., Leathers, D.J., Miller, J.R., and *Veron, D.E.*, 2009: Winter Northern Hemisphere weather patterns remember summer Arctic sea-ice extent. *Geophys. Res.Lett. 36*, L07503. https://doi.org/10.1029/2009GL037274

Grange, S.K., 2014: Technical note: Averaging wind speeds and directions. Technical report. University of Auckland, New Zealand. 12p.

Hwang, Y.T., Frierson, D.M.W., and *Kay, J.E.*, 2011: Coupling between Arctic feedbacks and changes in poleward energy transport. *Geophys. Res. Lett. 38*, L17704. https://doi.org/10.1029/2011GL048546

Knudsen, E.M., Orsolini, Y.J., Furevik, T., and *Hodges, K.I.*, 2015: Observed anomalous atmospheric patterns in summers of unusual Arctic sea ice melt. *J. Geophys. Res. Atmospheres 120*, 2595–2611. https://doi.org/10.1002/2014JD022608

Miller, G.H., Alley, R.B., Brigham-Grette, J., Fitzpatrick, J.J., Polyak, L., Serreze, M.C., and *White, J.W.C.*, 2010: Arctic amplification: Can the past constrain the future? *Quat. Sci. Rev.29*, 1779–1790. https://doi.org/10.1016/j.quascirev.2010.02.008

Overland, J.E., Francis, J.A., Hanna, E., and *Wang, M.*, 2012: The recent shift in early summer Arctic atmospheric circulation. *Geophys. Res. Lett. 39*, 1–6. https://doi.org/10.1029/2012GL053268

Péczely, Gy., 1961: The climatological characterisation of the macrosynoptic situations in Hungary. (in Hungarian) Magyarország makroszinoptikus helyzeteinek éghajlati jellemzése. OMSz Kisebb Kiadványai 32. Országos Meteorológiai Szolgálat, Budapest. (In hungarian)

Peings, Y. and *Magnusdottir, G.*, 2014: Response of the wintertime northern hemisphere atmospheric circulation to current and projected arctic sea ice decline: A numerical study with CAM5. *J. Climate 27*, 244–264. https://doi.org/10.1175/JCLI-D-13-00272.1

Péliné N.Cs., Bartholy J., Pongrácz R., and *Radics K.,* 2016: Analysis of climate change influences on the wind characteristics in Hungary. *Időjárás 120*, 53–71.

Screen, J.A. and *Simmonds, I.*, 2010: The central role of diminishing sea ice in recent Arctic temperature amplification. *Nature 464*, 1334–1337. https://doi.org/10.1038/nature09051

Screen, J.A., and *Simmonds, I.*, 2013: Exploring links between Arctic amplification and mid-latitude weather. *Geophys. Res. Lett. 40*, 959–964. https://doi.org/10.1002/grl.50174

Vince, E., 2013: Weather of winter 2012/2013. A 2012/13-as tél időjárása. *Légkör 58*, 40–42. (in Hungarian)

Zhang, X., Lu, C. and *Guan, Z.*, 2012: Weakened cyclones, intensified anticyclones and recent extreme cold winter weather events in Eurasia. *Environ. Res. Lett*, *7*, 44044–44051. https://doi.org/10.1088/1748-9326/7/4/044044

IDŐJÁRÁS

Dust deposition, microscale flow- and dispersion model of particulate matter, examples from the city center of Budapest

Orsolya Farkas and **Ákos Török**[*]

Budapest University of Technology and Economics,
Department of Engineering Geology and Geotechnics
Műegyetem rakpart 3, 1111 Budapest, Hungary

[*]Corresponding author E-mail: torokakos@mail.bme.hu

Abstract— Despite the air quality improvement, air pollution is still a severe problem in Budapest, and the city is one of the most polluted capitals of Europe. Dust has an adverse health effect, and it also causes aesthetic changes to buildings. Dust contributes to the damage of stone and may also result material loss. The paper analyzes the composition of dust and also describe its flow patterns in the city center of Budapest. The study area is located in one of the most polluted areas of Budapest, at Margit Boulevard. Dust samples were collected from the facades of buildings. Samples were analyzed with particle size analysis with laser diffraction, point counting of particles by optical microscopy, and X-Ray Diffraction (XRD). To simulate the airflow and the dispersion of particulate matter (PM_{10}), a computational fluid dynamics code called MISKAM (Mikroskaliges Strömung- und Ausbreitungsmodell - microscale flow and dispersion model for built up areas) was used. The results suggest that dust deposition is controlled by the flow pattern. Analyzed dust samples contain wind driven mineral grains (quartz, dolomite) and also human activity related pollutants such as fly ash and soot.

Key-words: dust, air pollution, mineralogy, MISKAM, historical buildings

1. Introduction

The high concentration of dust (particulate matter) has an adverse effect on human health and also causes alterations in structures and monuments (*Brimblecombe* and *Grossi,* 2009). Natural sources of airborne dust may include soil erosion, volcanic activity, forest fires, etc. (*Querol et al.,* 2004; *Gieré* and

Querol, 2010). The main anthropogenic sources of dust are from burning coal, oil, wood (*Pósfai* and *Buseck,* 2010), and waste, furthermore the road traffic emissions also have significant contribution to dust (*Grobéty et al.,* 2010; *Salma et al.,* 2017). In addition, the already deposited dust can be remobilized, stirred, and after redeposited again (*Salma et al.,* 2004a).

The health risks of particulate matter and the relationship between the fine particulate pollutants in the air and mortality have been studied in details in the past decades (*Reichardt,* 1995; *Lippman et al.,* 2000; *Samet et al.,* 2000; *Wichmann et al.,* 2000; *Pope et al.,* 2002). There is a linear correlation between concentrations of particulate pollutants and the number of diseases (*Dockery et al.,* 1993).

Diesel-engine vehicles have a more significant contribution to the airborne dust emissions than petrol fueled ones. The harmful effects of emissions of diesel-powered engines have been studied by applying C isotopic analysis (*Hildemann et al.,* 1994).

The particulates cause a visual damage on the buildings. Besides their optical effect, particulates contribute to the black crust formation and damage of building stones. Dust attracts sulphur dioxide and has a catalytic role in the formation of gypsum crystals (*Rodriguez-Navarro* and *Sebastian*, 1996) that damage buildings during their crystallization. The atmospheric sulphur concentration and deposition in Hungary have reduced in the past years, and previous simulations (*Bozó*, 1998; *Havasi et al.,* 2001) clearly demonstrated their pathways and deposition.

Previous studies have demonstrated that from polymorph varieties of SiO_2, the tridimite and crystobalite are more harmful when inhaled than the quartz. The amorphous SiO_2 varieties seem to have limited health effects (*Heaney* and *Banfield*, 1993).

The composition of settling dust was studied in Transsylvania (*Farkas* and *Weiszburg*, 2006). In this study, samples collected from 18 sites were compared. The results clearly reflected the influence of different industrial activities, however, the transportation related contribution to dust was not related.

Most of the comprehensive studies are focusing on air quality and urban climate in European capital cities (*Borbély-Kiss et al.,* 1999; *Kukkonen,* 2003; *Borsós et al.,* 2012; *Probáld,* 2014; *Ferenczi* and *Bozó*, 2017; *Leelőssy et al.,* 2017).

In the current paper, the terminology of *Gieré* and *Querol* (2010) was used. Particulate matter includes all particles with all size-ranges; fine particles less than 2.5 μm in diameter ($PM_{2.5}$) and coarse particles larger than 2.5 μm in diameter (including particles larger than PM_{10}). Dust term includes very fine to very coarse particles (up to a few mm in diameter), without indicating its source. Hence, settling dust has a size-range of nanometre to a few mm, but the lowest particle size analyzed in this paper was 0.02 μm.

In this paper we follow the above listed findings. To describe air pollution, two main tools were applied to assess the dust in the city centre. Dust samples were collected and analyzed to understand their composition and judge the contribution of anthropogenic sources. Besides sample collection, the PM_{10} deposition was also modeled by using a computational fluid dynamics (CFD) software to describe the sites, where highest amount of particulate matter is expected to accumulate. The combination of these two approaches allowed demonstrating the interaction between particulate matter deposition and flow patterns.

2. Materials and methods

2.1. Sampling sites

The study area is located in Hungary, in the second district of Budapest, at Margit Boulevard *(Fig. 1)*. It is a very busy, often traffic congested boulevard with high air pollution levels.
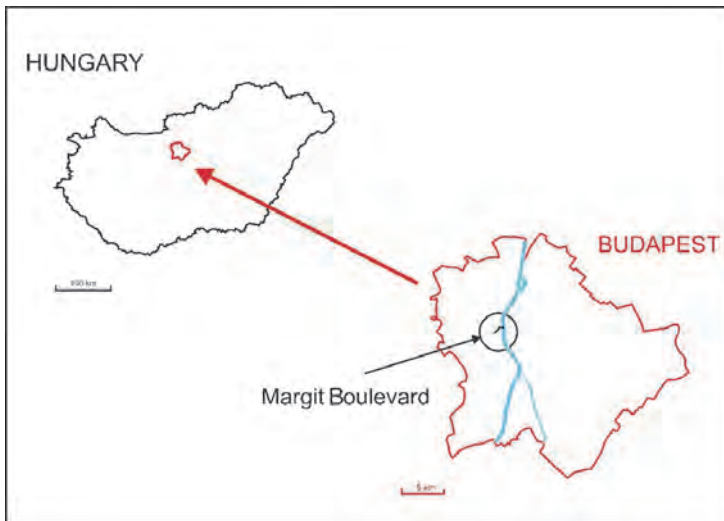
Fig. 1. Location of study area in Hungary and in Budapest

Seven dust samples were collected from the main boulevard and from the adjoining smaller streets. The sampling points and selected buildings are shown in *Fig. 2*. The description of sampling localities, the host rock of the samples, and sample codes are given in *Table 1*. Four samples are from the facades of three monuments (Semmelweis Medical Historical Library, Bauhaus style building in Margit Boulevard 15–17., and Margit-house), while the rest of the samples are coming from non-protected buildings.

Fig. 2. Sampling points in the city center of Budapest (see detailed description of sampling sites in *Table 1*).

Table 1. Sample codes, description of sample localities and host rock

Sample	Locality	Elevation above ground level [m]	Host rock	Description of the sampling site
T1	Budapest, Török Street 12. (Semmelweis Medical Historical Library)	1.3	Breccia	Window ledge
T2	Budapest, Török Street 12. (Semmelweis Medical Historical Library)	2.0	Breccia	Small cavities of ashlars
T3	Budapest, Török Street 6.	1.1	Tardos limestone	Top of footing
T5	Budapest, Török Street 1-3.	0.6	Tardos limestone	Window ledge
MK1a	Budapest, Margit Boulevard 15-17.	0.8	Travertine	Window ledge
MK5	Budapest, Margit Boulevard 5/A. (Margit-house)	1.0	Travertine	Window ledge
TF1	Budapest, Tölgyfa Street 30.	0,5	Travertine	Ledge inlet and ledge corner

2.2. Analytical methods

The dust samples were analyzed by using three techniques: (i) point counting of particles by optical microscopy (ii) X-Ray diffraction (XRD), and (iii) particle size analysis by laser diffraction *(Table 2)*.

Table 2. Analytical techniques and samples

Sample	Point counting of particles by optical microscopy	X-Ray Diffraction	Particle size analysis with laser diffraction
T1	✓		
T2	✓	✓	✓
T3	✓		✓
T5	✓	✓	✓
Mk1a	✓	✓	✓
Mk5	✓		✓
Tf1	✓	✓	

The proportion of components was determined by Dino Lite Microscopy resolution of 1.3 megapixel, magnification of 10 to 200x.

It was possible to measure and label particles by using the software of microscope. 3 areas 1 mm^2 each, were selected in the samples, where the mineralogical composition were evaluated based on particle counting. The results are presented as mean values of three counting.

The mineralogical composition was determined by X-Ray diffraction (XRD) with a Phillips Diffractometer (PW 1800, Cu-anode, 45 kV, 30 mA, Göttingen, Germany). Powder X-Ray patterns were obtained using PANalytical X'Pert HighScore Plus software. The diffraction data were recorded from 2° to 70° 2Θ via a continuous scan with a routine scan program.

Particle size distribution was measured by laser diffraction *(Jones*, 2003). Low Angle Laser Light Scattering (LALLS) was used for particle sizes of 0.02 to 2000 μm.

Sample preparation was made by using ultrasonic sample segregation (equipment: Bandelin, energy: 0.24 kJ, run time: 30 sec). The analysis took 90 sec with Beckman Coulter, LS 13 320.

2.3. Flow- and dispersion model MISKAM

To simulate the airflow and the dispersion of pollutant PM_{10}, a computational fluid dynamics (CFD) model was used. This particulate range was used since PM_{10} emission factors were available; i.e., this is the largest particle size for which transportation related emission factors were available. The main aim of the model was to identify flow patterns and link it to concentration differences of particulate matter. The CFD simulations are generally used to identify flow patterns and to simulate pollution dispersion. In addition, the results of modeling are commonly applied in urban development planning and design. As part of environmental impact analysis, the results of the pollution dispersion pattern can be directly implemented in development plans. MISKAM (Mikroskaliges Strömung- und Ausbreitungsmodell) was developed by *J. Eichhorn* (University of Mainz) to simulate pollution dispersion in urban areas (*Eichhorn*, 2008). The model incorporates a Reynolds-averaged Navier-Stokes solver adopting the Boussinesq-approximations to eliminate sound waves with a modified k – ε turbulence closure (*Eichhorn* and *Kniffka*, 2010).

The study area is a busy intersection, and its surroundings (400m × 400m) are located close to the city center of Budapest, at the intersection of Margit Boulevard and Török Street (*Fig. 2*).

For the input of model parameters, such as geometry, topography, MISKAM Data Processing software (developed by the Department of Fluid Mechanics, Budapest University of Technology and Economics) was used. Tecplot 360 software was used to visualize the results of simulations (wind flow, concentration distribution, etc.).

Medium-rise buildings with 4–5 floors are found in the modeled area. Additional input parameters were the ground plan and the elevation of buildings. For the meteorological characteristics, wind-statistics were created. The prevailing wind direction is from the WNW (west-northwest), while for the wind speed, a 2 m/s velocity was used at an elevation of 10 m. For this wind speed the software generated a logarithmic wind profile.

A 1 cm of surface roughness value was added for the ground surface, and the same value was applied for the buildings. Additional input data were: (i) leaf area density (LAD) of 0.5 m^2/m^3 and (ii) vegetation coverage (b) of 1 m^2/m^2. The pollution concentration of inflowing air to the model area was 0 kg/m^3, but when pollution concentration of the study area was calculated, the background concentration of PM_{10} was added, which was taken from the dataset of a nearby air quality monitoring station (Széna Square, Budapest I. district).

The traffic load of the roads was defined by traffic count by the authors. The traffic count was performed at one intersection (Margit Boulevard, Török Street and Margit Street) from 4 directions in 3 time periods (peak hours: morning, afternoon, peak-off hours: evening). Estimated traffic volumes were assigned to the surrounding streets. PM_{10} emissions were calculated by using

HBEFA (Handbook Emission Factors for Road Transport) and KTI (Institute for Transport Sciences Non-Profit Ltd.) databases, taking into account the various emission factors of vehicles (*Infras,* 2004).

3. Results and discussion

For each sample, the two most important components are quartz and soot. The amount of these components depends on the location and geometry of the sampling site (height, footing, or ledge, *Table 1*). The sample analyses suggest, that the higher proportion of soot is observed in the samples taken from Török Street (T2, T3, T5), where there is a wind-protected area. It is a narrower street, the soot particles can settle down, and the wind does not take the fine grains. The higher ratio of quartz (Mk1a, Mk5, TF1) is more likely to be linked to Margit Boulevard (*Table 3*). Here, the volume of traffic and disturbed dust are higher and probably the wind is stronger, thus it is easier to grab particles of small fraction (fly ash, soot).

Table 3. Point counting results (percentage) of particles by optical microscopy

	Quartz [%]	Fly ash [%]	Soot [%]	Carbonated parts [%]	Other [%]
Mk1a	64	10	15	6	5
Mk5	55	8	15	4	18
T2	49	5	40	2	4
T3	36	4	48	3	9
T5	43	6	37	4	10
TF1	57	7	21	2	13
T1	50	6	26	4	14

The results of the X-ray diffraction analysis are very similar, but some differences exist between the samples. The proportion of compounds is slightly different (*Table 4*). Our findings are in good agreement with the previous studies (*McAlister et al.,* 2006) that quartz particles are commonly found in the dust of Budapest. The peaks identified on XRD diffractograms (*Fig. 3*) clearly confirm the prevalence of quartz in the studied samples.

Table 4. Inorganic compounds in analyzed samples by XRD / Main mineral phases of settled dust

		Inorganic compounds/Main mineral phases (++ major element, + minor element, ~ trace element)						
	Quartz	**Dolomite**	**Calcite**	**Gypsum**	**Albite**	**Orthoclase**	**Chlorite**	**Illite**
MK1a	++	++	++		+	~	~	~
T2	++	++	+	+	+	~	~	~
T3	++	++	++		+	~	~	~
T5	++	++	+		+	~	~	~
TF1	++	++	++		+	~	~	~

Quartz: SiO_2 Albite: $NaAlSi_3O_8$
Dolomite: $CaMg(CO_3)_2$ Orthoclase: $KAlSi_3O_8$
Calcite: $CaCO_3$ Chlorit: $(Mg,Fe^{2+})_5Al(AlSi_3O_{10})(OH)_8$
Gypsum: $CaSO_4.2H_2O$ Illite: $K_{0,65}Al_{2,0}Al_{0,65}Si_{3,35}O_{10}(OH)_2$
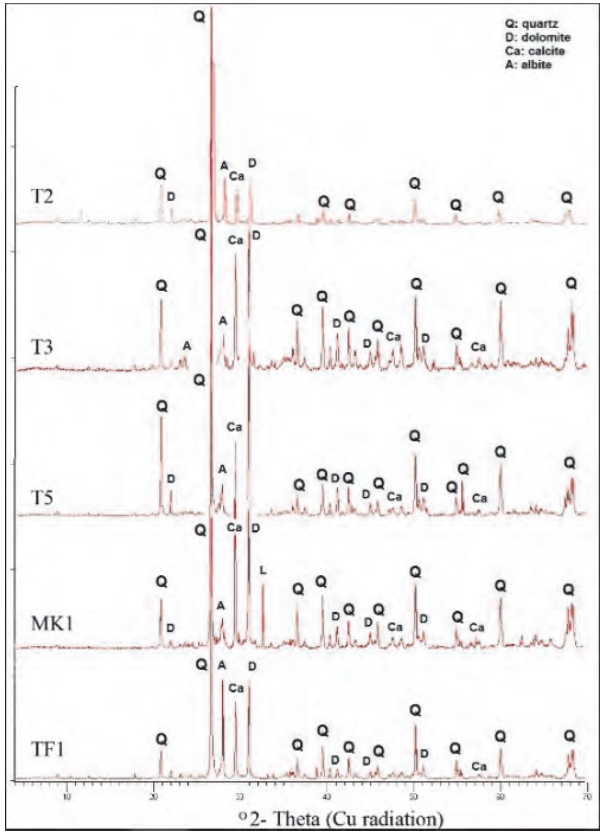
Fig. 3. X-ray diffractograms of analyzed samples.

The settled dust contains quartz, dolomite, calcite, and albite, and a small amount of gypsum is found in sample T2. Orthoclase, chlorite, and illite are present in traces. Calcite is the main mineral of the carbonate rocks, which was used in many buildings in Budapest and was found in all collected dust samples. The quartz and feldspar content can be attributed to wind-driven mineral grains (*Smith et al.,* 2003; *Török et al.,* 2011; *Farkas et al.,* 2018).

The organic compounds of dust were not analyzed, but it is known that it contains high amount of elemental and organic carbon (*Salma et al.,* 2014b*)*. The proportion and composition of these organic compounds changes with time, as it was documented by *Salma* and *Maenhaut (*2006). The changes are not restricted to urban areas but also indicative for rural ones (*Temesi et al.,* 2003*; Török et al.,* 2011).

The results of laser diffraction particle analyses are summarized in *Fig. 4*. Although the samples were taken from similar buildings, the size distribution of dust is markedly different. T2 and T3 dust samples were the finest. In these samples, more than 40% of particles are smaller than 20 μm in diameter. The statistical analyses of particle sizes show that Mk5 and T5 contains larger particles, and d_{90} values of these two samples are larger than 0.2 mm (*Table 5*). It is also clear that the samples that have the largest particles have a bimodal particle size distribution (*Fig. 4* and *Table 6*).
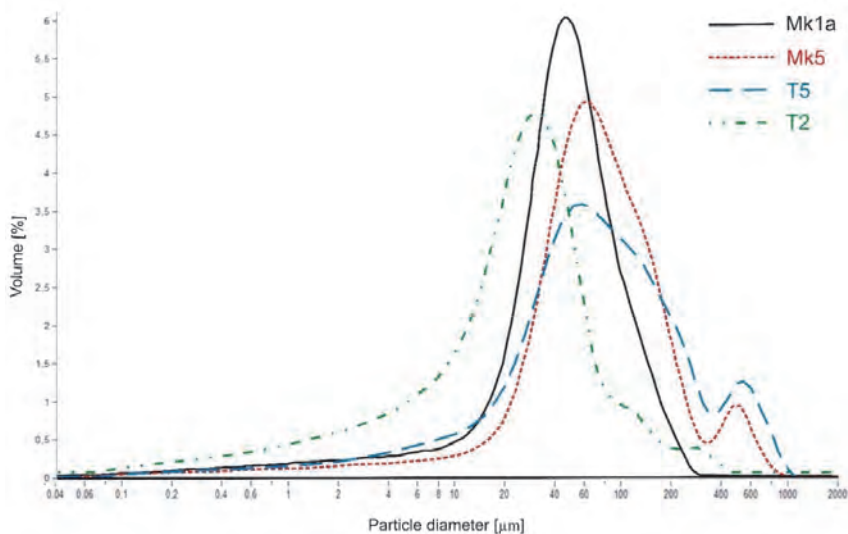
Fig. 4. Particle size distribution for four samples (Mk1a, Mk5, T5, T2) (particle diameter is shown in logarithmic scale).

Table 5. Statistic parameters for five samples (Mk1a, Mk5, T2, T3, T5) by laser diffraction particle analysis (values are given in micrometres)

	d_{mean}	d_{10}	d_{50}	d_{90}
Mk1a	60.1	13.09	49.97	119.6
Mk5	106.9	21.9	69.95	210.7
T2	34.7	2.795	23.89	68.3
T3	27.22	2.132	18.22	61.41
T5	113.1	9.137	60.77	272.8

d_{mean}: mean value
d_{10}: 10% percentile (10% of the data is smaller than this value)
d_{50}: 50% percentile (50% of the data is smaller than this value, equal to the median value)
d_{90}: 90% percentile (90% of the data is smaller than this value)

Table 6. Particle size distribution of analyzed samples (Mk1a, Mk5, T2, T3, T5), data obtained from laser diffraction particle analysis

Diameter of particles	MK1a [%]	MK5 [%]	T2 [%]	T3 [%]	T5 [%]
< 2 µm	3.79	2.62	7.95	9.51	3.75
2-6,3 µm	3.12	2.22	9.15	13.69	4.16
6,3-20 µm	6.89	4.35	25.10	30.20	9.49
20-63 µm	50.70	35.41	46.50	37.10	33.90
63-200 µm	33.90	44.40	9.50	9.30	33.50
200-630 µm	1.60	10.10	1.80	0.20	13.40
630-2000 µm	0.00	0.90	0.00	0.00	1.80

The critical locations with higher pollution concentration can be outlined with the help of the simulation dispersion of PM_{10} pollutants. The most important parameters of the model are the geometry and wind direction. Flow fields including the recirculation bubbles and street canyon vortices were identified by using a computational fluid dynamics (CFD) code (MISKAM). The use and advantages of CFD has been previously described by *Goricsán et al. (*2011) and *Leelőssy et al.* (2017). The MISKAM code was applied at 6 sites within the study area. The flow patterns and PM_{10} concentration were modeled at these sites (*Fig. 5*).
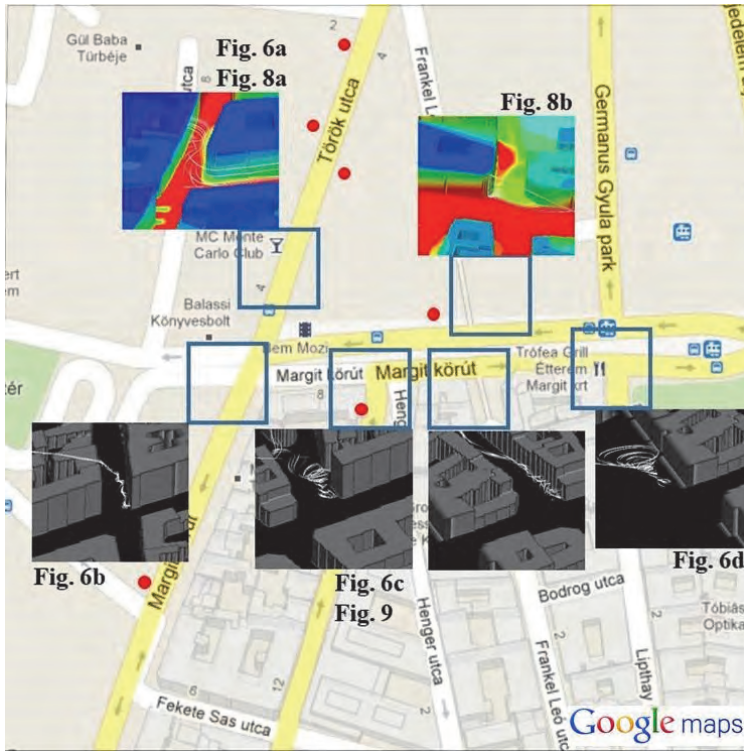
Fig. 5. Study site showing selected locations where flow patterns were detected using computational fluid dynamics (CFD) - MISKAM software.

With the help of CFD, flow patterns were observed. Recirculation in street canyon vortex, corner vortices, as well as outflow and vortex shedding were identified (*Fig. 6*). Flow patterns typical for urban canopy (*Balczó* and *Lajos*, 2015) were also observed in our simulation.

There is mounting evidence that local concentrations of air pollutants are greatly affected by the form of the city. The shape of the urban street canyon can greatly affect heat flow and wind flow patterns. Some possible interactions between wind, pollutants, and pedestrians are given in *Fig. 7.*
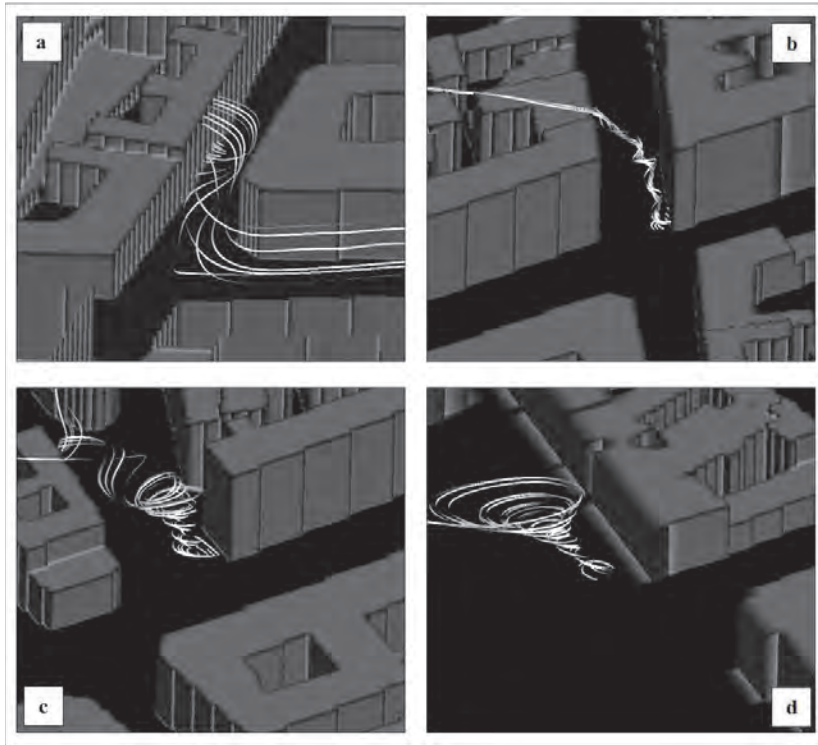
Fig. 6. Flow visualization with 3D streamlines (a. street canyon vortex, b-d. corner vortices and vortices shedding).
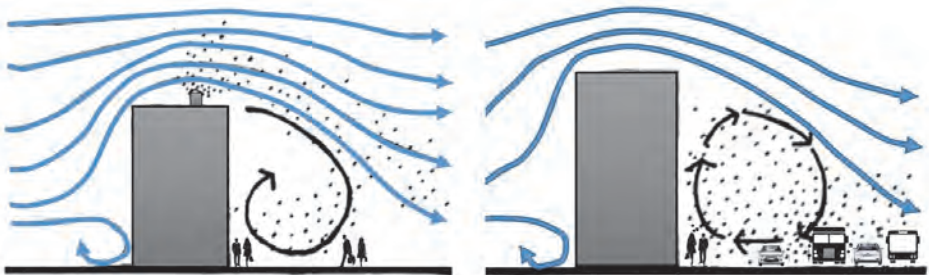
Fig. 7. The flow can sweep pollutants from above buildings or along traffic corridors into pedestrians' path (modified after *Spirn* (1986)).

Ideally a street canyon is a relatively narrow street with tall, continuous buildings on both sides of the road. Now the term street canyon is used more broadly, and the geometrical details of the street canyon can be used to set up

different categories (*Vardoulakis et al.,* 2003). In this study there were symmetric (or even) canyons, because the buildings that made the canyon had approximately the same height. When the roof level/background wind direction was perpendicular to the street, a vertically rotating wind flow was created with a centered primary vortex inside street canyons at the Török Street-Margit Boulevard corner (*Fig. 8a*).
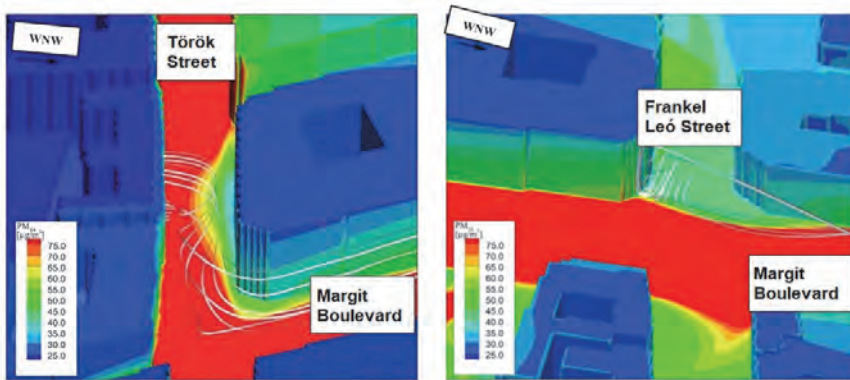
Fig. 8. Street canyon vortex (a) and outflow (b) with PM_{10} concentration values between 25–75 µg/m^3.

Outflow was identified at the intersection of Frankel Leó Street and Margit Boulevard (*Fig. 6a*). There are much lower concentrations at this side of the street (*Fig. 8b*).

Corner vortex was also identified with CFD modeling at Tölgyfa Street corner (*Fig. 6d* and (*Fig. 9*). For such vortices, a vertical axis spiral is formed at the corners of the building, where the pollution is enriched.
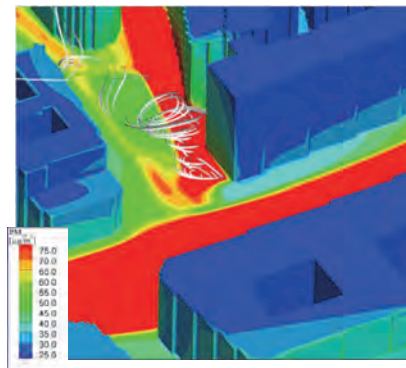
Fig. 9. Corner vortex at the corner of Tölgyfa Street and Margit Boulevard

We did not analyze the effect of climate change on wind characteristics and changes on flow patterns, but it is known that climate change will significantly influence the wind patterns in Hungary (*Péliné et al.,* 2016), and thus it is very probable, that it will also cause changes in small scale flow patterns such as street vortices.

Additional studies and a large data base with significant amount of dust samples and flow modeling would be required to make a larger scale model that would provide information on the past and present small scale flow patterns of the city center of Budapest.

4. Conclusion

The laser particle size analyses of collected dust samples indicate that there are differences in the particle-size distribution of samples. Samples characterized by larger particles often show a bimodal size distribution with particles larger than 200 µm in size.

The X-ray diffraction analyses of dust proved that from mineralogical point of view, the major constituents are quartz, dolomite, and calcite. The microscopic study revealed that besides the mineral grains, significant amount of fly ash and soot is also present in the studied samples. The composition of the samples is different, reflects the flow patterns, and also provides information on the geology of the hinterland and the substrate rock (i.e., the ashlar or wall cladding rock). The carbonate content of the dust samples taken from carbonate substrate was always higher than the dust samples taken from other substrate.

With application of MISKAM, a code CFD, taking into account the street geometries, it was possible to identify flow patterns such as recirculation in street canyon vortex, corner vortices, as well as outflow and vortex shedding.

Flow patterns were obtained from CFD. The results of transportation related PM_{10} emissions were obtained from traffic count and PM_{10} emission factors. Pollution concentration was calculated by using MISKAM. These results provide important information on the distribution and concentration of PM_{10}. The obtained trends can be used to describe the distribution of larger particles (larger than PM_{10}), too.

Street canyon vortex was identified at Török Street. Namely, the dust sample taken from one side of the street (houses with even number, sample T2) has smaller particle sizes, than the samples taken from the other side of the street (houses with odd numbers, sample T5) due to the flow pattern of the street canyon vortex. The central part of the canyon vortex has the lowest velocity, thus the smallest dust particles can also settle.

Additional studies are required to refine and extend the model and to provide an even better correlation between flow patterns, dust deposition, and particle size distribution of dust. With developing a data base, it would be possible to create a model to the entire city center.

References

Balczó, M. and *Lajos, T.,* 2015: Flow and dispersion phenomena in a simplified urban square. *Periodica Polytechnica Civil Engineering 59,* 347–360. https://doi.org/10.3311/PPci.7852

Borbély-Kiss, I., Koltay, E., Szabó, Gy., Bozó, L., and *Tar, K.,* 1999: Composition and sources of urban and rural atmospheric aerosol in Eastern Europe. *J. Aerosol Sci. 30,* 369–391. https://doi.org/10.1016/S0021-8502(98)00051-2

Borsós, T., Řimnáčová, D., Ždímal, V., Weidinger, T., Smolík, J., Wagner, Z., Burkart, J., Steiner, G., Reischl, G., Hitzenberger, R., Schwarz, J., and *Salma, I.,* 2012: Comparison of particulate number concentrations in three Central European capital cities. *Sci. Total Environ. 433,* 418–426. https://doi.org/10.1016/j.scitotenv.2012.06.052

Bozó, L., 1998: Temporal variation of the atmospheric sulfur budget over Hungary during 1980-1996. *Időjárás 102,* 141–147.

Brimblecombe, P. and *Grossi C.M.,* 2009: Millennium-long damage to building materials in London. *Sci. Total Environ. 407,* 1354–1361. https://doi.org/10.1016/j.scitotenv.2008.09.037

Dockery, W.D., Pope, C.A., Xu, X., Spengler, J.D., Ware, J.H., Fay, M.E., Ferris, B.G., and *Speizer, F.E.,* 1993: An Association between Air Pollution and Mortality in Six U.S. Cities. *New England J. Medic. 329,* 1753–1759. https://doi.org/10.1056/NEJM199312093292401

Eichhorn, J., 2008: MISKAM Manual for version 5.

Eichhorn, J. and *Kniffka, A.,* 2010: The Numerical Flow Model MISKAM: State of Development and Evaluation of the Basic Version. *Meteorol. Zeit. 19,* 81–90. https://doi.org/10.1127/0941-2948/2010/0425

Farkas, I. and *Weiszburg, T.,* 2006: Kolozs megyéből (Románia) gyűjtött ülepedő és szálló porok ásványtani vizsgálata. *Földtani Közlöny 136,* 547–572. (In Hungarian)

Farkas, O., Siegesmund, S., Licha, T., and *Török, Á.,* 2018: Geochemical and mineralogical composition of black weathering crusts on limestones from seven different European countries. *Environ. Earth Sci. 77,* 211. https://doi.org/10.1007/s12665-018-7384-8

Ferenczi, Z. and *Bozó, L.,* 2017: Effect of the long-range transport on the air quality of greater Budapest area. *Int. J. Environ. Poll. 62,* 407–416. https://doi.org/10.1504/IJEP.2017.089428

Gieré, R. and *Querol, X.,* 2010: Solid particulate matter in the atmosphere. *Elements 6,* 215–222. https://doi.org/10.2113/gselements.6.4.215

Goricsán, I., Balczó, M., Czáder, K., Rákai, A., and *Tonkó, C.,* 2011: Simulation of flow in an idealised city using various CFD codes. *Int. J. Environ. Poll. 44,* 359–367. https://doi.org/10.1504/IJEP.2011.038437

Grobéty, B., Gieré, R., Dietze, V., and *Stille, P.,* 2010: Airborne Particles in the Urban Environment. *Elements, 6,* 229–234.

Havasi, Á., Bozó, L., and *Zlatev, Z.,* 2001: Model simulation on the transboundary contribution to the atmospheric sulfur concentration and deposition in Hungary. *Időjárás 105,* 135–144.

Heaney, P.J. and *Banfield, J.A.,* 1993: Structure and chemistry of silica, metal oxides, and phosphates. In: (eds. *Guthrie, G.D., Mossman, B.T.,*) Reviews in Mineralogy, Vol. 28, Health Effects of Mineral Dusts, Chelsea, MI, Book Crafters, 185–233. https://doi.org/10.1515/9781501509711-008

Hildemann, L.M., Klinedinst, D.B., Klouda, G.A., Currie, L.A., and *Cass, G.R.,* 1994: Sources of Urban Contemporary Carbon Aerosol. Environ. Sci. Technol. 28, 1565–1576. https://doi.org/10.1021/es00058a006

Infras, 2004: Handbook of Emission Factors for Road Transport (HBEFA) version 2.1.

Jones, R.M., 2003: Particle size analysis by laser diffraction: ISO 13320, standard operating procedures, and Mie theory. *Amer. Laborat. 35,* 44–47.

Kukkonen, J., Bozó, L., Palmgren, F., and Sokhi, R.S., 2003: Particulate Matter in Urban Air. In (ed.: *Moussiopoulos, N.*) Air Quality in Cities. Berlin; Heidelberg; New York: Springer-Verlag, 2003. 92–120. https://doi.org/10.1007/978-3-662-05217-4_6

Leelőssy, Á., Molnár, F., Izsák, F., Havasi, Á., Mészáros, R., and Lagzi, I., 2014: Dispersion modelling of air pollutants: a review. *Centr. Europ. J. Geosci. 6,* 257–278.

Leelőssy Á., Lagzi I., and Mészáros R., 2017: Spatial and temporal pattern of pollutants dispersed in the atmosphere from the Budapest Chemical Works industrial site. *Időjárás 121,* 101–115.

Lippman, M., Ito, K., Nádas, A., and Burnett, R.T., 2000: Association of particulate matter components with daily mortality and morbidity in urban pollutions. Research Report 95. Health Effects Institute, Cambridge, USA.

McAlister, J.J., Smith, B.J., and Török, Á., 2006: Element partitioning and potential mobility within surface dusts on buildings in a polluted urban environment, Budapest. *Atmos. Environ. 40,* 6780–6790. https://doi.org/10.1016/j.atmosenv.2006.05.071

Péliné Németh, Cs., Bartholy, J., Pongrácz, R., and Radics, K., 2016: Analysis of climate change influences on the wind characteristics in Hungary. *Időjárás 120,* 53–71.

Pope, C.A., Burnett, R.T., Thun, M.J., Calle, E.E., Krewski, D., Ito, K., and Thurston, G.D., 2002: Lung cancer, cardiopulmonary mortality, and long-term exposure to fine particulate air pollution. *JAMA 287,* 1132–1141. https://doi.org/10.1001/jama.287.9.1132

Pósfai, M. and Buseck, P.R., 2010: Nature and climate effects of individual tropospheric aerosol particles. *Ann. Rev. Earth Planet. Sci. 38,* 17–43.
https://doi.org/10.1146/annurev.earth.031208.100032

Probáld, F., 2014: The urban climate of Budapest: past, present and future. *Hungarian Geograph. Bull. 63,* 69–79.

Querol, X., Alastuey, A., Ruiz, C.R., Artiňano, B., Hansson, H.C., Harrison, R.M., Buringh, E., ten Brink, H.M., Lutz, M., Bruckmann, P., Straehl, P., and Schneider, J., 2004: Speciation and origin of PM_{10} and $PM_{2.5}$ in selected European cities. *Atmos. Environ. 38,* 6547–6555.
https://doi.org/10.1016/j.atmosenv.2004.08.037

Reichhardt, T., 1995: Weighing the health risk of airborne particulates. *Environ. Sci. Technol. 29,* 360–364. https://doi.org/10.1021/es00008a744

Rodriguez-Navarro, C. and Sebastian, E., 1996: Role of particulate matter from vehicle exhaust on porous building stones (limestone) sulfation. *Sci. Total Environ.187,* 79–91.
https://doi.org/10.1016/0048-9697(96)05124-8

Salma, I., Maenhaut, W., Weidinger, T., and Pinto, J., 2004a: Temporal variation of secondary organic aerosol in downtown Budapest. *J. Aerosol Sci. 35S1,* 153–154.

Salma, I., Chi, X., and Maenhaut, W., 2004b: Elemental and organic carbon in urban canyon and background environments in Budapest, Hungary. *Atmospheric Environment 38,* 27–36.

Salma, I. and Maenhaut, W., 2006: Changes in elemental composition and mass of atmospheric aerosol pollution between 1996 and 2002 in a Central European city. *Environ. Pollut. 143,* 479–488.
https://doi.org/10.1016/j.envpol.2005.11.042

Salma, I., Németh, Z., Weidinger, T., Maenhaut, W., Claeys, M., Molnár, M., Major, I., Ajtai, T., Utry, N., and Bozóki, Z., 2017: Source apportionment of carbonaceous chemical species to fossil fuel combustion, biomass burning and biogenic emissions by a coupled radiocarbon–levoglucosan marker method. *Atmos. Chemist. Physics 17,* 13767–13781.
https://doi.org/10.5194/acp-17-13767-2017

Samet, J.M., Dominici, F., Curriero, F.C., Coursac, I., and Zeger, S.L., 2000: Fine particulate air pollution and mortality in 20 U. S. cities, 1987-1994. *New England J. Medic. 343,* 1742–1749.
https://doi.org/10.1056/NEJM200012143432401

Smith, B.J., Török, Á., McAlister, J.J., and Megarry, Y., 2003: Observations on the factors influencing stability of building stones following contour scaling: a case study of oolitic limestones from Budapest, Hungary. *Build. Environ. 38,* 1173–1183.
https://doi.org/10.1016/S0360-1323(03)00076-3

Spirn, A.W., 1986: Air Quality at the Street-Level: Strategies for Urban Design. Prepared for: Boston Redevelopment Authority.

Temesi, D., Molnár, A., Mészáros, E., and *Feczkó, T.,* 2003: Seasonal and diurnal variation in the size distribution of fine carbonaceous particles over rural Hungary. *Atmos. Environ. 37,* 139–146. https://doi.org/10.1016/S1352-2310(02)00773-2

Török, Á., Licha, T., Simon, K., and *Siegesmund, S.,* 2011: Urban and rural limestone weathering; the contribution of dust to black crust formation. *Environ. Earth Sci. 63*, 675–693. https://doi.org/10.1007/s12665-010-0737-6

Vardoulakis, S., Fischer, B.E.A., Pericleous, K., and *Gonzalez-Flesca, N.,* 2003: Modelling air quality in street canyons: a review. *Atmos. Environ. 37,* 155–182. https://doi.org/10.1016/S1352-2310(02)00857-9

Wichmann, H.E., Spix, C., Tuch, T., Woelke, G., Peters, A., Heinrich, J., Kreyling, W.G., and *Heyder, J.*, 2000: Daily mortality and fine and ultrafine particles in Erfurt, Germany. Part I: Role of particle number and particle mass. Health Effects Institute Research Report 98, Cambridge, USA.

IDŐJÁRÁS

Thermal conditions in the summer season on the Polish coast of the Baltic Sea in 1966–2015

Arkadiusz M. Tomczyk[1*], **Sebastian Kendzierski**[1], **Magdalena Kugiejko**[2], and **Natalia Pilguj**[3]

[1]*Department of Climatology, Adam Mickiewicz University in Poznań,
B. Krygowskiego 10, 61-680 Poznań, Poland*

[2]*Department of Tourism and Recreation, Adam Mickiewicz University in Poznań,
B. Krygowskiego 10, 61-680 Poznań, Poland*

[3]*Department of Climatology and Atmosphere Protection,
University of Wroclaw,
A. Kosiby 8, 51-621 Wrocław, Poland*

* Corresponding author E-mail: atomczyk@amu.edu.pl

Abstract—The Baltic Sea coast is characterized by a large frequency of days with biometeorologically adverse effects. In many Polish and foreign studies there are issues related to the increase in the frequency of warm days, hot days, and heat waves. The present study introduces the characteristics of thermal conditions on the Polish coast in the 1966–2015 multiyear period, as well as the identification of circulation conditions favoring the occurrence of extremely warm periods. The analysis included the maximum temperature data (obtained from five measurement stations), on the basis of which the characteristics such as: average maximum air temperature, sum of maximum air temperatures occurring in summer, warm days (T_{max} >25 °C), hot days and heat waves (T_{max} >30 °C) were determined. The existing thermal classification proposed by *Lorenc* (2000) was also used in relation to the maximum daily temperature. In addition, there appeared a topic of atmospheric circulation regarding the determination of conditions for the occurrence of exceptionally warm months (mean T_{max} >T_s+1.5σ). The research results indicate an increase in the average maximum temperature (T_{max}) in the summer season in 1966–2015. The changes are particularly visible in the western part of the research area (0.43 °C/10 years). Furthermore, the observed warming was translated into a higher occurrence of warm and hot days, which was discussed by other authors in the context of the whole of Poland. The occurrence of exceptionally warm months has reached the maximum frequency in the last 15 years, which is associated with positive anomalies of the sea level pressure and the 500 hPa isobaric surface. Periods of occurrence of the above mentioned anomalies were related to the presence of high pressure systems and the advection of air masses from the eastern sector (according to the presented T850 maps).

Key-words: air temperature, atmospheric circulation, summer season, climate change, Baltic Sea

1. Introduction

According to the bioclimatic regionalization of Poland, the Baltic Sea coast is classified as a coastal region and is considered the strongest stimulus (*Kozłowska-Szczęsna et al.,* 1997). The coastal bioclimate stands out from other climates due to the predominance of climatic stimuli associated with the greater impact of the cooling air value due to the combined effect of low temperature, higher wind speed and air humidity (*Kolendowicz et al.,* 2018). In this region, about 40% of days a year are considered burdensome in terms of biometeorological conditions (*Kozłowska-Szczęsna et al*., 2002).

The climate change observed today, manifesting itself, among others, through the increase in air temperature (*IPCC,* 2013) is of particular importance in regions that are heavily used for tourism. In Poland, the seasonality of tourist traffic is conditioned mainly by the climate and weather changes during the year (*Stasiak*, 2011; *Koźmiński* and *Michalska*, 2016a). According to *Krzyżewska* (2010), extreme weather phenomena cause not only a decrease in profits from tourism, but also pose a threat to human life and health. This has been particularly important in the last decades, in which an increase in the frequency of hot days and heat waves is observed (*Sulikowska et al.,* 2016; *Tomczyk* and *Bendorz,* 2016; *Tomczyk* and *Sulikowska,* 2017), which results in a significant increase in the number of deaths caused by biometeorological conditions affecting human body systems (*Kuchcik,* 2001; *Paldy* and *Bobvos,* 2009; *Bobvos et al.,* 2015; *Revich et al.,* 2015). The progressive climate warming will also have a positive impact by extending the summer tourist season mitigating the seasonality phenomenon and, consequently, also the environmental nuisance (*Koźmiński* and *Michalska*, 2016a).

Tourism plays a special role in the socio-economic development of coastal towns, where services related to the organization and operation of tourism are the main sources of income (*Jażewicz* and *Rydz*, 2001; *Matczak* and *Rydz,* 2001; *Schwichtenberg,* 2006; *Jażewicz,* 2011; *Parzych,* 2011). Taking into account the Schneider's index (*Warszyńska,* 1985*; Szromek,* 2012), it follows that for 2016, its highest values were reached by voivodships located in the northern part of the country *(Central Statistical Office Report,* 2017). Comparing the data from 2004 and 2014, the sustainable development of the tourist function was confirmed in the following voivodeships: the Pomeranian, West Pomeranian, and Warmian-Masurian (*Koźmiński* and *Michalska,* 2016b).

Bearing in mind the increase in the intensity of tourist traffic in northern Poland, it is reasonable to analyze the thermal conditions and their changes. In connection with the above, the following objectives were adopted:

1) characteristics of thermal conditions on the Polish coast of the Baltic Sea in 1966–2015;

2) characteristics of circulation conditions for the occurrence of exceptionally warm months in 1966–2015.

2. Data and methods

The article uses the daily values of maximum air temperature (T_{max}) from 1966 to 2015 for five stations located on the Polish coast of the Baltic Sea (*Fig. 1*). The data was obtained from the resources of the Institute of Meteorology and Water Management - National Research Institute.
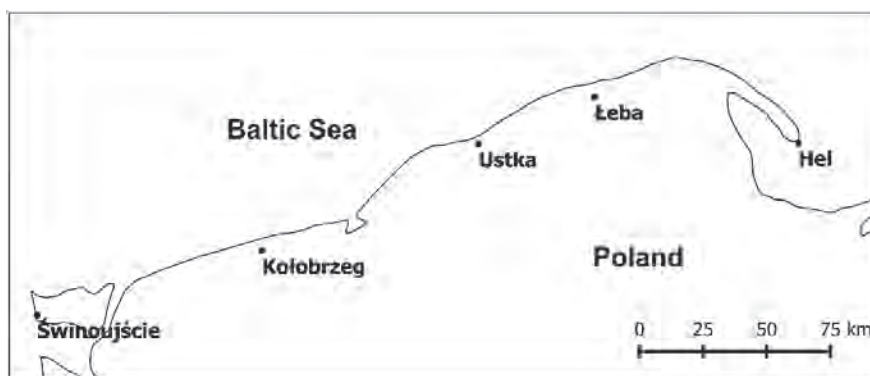
Fig. 1. Locations of the meteorological stations.
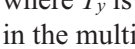
Based on the collected data, the basic characteristics were calculated, i.e., the average maximum air temperature in the summer seasons (June-August), as well as the warm (T_{max} >25 °C) and hot days (T_{max} >30 °C) and heat waves were determined. Heat wave was defined as a sequence of at least 3 hot days. In addition, a thermal classification proposed by *Lorenc* (1994) was carried out for months and seasons.

The Lorenc classification is determined by classical measures based on a standardized deviation from the average air temperature. The original Lorenc classification (1994) was based on a 9-class assessment of the average annual air temperature. Then it was extended to 11 classes (*Lorenc* and *Suwalska-Bogucka,* 1996; *Lorenc,* 2000) and applied to assessment of thermal conditions shorter than one year. The assumptions of this method were used in the classification of average values of monthly, annual, and seasonal air temperatures used in the Institute of Meteorology and Water Management - National Research Institute. Despite the existence of other methods for determining thermal classification and the fact that this method has advantages and disadvantages (*Czernecki* and *Miętus,* 2011), it was used for the purposes of this article because it is applicable when determining the results for the average maximum air temperature. For the period 1966–2015, individual thermal periods were defined, with distinction between

monthly and seasonal values, for the reference period 1971–2000. Detailed criteria for determining periods and their names are presented in *Table 1*.

Table 1. Thermal classification of months, seasons and years according to *Lorenc* (2000)

Color	Class number	Name of the period	Threshold values for air temperature
	1	extremely warm	$T_y > T_{avg} + 2.5\sigma$
	2	anomaly warm	$T_{avg} + 2.0\sigma < T_y \leq T_{avg} + 2.5\sigma$
	3	very warm	$T_{avg} + 1.5\sigma < T_y \leq T_{avg} + 2.0\sigma$
	4	warm	$T_{avg} + 1.0\sigma < T_y \leq T_{avg} + 1.5\sigma$
	5	slightly warm	$T_{avg} + 0.5\sigma < T_y \leq T_{avg} + 1.0\sigma$
	6	normal	$T_{avg} + 0.5\sigma \leq T_y \leq T_{avg} + 0.5\sigma$
	7	slightly cool (slightly frosty)	$T_{avg} - 1.0\sigma \leq T_y < T_{avg} - 0.5\sigma$
	8	cool (frosty)	$T_{avg} - 1.5\sigma \leq T_y < T_{avg} - 1.0\sigma$
	9	very cool (frosty)	$T_{avg} - 2.0\sigma \leq T_y < T_{avg} - 1.5\sigma$
	10	anomaly cold (cold)	$T_{avg} - 2.5\sigma \leq T_y < T_{avg} - 2.0\sigma$
	11	extremely cold (frosty)	$T_y < T_{avg} - 2.5\sigma$

where T_y is the average annual air temperature, T_{avg} is the average air temperature in the multiyear period 1971–2000, and σ is the standard deviation.

In addition, the circulation conditions for the occurrence of exceptionally warm months, i.e., months with an average $T_{max} > T_s + 1.5\sigma$, were analyzed. According to the Lorenc thermal classification, exceptionally warm months included very warm, anomalously warm, and extremely warm months. In order to determine the pressure conditions, the daily values of atmospheric pressure at sea level *(SLP)*, the height of the 500 hPa isobaric surface (*z500* hPa) and the air temperature at the 850 hPa isobaric surface (*T850*) were used. Data was obtained from the National Center for Environmental Prediction/National Center for Atmospheric Research (NCEP/NCAR) reanalysis (*Kalnay et al.,* 1996), which are available in the archives of the NOAA ESRL PSD (Earth System Research Laboratory Physical Science Division). On the basis of the aforementioned data, there were averaged maps drawn up for the sea level pressure, together with maps of height of 500 hPa isobaric surface and temperature at the 850 hPa isobaric surface, as well as maps of anomalies. Anomalies were calculated as the difference between average values of individual parameters of selected months and average values for those months from the entire multiyear period. In addition, the Großwetterlage circulation calendar was used to characterize the atmospheric circulation.

3. Results

3.1. Average T_{max} in summer

The average maximum air temperature in the summer season on the Polish coast of the Baltic Sea in the years 1966–2015 ranged from 20.1 °C in Łeba and Ustka to 21.1 in Świnoujście. The lowest average summer T_{max} ranged from 18.0 °C in Łeba to 19.2 °C in Świnoujście. The coldest seasons were primarily in the first half of the analyzed multiyear period and took place in 1974, 1987, and also in 1993 (*Fig. 2*). In turn, the highest average T_{max} ranged from 22.2 °C in Łeba, Ustka and Kołobrzeg, to 23.6 °C in Świnoujście. The warmest seasons were in 1992, 2002 and 2006. The course of the average T_{max} in the analyzed years showed its considerable year-to year fluctuations. In the prevailing area, the variability of the mean T_{max} was similar, as evidenced by the low variation in the standard deviation values falling within the range of 0.9–1.0. The analyses showed a statistically significant increase in T_{max}, ranging from 0.20 °C/10 years (Hel) to 0.43 °C/10 years (Świnoujście). T_{max} changes in the first decade of the 21st century had a significant impact on the increase, when T_{max} generally exceeded the standard from the years 1966–2015.

In June, the average T_{max} ranged from 18.2 °C in Ustka to 19.5 °C in Świnoujście. In all stations an increase in T_{max} was observed, which was from 0.01 °C/10 years in Hel to 0.32 °C/10 years in Świnoujście, and only at this station the changes were statistically significant. In July, the average Tmax changed from 20.9 °C in Łeba to 21.9 °C in Świnoujście. In each station there was a statistically significant increase in T_{max} and it changed from 0.30 °C/10 years in Hel to 0.52 °C/10 years in Świnoujście. In turn, in August the average T_{max} ranged from 21.0 °C in Łeba to 21.1 in Świnoujście. Apart from Hel, T_{max} changes were statistically significant, ranging from 0.21 °C/10 years in Hel to 0.46 °C/10 years in Świnoujście.
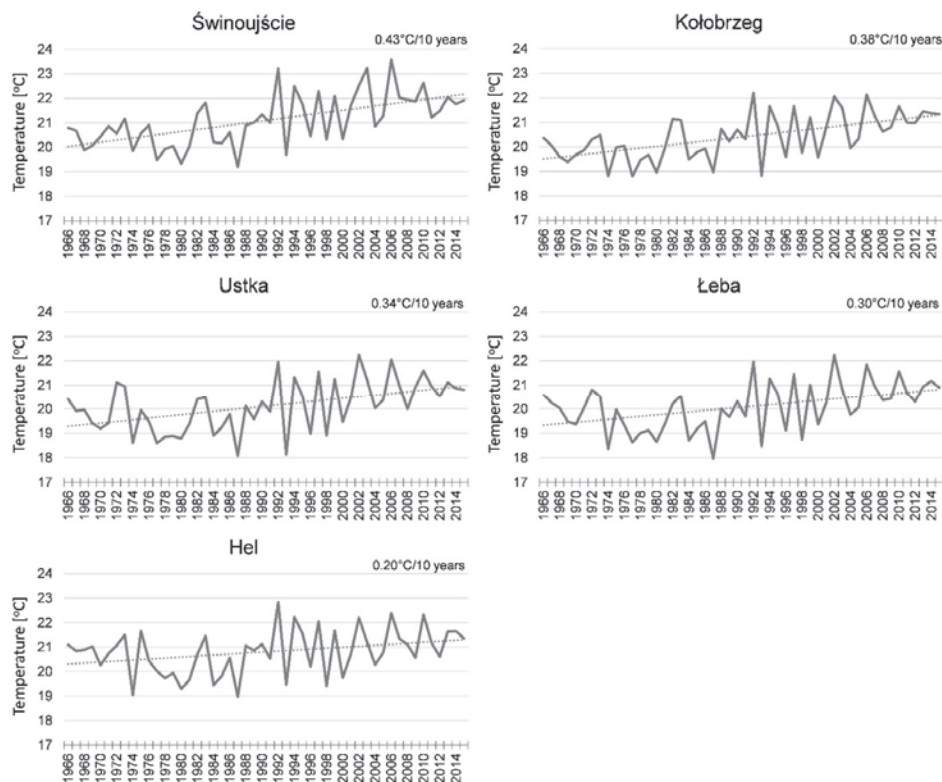
Fig. 2. Mean summer T_{max} values with trend line.

3.2. Characteristic days and heat waves

The total number of warm days (T_{max} >25 °C) in the analyzed multiyear period fluctuated from 455 in Łeba to 560 in Świnoujście, which gives an average of 9.1 and 11.2 days, respectively, in the season. The smallest number of warm days in the season ranged from 0 in Ustka to 3 in Świnoujście and was recorded mainly in 1977 (*Fig. 3*). The exception was the station in Hel, where the smallest number was recorded in 2008. In addition, in Świnoujście, the same number of warm days as in 1977 was found in 1968. In turn, the highest number of warm days, apart from the station in Łeba (2002), occurred in 2006. At the individual stations, the highest number of warm days ranged from 20 in Łeba and Kołobrzeg to 29 in Świnoujście. In the analyzed multiyear period, an increase in the number of warm days was observed, which ranged from 0.5 days/10 years in Łeba to 1.2 days/10 years in Świnoujście. Statistically significant changes were recorded in Ustka, Kołobrzeg, and Świnoujście.

The total number of hot days (T_{max} >30 °C) changed from 22 in Hel to 113 in Świnoujście. More than 100 days were also recorded in Ustka and Kołobrzeg. At each station, seasons without hot days were recorded and they occurred mainly in the first half of the analyzed multiyear. The maximum number of hot days in the season ranged from 5 in Hel to 9 in Kołobrzeg and Świnoujście. The days of the above category were most frequently recorded in the summer of 1992, 1994 and 2010 (*Fig. 3*). Hot days were most often recorded in July, and their share fluctuated from 42% in Świnoujście to 72% in Hel. In all stations there was an increase in the number of hot days, although statistically significant changes were found only in Świnoujście (0.6 days/10 years).

From among the hot days, heat waves were separated into sequences of at least 3 hot days. In the analyzed multiyear period, the smallest number of waves occurred in Hel, only 1, while the largest number was found in Świnoujście – 4 waves. The heat wave that occurred at the same time at all stations was the wave of the first half of July 2010. The longest wave occurred in Świnoujście and lasted 5 days, from July 9 to 13, 2010.
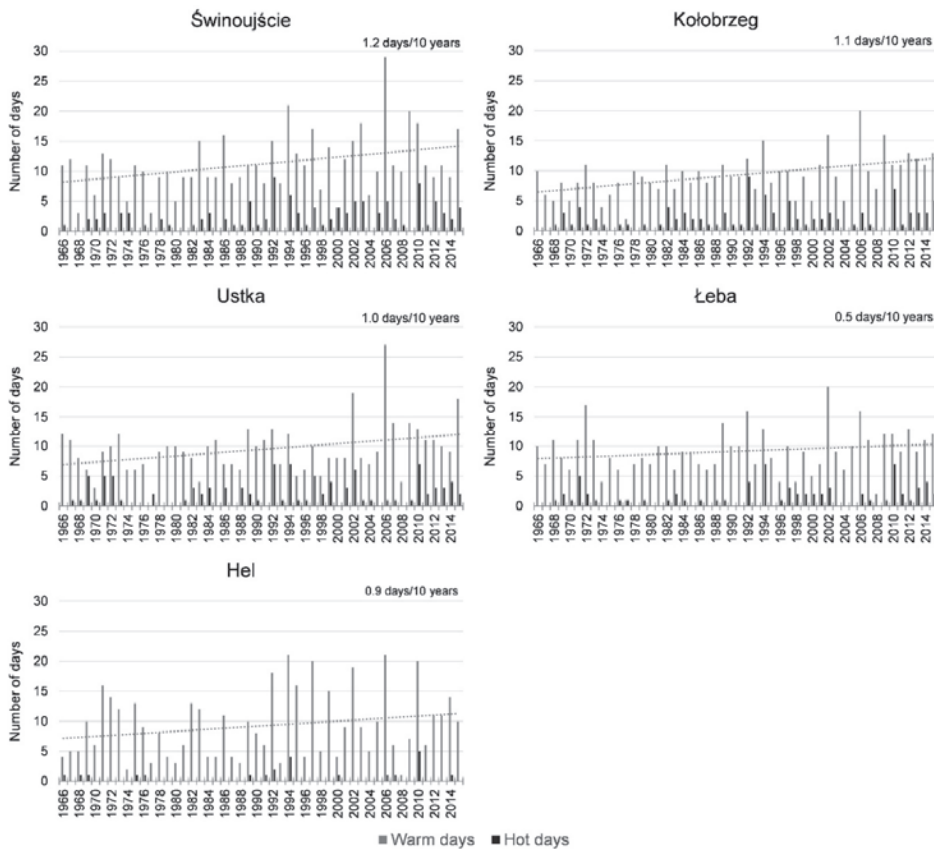
Fig. 3. Multiyear series of the annual number of warm and hot days with the trend line (warm days)

3.3. Thermal classification

For the daily maximum air temperature in 1966–2015, thermal classification of the summer months and the season was made (*Table 2*). Colder and warmer decades can be clearly distinguished. The period of 1966–1971 was characterized by the occurrence of lower temperatures, especially in the western part of the discussed area. 1974 turned out to be exceptionally cold, when the anomalously cold and extremely cold months occurred. In the years 1977–1981, the occurrence of temperatures below the normal range (cold, very cold) was again noticeable. However, during this period, June was different – at all stations the month was usually described as normal. The next colder period was 1984–1987. Then from the 90s, there were no colder subsequent years observed. The year 1993 was extremely cold, when the summer period was classified as very cold and anomalously cold. The years 1995–2001 were characterized by rapid changes in temperature; there were months both extremely warm (1997) and anomalously cold (1998). The first decade and the middle of the second decade of the 21st century were marked as normal and slightly warm. At that time there were months both extremely warm and anomalously warm (July 2006), anomalously warm and very warm (July 2010) as well as cold and very cold (June 2009). Considering the entire period under consideration, the occurrence of maximum temperatures classified as colder than the standard is noted int he period 1966–1990, and warmer months than the standard occured in the years 1992–2015. There is also a spatial differentiation of the classification distribution in the years 1966–1971 for warmer eastern stations and colder western ones.

Table 2. Thermal classification according to *Lorenc* (2000)

Year	Świnoujście				Kołobrzeg				Ustka				Łeba				Hel			
	VI	VII	VIII	JJA	VI	VII	VIII	JJA	VI	VII	VIII	JJA	VI	VII	VIII	JJA	VI	VII	VIII	JJA
1966	4	8	8	7	3	7	8	6	3	7	7	6	2	6	7	6	4	6	7	6
1967	8	6	7	7	8	6	7	7	8	6	6	7	7	6	6	6	7	6	6	6
1968	6	9	9	9	5	9	8	8	4	8	7	6	4	8	6	6	4	8	6	6
1969	10	6	9	8	10	6	9	9	9	6	8	7	9	5	8	7	6	6	6	6
1970	6	7	8	8	6	7	8	8	7	7	8	8	7	7	7	7	6	8	7	7
1971	9	6	6	7	9	7	6	8	11	7	5	7	9	6	4	6	8	6	5	6
1972	7	6	8	7	6	6	7	7	4	5	6	5	5	5	6	6	6	5	7	6
1973	6	6	6	6	6	6	6	6	5	6	6	6	6	6	6	6	5	6	6	6
1974	10	8	6	9	11	8	6	10	10	8	6	9	10	9	6	9	10	9	6	10
1975	11	6	6	7	10	6	5	7	9	6	5	6	10	6	5	6	7	5	4	5
1976	6	6	8	7	6	6	7	7	8	6	7	7	8	6	7	8	7	6	7	7
1977	6	9	10	10	6	9	10	10	6	9	9	9	6	9	9	9	5	8	8	8

Table 2. Continue

Year	Świnoujście				Kołobrzeg				Ustka				Łeba				Hel			
	VI	VII	VIII	JJA	VI	VII	VIII	JJA	VI	VII	VIII	JJA	VI	VII	VIII	JJA	VI	VII	VIII	JJA
1978	6	9	8	9	6	9	8	8	7	8	8	9	6	8	8	8	6	8	8	8
1979	5	10	7	8	3	10	7	8	4	11	7	8	3	10	8	8	3	10	8	8
1980	7	9	9	10	7	8	9	10	6	8	8	9	6	8	8	9	7	9	8	9
1981	7	7	9	8	6	7	8	7	6	7	8	8	6	7	8	7	7	8	8	8
1982	6	6	6	6	6	6	5	6	6	6	6	6	7	6	6	6	8	6	6	6
1983	6	6	6	6	6	6	6	6	6	6	6	6	6	6	6	6	6	5	6	6
1984	9	8	6	8	9	8	6	8	10	8	6	8	10	9	6	9	10	8	6	9
1985	10	6	7	8	9	6	6	8	8	7	7	8	9	6	7	8	9	7	7	8
1986	8	6	8	7	8	6	7	7	6	6	7	7	7	6	7	7	6	6	7	7
1987	8	8	10	10	8	7	9	10	8	8	9	10	8	9	9	10	8	8	10	10
1988	7	6	7	7	7	5	6	6	7	5	7	6	6	6	7	6	6	6	6	6
1989	6	6	7	7	6	6	7	7	7	6	7	7	7	6	7	7	6	6	7	6
1990	6	7	6	6	5	8	6	6	4	8	6	6	4	8	6	6	5	7	6	6
1991	8	6	6	7	7	6	6	7	8	6	6	7	8	6	6	7	9	6	6	7
1992	4	4	4	3	4	5	4	3	4	5	4	4	3	5	5	3	2	5	5	3
1993	8	8	9	9	8	8	9	10	9	8	9	10	8	8	8	9	7	8	9	9
1994	6	4	6	5	6	4	6	5	6	3	6	5	6	3	6	5	7	2	5	4
1995	8	5	5	6	8	5	6	6	7	6	6	6	6	6	6	6	6	6	5	5
1996	7	8	6	8	7	9	6	8	8	9	6	8	7	9	6	8	6	8	6	7
1997	6	7	1	5	5	7	1	5	5	7	2	4	5	6	3	4	6	6	2	4
1998	6	8	9	8	5	7	9	8	6	8	9	8	6	8	10	9	6	8	10	9
1999	5	5	6	5	5	5	7	6	4	5	6	5	5	5	6	5	5	5	6	5
2000	5	10	7	8	4	10	8	8	5	8	7	7	5	9	7	7	6	9	7	8
2001	8	5	5	6	9	5	5	6	8	5	6	6	9	5	6	6	9	5	6	6
2002	4	6	4	5	4	6	4	4	4	6	3	3	5	5	2	3	6	6	2	4
2003	2	5	5	3	4	6	6	5	4	6	6	5	5	6	6	6	5	6	6	6
2004	7	7	6	7	7	8	6	7	7	7	5	6	7	8	5	7	7	8	5	7
2005	6	6	8	6	6	6	8	7	6	6	7	6	7	5	7	6	7	5	7	6
2006	3	1	6	3	4	2	7	3	4	1	7	4	5	2	6	4	5	2	6	4
2007	4	6	6	6	3	6	6	5	5	6	6	6	3	7	6	5	3	7	6	6
2008	5	6	6	6	6	6	6	6	6	6	6	6	5	6	6	6	5	6	6	6
2009	8	5	4	6	9	5	5	6	8	5	5	6	9	5	5	6	9	6	6	7
2010	6	2	6	4	7	3	6	5	6	3	6	4	6	3	5	4	6	3	5	4
2011	5	8	6	6	4	7	6	6	4	6	6	6	4	6	6	6	4	6	6	6
2012	6	6	6	6	6	6	6	6	6	6	6	6	6	6	6	6	7	6	6	6
2013	6	6	5	6	5	6	5	5	5	6	5	5	5	6	6	5	4	6	6	5
2014	6	6	6	6	6	4	6	5	6	5	6	6	6	4	6	5	6	4	6	5
2015	7	6	4	6	6	6	3	5	7	6	3	6	7	6	3	6	6	6	4	6

3.4. *Very warm months and their circulation conditions*

In the analyzed multiyear period, the total number of exceptionally warm months ranged from 5 in Świnoujście to 9 in Łeba. Most of these months occurred in the last 15 years. The number of Junes classified as exceptionally warm months ranged from 1 in Ustka to 3 in Hel, Łeba, and Kołobrzeg. Among the months that were classified at more than one station, Junes of 1966, 1979, 1992, and 2007 should be mentioned. In addition, June of 2003 and 2006 were also classified at one station. The situation was different in the case of July, because no exceptionally warm month was found at any stations. At two stations (Kołobrzeg, Świnoujście), two exceptionally warm months were recorded, while there were three warm mounths at the other stations. It was July of 1994, 2006, and 2010. In turn, the number of Augusts classified as exceptionally warm months changed from 1 in Świnoujście to 3 in Łeba and Ustka. These months occurred in 1997, 2002, and 2015.

The occurrence of exceptionally warm months in June was connected with a ridge of high pressure lying across Europe, within which a local high-pressure area was formed with its centre over the Baltic Sea (>1015 hPa) (*Fig. 4*). Over Central and Northern Europe, the *SLP* was higher than the average in June in the analyzed multiyear period, and in the center of the system it was >2 hPa. The *SLP* anomalies over northern Poland ranged from 0 to >1.5 hPa. Contour lines of isobaric surface 500 hPa over Central Europe bent northward creating its clear elevation, and that indicates the presence of warm air masses on the analyzed days. The majority of the continent was within the range of the *z500* positive anomalies. Over the research area, it settled 30–40 m higher. This system generated the advection of warm and continental air masses from the southeast sector. The settling air masses were much warmer than the average in June, as indicated by the positive *T850* anomalies, whose center (>2 ºC) stretched from southern Poland to the Norwegian Sea. According to the Großwetterlage circulation calendar, the HNFZ (Norwegian Sea/Fennoscandia High), BM (Central European Ridge), and HB (British Isles High) types were recorded much more frequently than the average in the analyzed months.

Fig. 4. Mean *SLP* (color scale) and *z500* (dashed line) (a), SLP (color scale) and *z500* (dashed line) anomalies (b), and *T850* anomalies (color scale) (c) for the exceptionally warm months in June.

Similar pressure conditions caused exceptionally warm months in July. As in the case of June over Europe, there was a high-pressure ridge with a local high pressure area over the Baltic Sea (>1018 hPa) (*Fig. 5*). At the time the *SLP* over the major part of the continent was higher than the average in July, maximum >5 hPa. Over northern Poland, the anomalies ranged from 3.5 to 4.5 hPa. Contour lines of isobaric surface 500 hPa over Central Europe bent north-eastward creating its clear elevation, and that indicates the presence of warm air masses in the analyzed months. Over the research area the *z500* values settled higher than the average in July by about 100 m. The described situation provided the inflow of air masses from the south-east, much warmer than the average, as evidenced by the *T850* anomalies, which over northern Germany was >3.5 °C. According to the Großwetterlage circulation calendar, in the analyzed months, BM (Central European Ridge), TRW (Western Europe Trough), and HB (British Isles High) types were observed much more frequently than the average.

Fig. 5. Mean *SLP* (color scale) and *z500* (dashed line) (a), *SLP* (color scale) and *z500* (dashed line) anomalies (b), and *T850* anomalies (color scale) (c) for the exceptionally warm months in July.

The occurrence of exceptionally warm months in August was connected with a ridge of high pressure lying across Europe, within which an extensive high-pressure area was formed with its centre over Estonia and the Gulf of Finland (>1019 hPa) (*Fig. 6*). In the center of the system, the *SLP* was higher than the average in August by >6 hPa, and over northern Poland by 1.5–3.5 hPa. As in previous months, the contour lines of isobaric surface 500 hPa bent northward. Over the research area, it settled higher than the average by 70–85 m. This system caused the advection of air masses from the eastern and southeastern sectors. Much warmer air masses than the average in August covered the central and northern part of the continent. Over the northern part of Poland, *T850* anomalies were approximately 3 °C. According to the Großwetterlage circulation calendar, HFA (Fennoscandian High, anticyclonal), HFZ (Fennoscandian High, cyclonal), SWA (Southwest Circulation, anticyclonal), and TM (Central European Low) types were noted much more frequently in the analyzed months than average.
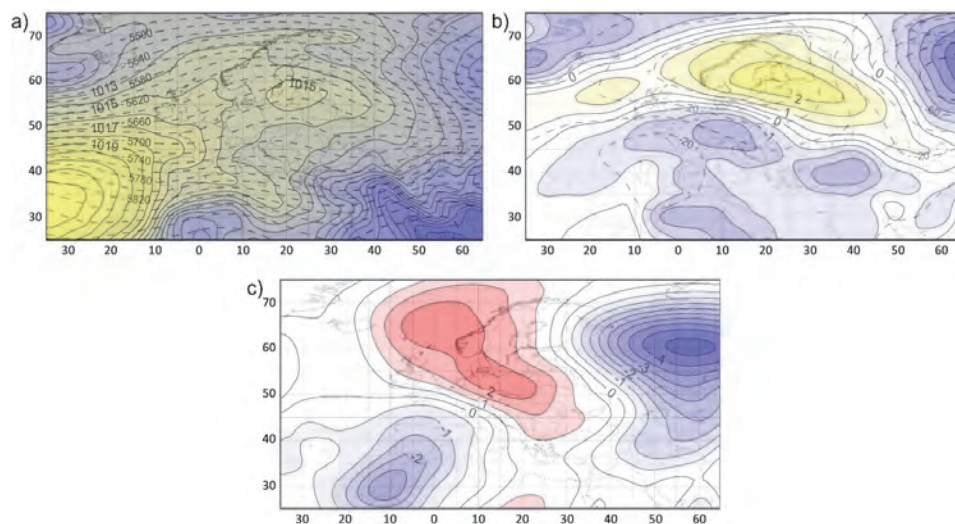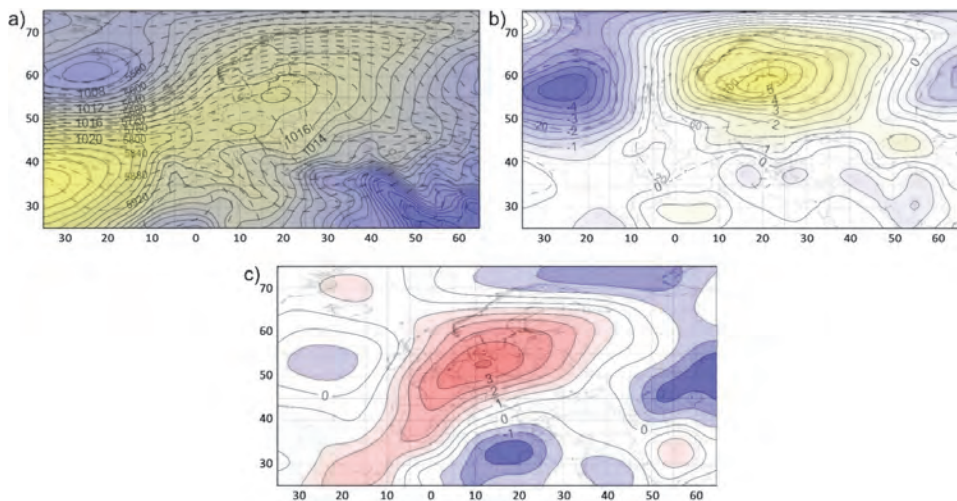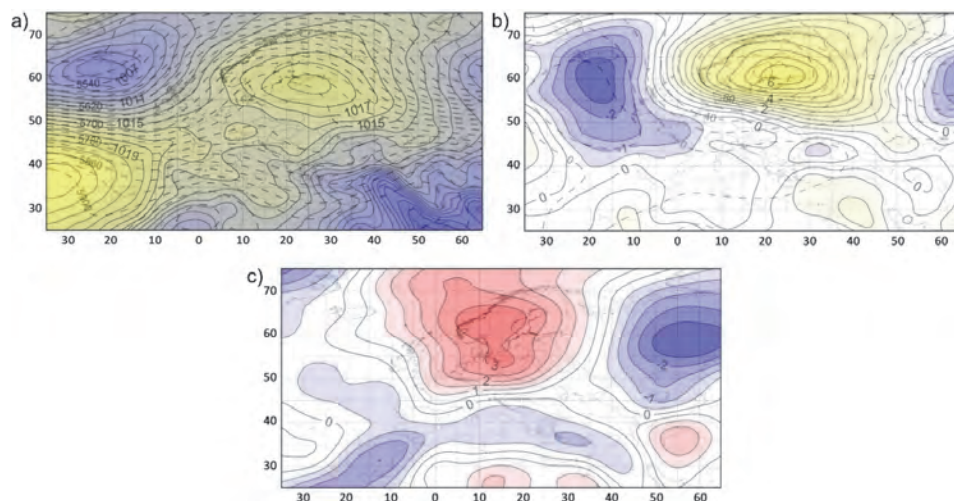
Fig. 6. Mean *SLP* (color scale) and *z500* (dashed line) (a), *SLP* (color scale) and *z500* (dashed line) anomalies (b), and the *T850* anomalies (color scale) (c) for the exceptionally warm months in August.

4. Discussion and summary

The research confirmed the increase in the mean T_{max} in the summer season in 1966–2015. The most intense changes were recorded in the western part of the Polish coast of the Baltic Sea and in Świnoujście, and these were 0.43 °C per 10 years. The previous studies of changes in air temperature, both average annual and average air temperature in particular seasons, have clearly indicated the increase (*Tylkowski,* 2013; *Tomczyk* and *Bednorz,* 2014). The size of these changes is strongly dependent on the adopted multiyear period. Numerous studies also confirm the warming of other Polish regions (*Michalska,* 2011; *Wójcik* and *Miętus,* 2014; *Owczarek* and *Filipiak,* 2016). When analyzing the spatial distribution of air temperature increase, it can be shown that the northern and western regions of the country are getting warmer a bit more intensively (*Biernacik et al.,* 2010). A common feature is the most intense warming in spring and summer (*Wójcik* and *Miętus,* 2014; *Owczarek* and *Filipiak,* 2016).

The observed warming is also translated into an increase in the frequency of warm and hot days. The statistically significant changes in the case of warm days were recorded in Ustka, Kołobrzeg, and Świnoujście, while in the case of hot days only in Świnoujście. Similarly, *Tomczyk* and *Bednorz* (2014) found an increase in hot days on the southern coast of the Baltic Sea. These authors adopted a

definition of characteristic days based on relative thresholds (the basis was the 95th percentile of T_{max}), and not on absolute values as in this article, which resulted in showing different rates of change. The increase in the number of warm and hot days has been demonstrated in numerous studies concerning the area of Poland (*Ustrnul et al.*, 2010; *Tomczyk,* 2014; *Owczarek* and *Filipiak,* 2016; *Sulikowska et al.*, 2016; *Bartoszek* and *Krzyżewska,* 2017), as well as other European regions (*Avotniece et al.,* 2010; *Kundzewicz* and *Huang,* 2010; *Kažys et al.,* 2011; *Tomczyk* and *Bednorz,* 2016; *Tomczyk* and *Sulikowska,* 2017). The increasing occurrence of warm and hot days has been also translated into the more frequent occurrence of heat waves. The changes taking place have been thoroughly documented by research from Poland (*Sulikowska et al.,* 2016; *Bartoszek* and *Krzyżewsk*a, 2017) as well as Europe (*Shevchenko et al.*, 2014; *Tomczyk,* 2016; *Tomczyk* and *Bednorz,* 2016; *Spinoni et al.,* 2015).

The conducted research also showed more frequent occurrence of exceptionally warm months, most of which occurred in the last 15 years. The more frequent occurrence of months and seasons above the standard is indicated in studies by *Twardosz* and *Kossowska-Cezak* (2013). According to these authors, currently observed warming occurs primarily through the increasingly frequent appearance of extremely hot summers, not through the disappearance of extremely cold summers.

The influence of atmospheric circulation on thermal conditions and the occurrence of thermal extremes have been the subject of great interest for many years (*Kažys et al.,* 2011; *Unkašević* and *Tošić,* 2015; *Tomczyk,* 2016). The occurrence of exceptionally warm months was associated with positive anomalies of the sea level pressure and the height of the 500 hPa isobaric surface, which indicates the presence of high pressure systems. During their occurrence, the advection of warm air masses from the eastern sector took place, which was also confirmed on the maps of T850 anomalies. The obtained results are consistent with earlier studies on circulation conditions for the occurrence of days with extreme temperatures, including heat waves in various regions of Central Europe. The occurrence of heat waves on the southern coast of the Baltic Sea was associated with anticyclonal circulation ensuring the advection of warm, continental masses from the southeast and northeast (*Tomczyk* and *Bednorz,* 2014). As established by *Tomczyk* and *Bednorz* (2016), the occurrence of heat waves in Central Europe was associated with three different types of circulation. In addition to the two types associated with high pressure systems, the occurrence of heat waves was possible during the settling of low pressure center, with its center west of Ireland. *Kažys et al.* (2011) showed that 1/3 cases of extremely hot weather in Lithuania were related to the advection of air masses from the southeast. A similar direction of inflow of air masses was distinguished for Latvia (*Avotniece et al.,* 2010) and Estonia (*Jaagus,* 2006).

References

Avotniece, Z., Rodinov, V., Lizuma, L., Briede, A. and *Kļaviņš, M.,* 2010: Trends in the frequency of extreme climate events in Latvia. *Baltica 23*, 135–148.

Bartoszek, K. and *Krzyżewska, A.,* 2017: The atmospheric circulation conditions of the occurrence of heatwaves in Lublin, southeast Poland. *Weather 72*, 176–180. https://doi.org/10.1002/wea.2975

Biernacik, D., Filipiak, J., Miętus, M. and *Wójcik, R*., 2010: Zmienność warunków termicznych w Polsce po roku 1951. Rezultaty projektu KLIMAT. In: (Eds.: *Bednorz, E., Kolendowicz, L.*): Klimat Polski na tle klimatu Europy. Zmiany i ich konsekwencje. Bogucki Wydawnictwo Naukowe, Seria: Studia i Prace z Geografii i Geologii 16. (in Polish)

Bobvos, J., Fazekas, B., and *Páldy, A.,* 2015: Assessment of heat-related mortality in Budapest from 2000 to 2010 by different indicators. *Időjárás 119*, 143–158.

Central Statistical Office Report, 2017: Tourism in 2016. Statistical Publishing Establishment, Warsaw.

Czernecki, B. and *Miętus, M.,* 2011: Porównanie stosowanych klasyfikacji termicznych na przykładzie wybranych regionów Polski. *Przegląd Geofizyczny 56*, 201–233. (in Polish)

IPCC, 2013: Climate change: The physical science basis. Contribution of Working Group I to the Fifth Assessment Report of the Intergovernmental Panel in Climate Change. Cambridge University Press, Cambridge.

Jaagus, J., 2006: Climatic changes in Estonia during the second half of the 20th century in relationship with changes in large–scale atmospheric circulation. *Theor. Appl. Climatol. 83,* 77–88. https://doi.org/10.1007/s00704-005-0161-0

Jażewicz, I. and *Rydz, E.,* 2001: Turystyka jako czynnik rozwoju społeczno-ekonomicznego Łeby. Zeszyty naukowe Wydziału Ekonomii i Zarządzania 8, Koszalin. (in Polish)

Jażewicz, I., 2011: Strategiczna rola turystyki w rozwoju Łeby. In: (Ed.: Jażdżewska, I.): Funkcja turystyczna miast, XXI Konserwatorium Wiedzy w Mieście, Uniwersytet łódzki, Łódź. (in Polish)

Kalnay, E., Kanamistu, M., Kistler, R., Collins, W., Deaven, D., Gandin, L., Iredell, M., Saha, S., White, G., Woollen, J., Zhu, Y., Leetmaa, A., Reynolds, R., Chelliah, M., Ebisuzaki, W., Higgins, W., Janowiak, J., Mo, K.C., Ropelewski, C., Wang, J., Jenne, R., and *Joseph, D.*, 1996: The NMC/NCAR 40-Year Reanalysis Project. *Bull. Am. Meteorol. Soc. 77*, 437–471. https://doi.org/10.1175/1520-0477(1996)077<0437:TNYRP>2.0.CO;2

Kažys, J., Stankūnavičius, G., Rimkus, E., Bukantis, A., and *Valiukas, D.,* 2011: Long–range alternation of extreme high day and night temperatures in Lithuania. *Baltica 24*, 71–82.

Kolendowicz, L., Półrolniczak, M., Szyga-Pluta, K. and *Bednorz, E.,* 2018: Human-biometeorological conditions in the southern Baltic coast based on the universal thermal climate index (UTCI). *Theor. Appl. Climatol. 134*, 363–379. https://doi.org/10.1007/s00704-017-2279-2

Kozłowska-Szczęsna, T., Błażejczyk, K., and Krawczyk, B., 1997: Bioklimatologia człowieka. Metody i ich zastosowanie w badaniach bioklimatu Polski. Monografie, IGiPZ, PAN, 1, Warszawa. (in Polish)

Kozłowska-Szczęsna, T., Błażejczyk, K., Krawczyk, B., and *Limanówka, D.,* 2002: Bioklimat uzdrowisk polskich i możliwości jego wykorzystania w lecznictwie. IGiPZ PAN, Warszawa. (in Polish)

Koźmiński, C. and *Michalska, B.,* 2016a: The seasonal nature of tourist flows in relation to meteorological conditions as illustrated by the case of Zachodniopomorskie Voivodeship. *Bulletin of Geography. Socio–economic Series 34*, 33–45.

Koźmiński, B. and *Michalska, C.,* 2016b: Sezonowość ruchu turystycznego w Polsce. Zeszyty Naukowe Uniwersytetu Szczecińskiego 3, 9–23. (in Polish)

Krzyżewska, A., 2010: Fale upałów jako zjawisko ograniczające turystykę w dużych miastach świata. Krajobrazy rekreacyjne-kształtowanie, wykorzystanie, transformacja. *Problemy Ekologii Krajobrazu 27*, 239–244. (in Polish)

Kuchcik, M., 2001: Mortality in Warsaw: is there Any connection with Feather and air pollution? *Geographia Polonica 74*, 29–45.

Kundzewicz, Z.W. and *Huang, S.,* 2010: Seasonal temperature extremes in Potsdam. *Acta Geophysica 58*, 1115–1133. https://doi.org/10.2478/s11600-010-0026-5

Lorenc, H., 1994: Ocena zmienności temperatury powietrza i opadów atmosferycznych w okresie 1901–1993 na podstawie obserwacji z wybranych stacji meteorologicznych w Polsce. *Wiad. IMGW, 38*, 43–59.

Lorenc, H. and *Suwalska-Bogucka, M.,* 1996: Thermal tendencies of winters in Poland as the indicator of climate variability. *Zesz. Nauk. UJ., Prace Geogr. 102*, 365–374.

Lorenc, H., 2000: Termiczno-opadowa ocena klimatycznych sezonów roku w Polsce oraz tendencje czasowo-przestrzenne. Projekt badawczy M-9, IMGW, Maszynopis.

Matczak, A. and *Rydz, E.,* 2001: Koncepcja monitoringu ruchu turystycznego w strefie brzegowej Bałtyku (na przykładzie rejonu Ustka-Rowy). Zeszyty Naukowe 1, Wyższa Pomorska Szkoła Turystyki i Hotelarstwa, Bydgoszcz. (in Polish)

Michalska, B., 2011: Tendencje zmian temperatury powietrza w Polsce. *Prace i Studia Geograficzne 47*, 67–75. (in Polish)

Owczarek, M. and *Filipiak, J.,* 2016: Contemporary changes of thermal conditions in Poland, 1951-2015. *Bulletin of Geography. Physical Geography Series 10.*

Paldy, A. and *Bobvos, J.,* 2009: Impact of the Unusual Heatwave of 2007 on Mortality in Hungary. *Epidemiology 20,* S126–S127. https://doi.org/10.1097/01.ede.0000362437.27958.17

Parzych K., 2011: Wybrane cechy ruchu turystycznego w Kołobrzegu i w świetle wyników pomiaru ruchu turystycznego, *Słupskie Prace Geograficzne 8,* 75–84. (in Polish)

Revich, B.A., Shaposhnikov, D.A., Podol'naya, M.A., Khor'kova, T.L., and *Kvasha, E.A.*, 2015: Heat Waves in Southern Cities of European Russia as a Risk Factor for Premature Mortality. *Studies on Russian Economic Development 26*, 142–150. https://doi.org/10.1134/S1075700715020100

Schwichtenberg, A., 2006, Gospodarka turystyczna polskiego wybrzeża, Politechnika Koszalińska, Koszalin. (in Polish)

Shevchenko, O., Lee, H., Snizhko, S., and *Mayer, H.,* 2014: Long-term analysis of heat waves in Ukraine. *Int. J. Climatol. 34*, 1642–1650. https://doi.org/10.1002/joc.3792

Spinoni, J., Lakatos, M., Szentimrey, T., Bihari, Z., Szalai, S., Vogt, J., and *Antofie, T.*, 2015: Heat and cold waves trends in the Carpathian Region from 1961 to 2010. *Int. J. Climatol. 35,* 4197–4209. https://doi.org/10.1002/joc.4279

Stasiak, A., 2011: Uwarunkowania i bariery rozwoju turystyki społecznej w Polsce. In: (Eds.: *Stasiak A.*): Perspektywy i kierunki rozwoju turystyki społecznej w Polsce, Łódź. (in Polish)

Sulikowska, A. Wypych, A. and *Woszczek, I.*, 2016: Fale upałów latem 2015 roku i ich uwarunkowania cyrkulacyjne. Badania Fizjograficzne, Seria A. *Geografia Fizyczna (A67)*, 205–223. (in Polish)

Szromek, A., 2012: Wskaźniki funkcji turystycznej. Koncepcja wskaźnika funkcji turystycznej i uzdrowiskowej, Wydawnictwo Politechniki Śląskiej, Gliwice. (in Polish)

Tomczyk A.M., 2014: Cyrkulacyjne uwarunkowania występowania fal upałów w Poznaniu. *Przegląd Geograficzny 86,* 41–52. (in Polish) https://doi.org/10.7163/PrzG.2014.1.3

Tomczyk, A.M., 2016: Impact of atmospheric circulation on the occurrence of heat waves in southeastern Europe. *Időjárás 120*, 395–414.

Tomczyk, A.M. and *Bednorz, E.,* 2014: Heat and cold waves on the southern coast of the Baltic Sea. *Baltica 27*, 45–54. https://doi.org/10.5200/baltica.2014.27.05

Tomczyk, A.M. and *Bednorz, E.,* 2016: Heat waves in Central Europe and their circulation conditions. *Int. J. Climatol. 36*, 770–782. https://doi.org/10.1002/joc.4381

Tomczyk, A.M. and *Sulikowska, A.,* 2017: Heat waves in lowland Germany and their circulation-related conditions. *Meteorol. Atmos. Phys. 130,* 499–515. https://doi.org/10.1007/s00703-017-0549-2

Twardosz, R. and *Kossowska-Cezak, U.,* 2013: Exceptionally hot summers in central and eastern Europe (1951–2010). *Theor. Appl. Climatol. 112*, 617–628. https://doi.org/10.1007/s00704-012-0757-0

Tylkowski, J., 2013: Temporal and spatial variability of air temperature and precipitation at the Polish coastal zone of the southern Baltic Sea. *Baltica 26*, 83–94.

Unkašević, M. and *Tošić, I.,* 2015: Seasonal analysis of cold and heat waves in Serbia during the period 1949-2012. *Theor. Appl. Climatol. 120*, 29–40. https://doi.org/10.1007/s00704-014-1154-7

Ustrnul, Z., Czekierda, D. and *Wypych, A.,* 2010: Extreme values of air temperature in Poland according to different atmospheric circulation classifications. *Phys. Chem. Earth 35*, 429–436. https://doi.org/10.1016/j.pce.2009.12.012

Warszyńska, J., 1985: Funkcja turystyczna Karpat Polskich. In: Folia Geographica, Series Geographica–Oeconomica 18. (in Polish)

Wójcik, R. and *Miętus, M.,* 2014: Niektóre cechy wieloletniej zmienności temperatury powietrza w Polsce (1951–2010). *Przegląd Geograficzny 86*, 339–364. (in Polish) https://doi.org/10.7163/PrzG.2014.3.3

IDŐJÁRÁS

Investigation of soybean leaf area influenced by water supply

Angela Anda*, **Brigitta Simon**, **Gábor Soós**, **László Menyhárt**, and **Tamás Kucserka**

Department of Meteorology and Water Management,
University of Pannonia, Georgikon Faculty,
Deák Ferenc u. 16, H-8360 Keszthely, Hungary

*Corresponding author E-mail: anda-a@georgikon.hu; anda@keszthelynet.hu

Abstract— Soybean leaf area observations were carried out in two levels of water supply using two different varieties (*Sinara* and *Sigalia*) in Hungary. Half of the crops was grown using unlimited watering in evapotranspirometers, while the others received only 50% of their water requirements from the R1 (beginning bloom) stage (stressed crops). Out of four meteorological variables, the air temperature, the most easily accessible meteorological variable impacted the *LAI* (leaf area index) the most, irrespective of water supply. To obtain the variation in the vertical leaf area distribution, the LAI_{max} was selected and analyzed, when leaf area remained relatively invariable. Water deprivation in the reproductive phase significantly reduced the *LAI*, irrespective of the studied variety. The water stress condition significantly lowered the level-wise trifoliate area of *Sigalia* above the sixth leaf level but did not lower it in the case of *Sinara*. Increase of 1.5 in the number of leaf levels could be contributed to the higher *LAI* of crops with unlimited watering in comparison to water stressed ones. The area of the middle leaflet was significantly higher compared to the outer ones at the bottom and the top of the plant, but they were of about the equal size around the center of the plant height irrespective of the variety. According to our best knowledge, this morphological phenomenon has not been described yet.

Key-words: distribution of leaf area, soybean (*Glycine max* L.), evapotranspiration, water stress

1. Introduction

Leaf assimilatory surface size, photosynthesis, and crop biomass are the main crop indicators of final yield (*Kross et al.* 2015) including soybean. Most commonly, the ratio of the green leaf area in m^2 to the ground surface area (in m^2)

is expressed as leaf area index, *LAI*. Green leaf area is available for gas exchange processes (mainly CO_2 and water vapor) between the canopy and the atmosphere. *Vina et al.* (2011) specified these vegetation processes, including light and water interception (rainfall and fog), light attenuation through the crop stand, transpiration, photosynthesis, autotrophic respiration, and carbon and different nutrients' cycles. *Yang et al.* (2009) identified that the size of maximum *LAI* reflected the impacts of environmental conditions the most. *Malone et al.* (2002) concluded the soybean *LAI* reaches 3.5–4.0 in the growth stages from R2 (full bloom) to R5 (beginning seed) producing high seed yield. Similar values were also published by *Board et al.* (1997). In soybean evapotranspiration (*EVTR*), "threshold" *LAI* of 3.7 was communicated by *Campos et al.* (2017) at the University of Nebraska-Lincoln Research Centre, USA after which further growth in *LAI* does not increase canopy's evapotranspiration. This peak *LAI* was called as "saturation *LAI*" after *Bausch* (1993). In this study, the peak *LAI* was selected and analyzed from the growing period of soybean, where *LAI* remained relatively invariable (August). Selected time periods were also suitable for comparative water withdrawal investigations as growth stages between R4 (full pod) and R6 (full seed) are vulnerable to water deficiencies producing in significant yield loss (*Bagg et al.* 2009). *Hsiao* (1990) also highlighted *LAI* as affected by water stress as an important indicator of crop growth and final yield.

The green colored part of crop leaves is the photosynthetically active component which must be separated from the dried leaves.

Two main types of approaches were developed in the *LAI* estimation; direct (based on leaf collection) and indirect methods. In this second group, *LAI* is derived from one or more easily measurable leaf characteristics (*Jonckheere et al.* 2004). Indirect non-contact measurements are considered to be the most up-to-date, and non-destructive *LAI* observation group using remotely sensed canopy reflectance data that has been reviewed partially by *Verrelst et al.* (2015). Although it does not mean that other *LAI* estimation methods can not be of great significance under special circumstances.

The aim of this investigation was to find a simplified approach in soybean's leaf area estimation that allows easy experimental evaluation of the assimilatory (transpiration) surface size. Leaf area estimation (in the absence of planimeter) using empirical functions based on meteorological variables was also a vital part of the study target. The variation in the vertical distribution of the leaf area across two soybean varieties of three different water supply levels was also documented. To date, there are only limited number of studies that have attempted to take soybean leaflet area into account. Leaf area parameters are basic inputs for most of the crop models.

2. Materials and methods

Soybean (*Glycine max* L.) and meteorological observations were carried out at the Keszthely Agrometeorological Research Station (ARS) (latitude: 46°44′ N, longitude: 17° 14′ E, elevation: 124 m above sea level), over the vegetation period of 2017. A QLC-50 climate station fitted with a CM-3 pyranometer was operated at ARS. This standard station belongs to the Hungarian National Meteorological Network operated by the Hungarian Meteorological Service (OMSZ). On the recommendation of the seed supplier company of Karintia (2017), indeterminate *Sinara* (*Sin*), a water stress tolerant, and *Sigalia* (*Sig*), a variety bred for average weather conditions were included in the study. The length of the studied soybean's growing season ranged between 116 and 120 days. Soybean hand sowing occurred on May 9, 2017, and crops successfully emerged on May 17, 2017. The planting distance between the crop rows was 0.24 m (planting population: 600,000 seed ha^{-1}). Before planting, 300 kg ha^{-1} nitrogen-phosphorus-potassium (NPK) fertilizer was applied at the time of sowing (N:P:K=1:1:1).

The phenological phases of soybean were used after *Fehr* and *Caviness* (1977).

Some of the treatments were grown in the growing pots of Thornthwaite-type compensation evapotranspirometers. Half of them got unlimited water supply in line with the nature of the equipment (*ET*). Stressed soybean canopies received only 50% of their water requirement from the reproductive phase (R1), producing detectable water stress conditions (*RO*). The stressed vessels' control system (magnetic swimmer and Reed-switch) were disconnected and its water supplier switch was connected to the non-stressed vessel's reed switch, so the stressed vessel's water supply was regulated by the non-stressed water compensation unit. Water deprivation of stressed crops was ensured by closing the water supplier tap every second day. This setup allowed to reduce water supply in about half of the reproductive stage. A data logger of HYGACQ V1.3 type was connected to log the amount of water use. The calculated hourly sums were memorized. The collected hourly data were downloaded to a computer, using the WHYGACQ program (*Anda* and *Soós*, 2014). As stressed crop's tap was closed every second day, pentad sums and evapotranspiration totals were calculated (water balance) and presented in the study.

Altogether, two water treatments and two varieties were included in the study with the following experimental design:

- *Sin ET* (water stress tolerant variety, unlimited water supply);
- *Sig ET* (variety of average weather conditions, unlimited water supply);
- *Sin RO* (water stress tolerant variety, crops exposed to moisture stress from generative phase, R1);
- *Sig RO* (variety of average weather conditions, crops exposed to moisture stress from generative phase, R1).

The leaflet area, L was determined as follows. Given the oval shape of the leaflets, the area was expected to be directionally proportional to the product of the length (a) and width (b). The parameter (a) was measured from the base of the leaf to the terminal part of the leaf blade. The maximum width of the leaflet (b) was taken at the widest lobes of the lamina perpendicular to the lamina midrib:

$$L = x \cdot ab. \tag{1}$$

In addition, destructive L measurement using segmentation was carried out from separate growing pots excluded from the water supply study. Each leaflet was placed on a flat surface of an evenly colored red cardboard with a scale at the side, directly under a vertically mounted camera (Canon EOS 7D digital camera with 17.9 megapixels. Histogram based threshold segmentation was applied in the image processing program (SGDIP 0.1; of our own) to count the area of the region of interest.

The x multiplier in Eq. (1) was determined with linear regression without intercept based on about 350 trifoliates.

Plant height of the crops was also registered for the same crops where L measurements were carried out.

The effect of the water supply on the trifoliate level was analyzed with a 3-way ANOVA method. The area of the trifoliate was the response variable, the water supply, the variety of the plants, and the trifoliate level were considered as exploratory variables. In the first step, all 2-way and 3-way interactions were included in the model. Iteratively, the non-significant interaction and main effect with the highest p-value was removed from the model. Tukey HSD posthoc test was used, if it is necessary.

The area of the middle leaflet compared to the outer ones within a trifoliate was examined. The proportion of the middle leaflet within the whole trifoliate was calculated for each trifoliate level of each plant. Given the two outer leaflet are of about equal size, the proportion being greater than 1/3 implies that the middle leaflet is larger than the outer ones. This proportion was analyzed with a 3-way ANOVA method on the same way as described at the analysis of the area of the trifoliate level.

Two-tailed one-sample t-test was applied to compare the proportion of the middle leaflet assumed to be 1/3 of trifoliate area, on each trifoliate level, separately. Pooled standard deviation was used in the t-test. To facilitate the presentation of the results, 95% confidence interval was calculated for each trifoliate level. All plants were considered as a single sample.

To illustrate the impact of meteorological elements (air temperature, T_a; water vapor pressure, e_a; wind speed, u; precipitation, P) on LAI, the Pearson's correlation analysis was applied. Multiple stepwise regression analysis was carried out to get the combined effect of different meteorological variables on

LAI. The Akaike information criterion (*AIC*) was applied to estimate different *LAI* projections (*Motulsky* and *Christopoulos,* 2004):

$$AIC = N \times \ln\left(\frac{SS}{N}\right) + 2K \quad , \tag{2}$$

where N is the number of data points, K is the number of parameters fit by the regression plus one, SS is the residual sum of squares value taken from the ANOVA-table of the regression analysis. The model with the smallest *AIC* value is most likely to be correct.

The tests were carried out with the SPSS Statistics software (IBM Corp., New York, USA) and R statistical software (R, 2017).

3. Results and discussion

3.1. Weather, crop development, and evapotranspiration (EVTR)

On a soybean seasonal average basis, the vegetation period in 2017 was 1.3 °C warmer ($p < 0.622$) than that of the long-term mean at Keszthely (1971–2000). Warmer months were particularly noticeable in summer (June-August), when the difference from the climate norms was 1.8–2.7 °C. The growing season's precipitation sum P was 37.0 mm lower ($p < 0.738$) than that of the long-term P total (384.4 mm). Monthly P sums in the growing season reduced with 17.4–37.4 mm in comparison to their climate norms (1971–2000). Although the distribution of monthly P sum was quite even during the soybean growing season in 2017. The only increased P in September was out of the soybean's vegetation period.

Durations of the soybean phenological stages were similar across all treatments (data not shown). The maximum difference in the length of the vegetation periods was only restricted to a few days (1–2 days).

Barely different seasonal daily mean *EVTR* rates of 5.88 and 5.63 mm day^{-1} was measured in *Sin ET* and *Sig ET*, respectively. Using unlimited watering, increase of 4.51% in daily average *EVTR* rate of *Sin ET* was not significant ($p < 0.224$), indicating no variation in *EVTR* rates between the two varieties with different water requirements. Irrespective of variety, 50% water withdrawal of the crop water requirement declined the seasonal daily mean *EVTR* rate by more than half (*Sin*: 74.68%, $p < 0.001$; *Sig*: 75.51%, $p < 0.001$). Surprisingly, there was no significant impact of variety on daily mean *EVTR* rates at both water supply levels (*ET*: 4.51%, $p < 0.224$; *RO*: 5.48%, $p < 0.165$). Even over water deprivation, the variety *Sin* bred for water shortage conditions statistically used the same amount of water as *Sig*.

Distribution in evapotranspiration pentad sums followed the usual pattern (*Fig. 1*); the peak 5-day evapotranspiration sums in the middle of the growing

season were 51.6 (*Sin*) and 57.4 mm pentad^{-1} (*Sig*) for the *ET* in the middle of July, and 23.0 (*Sin*) and 24.7 mm pentad^{-1} (*Sig*) for the *RO* treatments, respectively, in the middle of August. Top water losses of water deprived treatments were late about one month in comparison to unlimited the water supply treatment. From the beginning of August, variety *Sin* generally had higher peak 5-day *EVTR* sums than the variety *Sig* in both water supplies. In August, the stressed soybean probably "addicted" to water shortage, and the evapotranspiration curves of *RO* got closer to the evapotranspiration curves of *ET*.
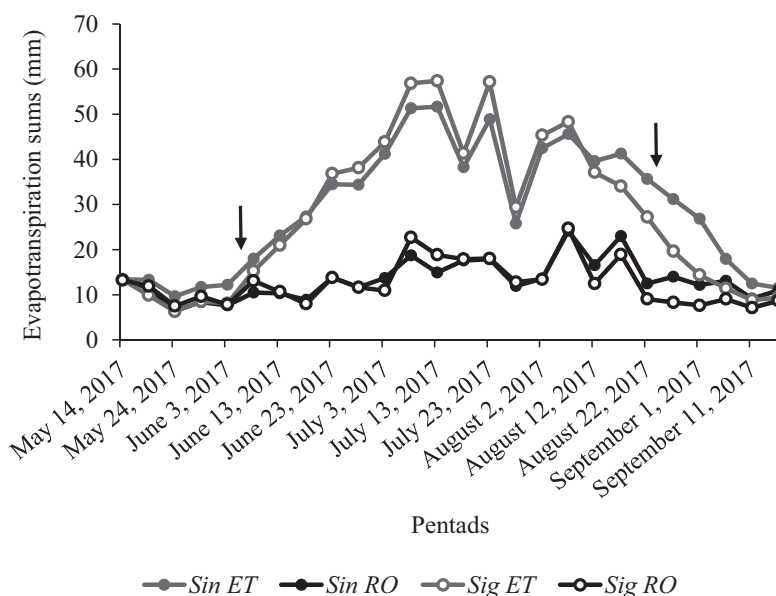
Fig. 1. Pentad sums of evapotranspiration in two soybean varieties (*Sinara* (*Sin*) and *Sigalia* (*Sig*)), using unlimited (*ET*) and water stressed (*RO*) canopies at Keszthely, during 2017. The arrows show the beginning and end of water deprivation.

The cumulative *EVTR* of 346.4 and 327.9 mm in *Sin RO* and *Sig RO*, respectively, stayed near the cumulative *P* of the growing period (2017: 347.4 mm) (*Fig. 2*). *EVTR* totals of both *ET* treatments (*Sin*: 759.3 mm; *Sig*: 725.8 mm) were about twice as high as the cumulative seasonal *P* at Keszthely, indicating that soil water coming from *P* probably would not be enough to satisfy soybean water needs. *Montoya et al.* (2017) reported similar *EVTR* totals ranging from about 400 to 800 mm for rainfed and 50–75% deficit irrigated soybeans (cultivar Don Mario) in Uruguay (31°22'S).
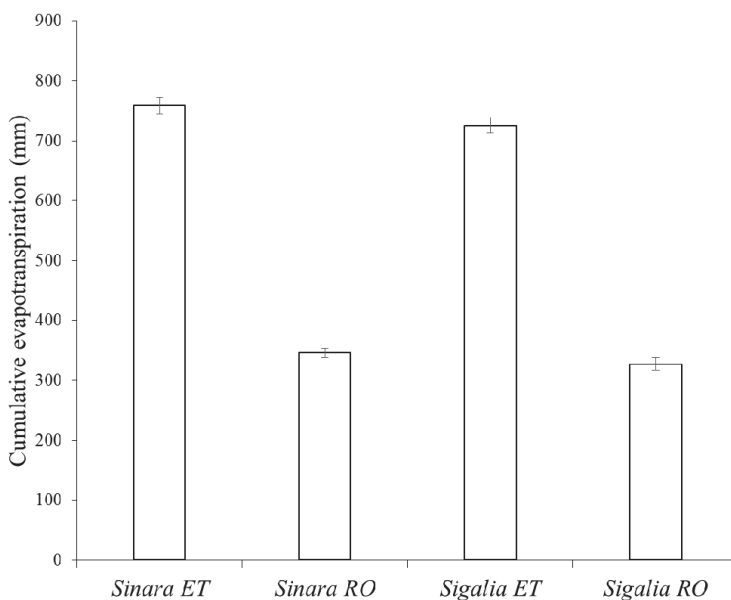
Fig. 2. Cumulative evapotranspiration of the two varieties *Sinara* (*Sin*) and *Sigalia* (*Sig*) using two levels of water supply; unlimited (*ET*) and water stressed (*RO*) canopies at Keszthely, during 2017.

3.2. *Seasonal variation in LAI*

Until photosynthesis shows an immediate response to environmental conditions, crop growth is the end result of photosynthesis, responds more slowly to environmental variation (*Lessmann et al.* 2001). This is why consecutive tracking of *LAI* is appropriate in crop growth monitoring.

LAI of soybean showed a period of increase that followed by a maximum value maintained for a shorter time period before decreasing. Weekly mean *LAI* increased from a minimum of 0.3 on June 6 to a maximum of 9.6 (both *ET*) on August 2 (*Fig. 3*). LAI_{max} of 6.5 in *Sin RO* was only slightly lower than that of LAI_{max}=7.0 measured by *Montoya et al.* (2017) in soybean (cultivar: Don Mario) at Salto, Uruguay (31°22' S). *Setiyono et al.* (2008) also detected somewhat lower LAI_{max} of 7.8 in irrigated soybean (variety P93M11) at Lincoln, NE (40°49' N). Natural senescence slightly declined the *LAI* to a value of 0.1 (*RO*). Seasonal mean *LAI* ranged from 5.3 (*Sin ET*) to 3.0 (*Sig RO*) over the growing season of 2017. Only, like a tendency, the seasonal mean *LAI* in *Sin* tended to be 1.9 (*ET*; $p < 0.349$) and 12.4% (*RO*; $p < 0.154$) higher than that of the average *LAI* of *Sig*. In turn, the seasonal mean *LAI* of both varieties were strongly impacted by water deprivation. Declines of 39.4 ($p < 0.001$) and 49.3% ($p < 0.001$) in water stressed *Sin* and *Sig* were observed, respectively, in comparison to *LAI* of crops with

unlimited watering. *Kross et al.* (2015) explained lower soybean *LAI* under dryer conditions to have resulted from a greater investment in the root structure. Descending branch of weekly *LAI* curve was slightly steeper in the water stressed pots than that of in the *ET* treatments.
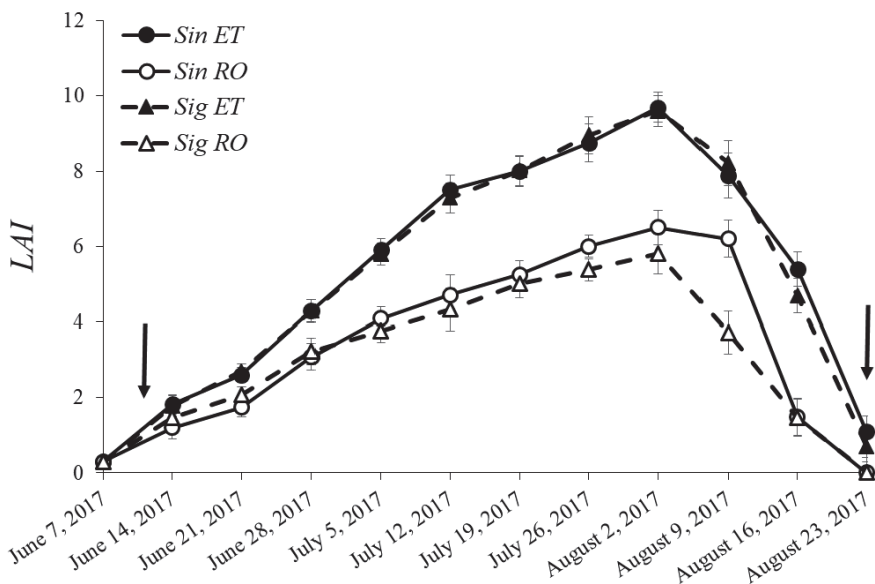
Fig. 3. Weekly variation in leaf area index (*LAI*) of varieties *Sinara* (*Sin*) and *Sigalia* (*Sig*) using two levels of water supply (*ET*: unlimited watering; *RO*: water stressed crops) in 2017. The arrows show the beginning and end of water deprivation.

3.3. Soybean's canopy structure

The LAI_{max} was selected for evaluation of canopy architecture, as during this growth period (R6), the final height of crops was reached and the *LAI* remained relatively invariable. *Yang et al.* (2009) concluded that LAI_{max} well reflects the impact of environmental conditions on the growth of crops.

The average number of leaf storeys were 15.0 ± 2.18 and 13.5 ± 1.75 in *ET* and *RO*, respectively. Due to the lower number of leaf levels, crop height in *ET* increased with 0.13 m ($p <0.001$) comparing to the height of *RO*. Unlimited water supply stimulated the plant growth through emerging more trifoliate layers contributing to increased *LAI*.

The multiplier *x* in Eq. (1). was determined with linear regression without intercept based on measured data of about 350 trifoliates:

$$L = 0.708 \; ab. \tag{3}$$

Fig. 4 shows the calculated leaflet area values.
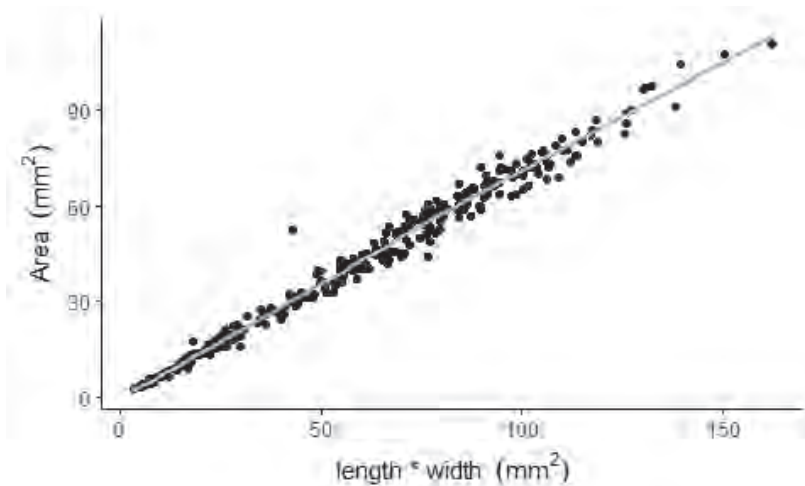
Fig. 4. Calculated leaflet area values based on Eq. (3).

The effect of the water supply was analyzed with a 3-way full factorial ANOVA. The 3-way interaction and two 2-way interactions were not significant, they were removed from the model. Finally, the main effect of the trifoliate level ($p = 3 \cdot 10^{-10}$), the water supply ($p = 0.0005$) and the water supply and variety interaction ($p = 0.034$) were found to be significant. The fact that interactions including trifoliate level were not significant shows that the effect of the water supply and the variety were much the same on each trifoliate level. To reveal the information hidden in the water supply – variety interaction, these two variables

were combined into a single variable having four levels. The pairwise comparison was performed using the Tukey-HSD test. It pointed out that the trifoliate area was significantly lower in the case of *Sig* with water stress condition than in the other three groups (each $p < 0.05$). The difference among the other three groups was not significant (*Fig. 5*).
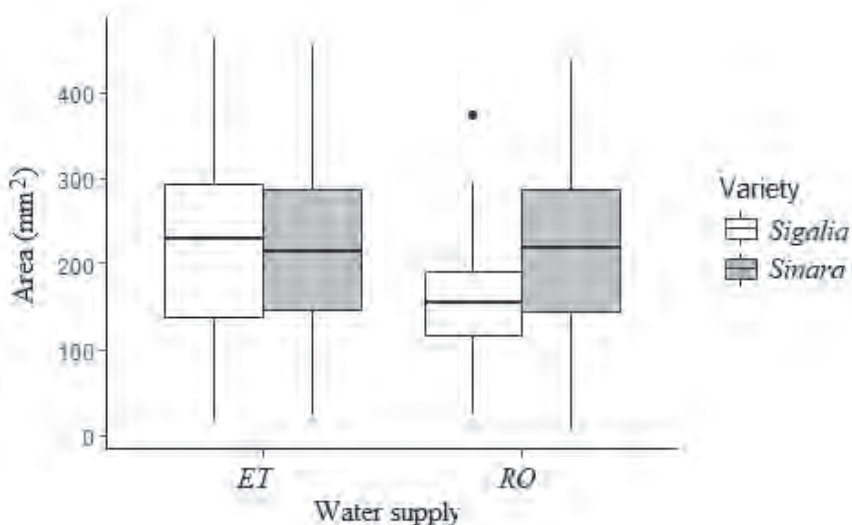
Fig. 5. Trifoliate area by water supply and variety of soybean. *ET*: unlimited watering, *RO*: water stress.

Analysis was carried out on the proportion of the middle leaflet within the whole trifoliate with 3-way ANOVA model. After removing the non-significant interactions and main effects, the final model contained only the intercept. Therefore, none of the factors had significant effect on the proportion of the middle leaflet. The mean of the proportion was compared to 1/3 using a one-sample *t*-test. The trifoliate levels above the 13th level were excluded from the analysis due to the low sample size. The results are shown in *Fig. 6*. The curve is bowl-shaped, the proportion of the middle leaflet is significantly higher than 1/3 on the lower four levels and from the 10th level with the exception of the 12th level. It shows that the area of the middle leaflet is approximately equal to the area of the outer ones around the center of plant height, but is greater at the bottom and the top of the plant height.
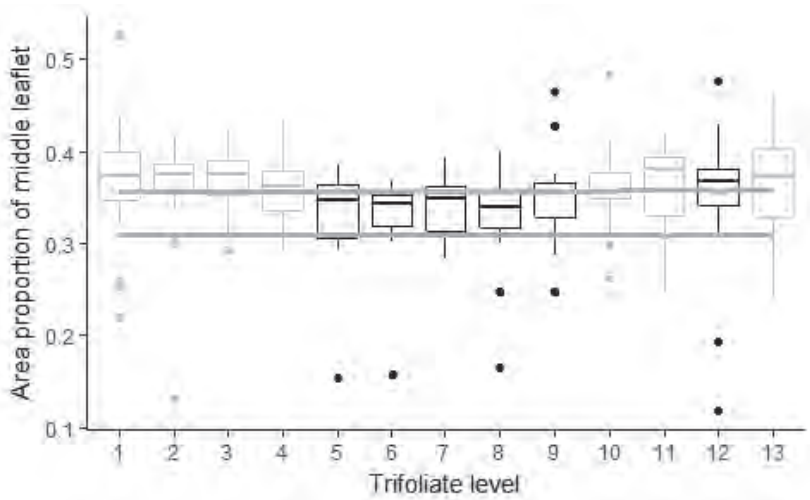
Fig. 6. Area of the middle leaflet compared to the whole area of the trifoliate. Thick grey line shows the 95% confidence interval. Boxplot is colored grey if the difference from the 1/3 is significant.

3.4. *Impact of weather on the LAI*

The influence of four meteorological variables (air temperature, T_a; vapor pressure, e_a; precipitation, P; and wind speed, u) on the weekly mean *LAI* of the two varieties using two levels of water supply was assessed by a correlation analysis (*Table 1*). Irrespective of the variety and water supply, the highest correlation coefficients (r) ranging from 0.59 (*Sig RO*) to 0.62 (both *ET* treatments) were computed between *LAI* and T_a. T_a alone explained at about 60–62% of the variability of *LAI*. Among four studied parameters (water stress, phenology, T_a, and light use), T_a significantly improved the vegetation production metrics, included *LAI* (*Nguy-Robertson et al.* 2015) in Nebraska, USA (41.165°N). Slightly lower positive correlations of 0.46 (*Sig RO*) – 0.56 (*Sin RO*) were observed between *LAI* and e_a. Weak negative correlations [(–0.07) – (–0.15)] between *LAI* and P were expected as crops were grown in evapotranspirometer under unlimited watering. Unexpectedly, negative correlation [(–0.21) – (–0.45)] between *LAI* and u was found referring to the favorable effect of calm weather conditions on soybean leaf growth. The correlation between *LAI* and u was only significant in *Sig RO*, see also *Table 1*. The probably reason might has been that the *LAI* values were the lowest in *Sig RO*, creating the most open canopy structure mostly exposed to the influence of wind. More closed soybean stands with higher *LAI* could hinder the impact of the wind.

Table 1. Correlation coefficients (*r*) for weekly measured leaf area index (*LAI*) and weekly weather variables (weekly means of air temperature, T_a; weekly means of water vapor pressure, e_a; weekly precipitation sums, *P*; weekly mean wind speed, *u*) included in the study. Number of observations was 12 for each correlation.

LAI	Sin ET	Sin RO	Sig ET	Sig RO
T_a [°C]	0.62[**]	0.61[**]	0.62[**]	0.59[**]
e_a [kPa]	0.51[**]	0.56[**]	0.52[**]	0.46[**]
P [mm]	−0.15	−0.07	−0.14	−0.08
u [m/s]	−0.21	−0.32	−0.24	−0.45[*]

* Marginally significant correlation $|r|>0.1$, $p<0.01$
** Marginally significant correlation $|r|>0.1$, $p<0.001$

All of the meteorological variables mentioned above were included in the multiple stepwise regression analysis. In this statistical analysis the variables included stepwise in the resulted equations are dimensionless. As there was hardly enough difference in *r* between the two studied varieties (*ET*: $p<0.809$; *RO*: $p<0.115$), their data were treated together (*Table 2*) when identifying regression equation. On the basis of the Akaike information criterion (*AIC)* and the adjusted multiple correlation (R^2), T_a impacted the *LAI* the most, irrespective of water supply (in *ET*: $LAI = 0.996T_a - 16.796$, $R^2 = 0.322$, AIC= 20.77; in *RO*: $LAI = 0.728T_a - 12.746$, $R^2 = 0.309$, AIC= 13.25). It is a favorable response as T_a is the most easily accessible meteorological variable for all potential users including farmers. *Nielsen* (1990) called the attention for the importance of ambient T_a in governing soybean's physiological processes in USDA Central Great Plains Research Statin (40°9'N), as shown even for leaf growth in this study.

Table 2. Result of multiple stepwise regression analysis between meteorological variables and leaf area index, *LAI* in unlimited water supply, *ET* and using 50% water withdrawal, *RO*. Only one meteorological variable, the air temperature T_a remained in the regression equations. Equations included data of both varieties studied. *R* and *AIC* denoted coefficient of multiple correlation and Akaike Information Criterion, respectively.

	Adjusted R^2	F-value	Sig. of F	Standard Error of coefficient	Regression equation	AIC
ET	0.322	6.223	0.032	Const.=8.88 T_a=0.399	$LAI = 0.996T_a - 16.796$	20.77
RO	0.309	5.925	0.035	Const.=6.65 T_a=0.299	$LAI = 0.728T_a - 12.746$	13.25

3.5. Seed yield of the treatments

Based on a two-way ANOVA (F) test for seed yield, there were significant main effects of water supply (F (1, 16) = 87.396; p = 0.000) and variety (F (1, 16) = 8.082; p = 0.012) (The numbers in the bracket are the between-groups and the within-groups degrees of freedom separated by a comma. After the = are the F statistic and the significance level). The water x variety interaction on seed yield was not significant (F (1, 16) = 1.644; p = 0.218), indicating that the impact of the water supply was about the same on both varieties (*Fig. 7*).

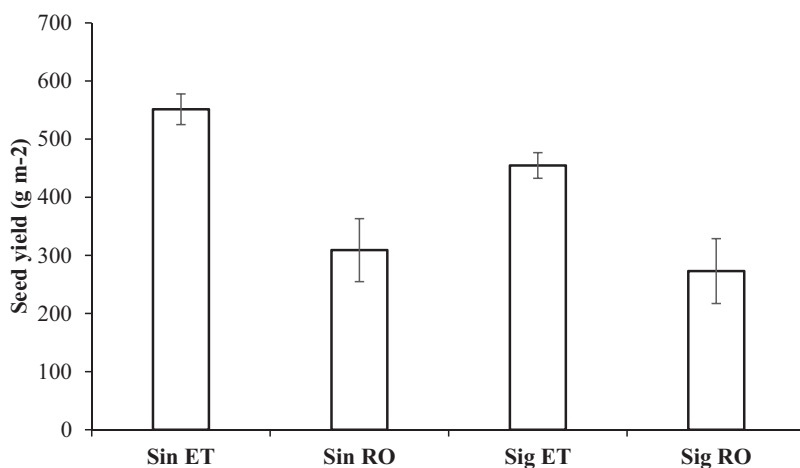*Fig. 7.* Seed yield of soybean varieties *Sinara* (*Sin*) and *Sigalia* (*Sig*) in two watering levels (unlimited: *ET*; water stressed: *RO*).

4. Conclusion

Accounting different varieties and water supply levels, this study contributed to the better understanding of soybean canopy architecture. The new information – produced by the research – can widen the application related to the crop structure used in crop modeling.

References

Anda, A. and *Soós, G*., 2012: Evapotranspiration of cadmium treated maize. *Növénytermelés. 61,* 369–372.

Bagg, J., Banks, S., Baute, T., Bohner, H., Brown, C., Cowbrough, M., Hall, B., Hayes, A., Johnson, P., Martin, H., McDonald, I., Quesnel, G., Reid, K., Spieser, H., Stewart, G., Tenuta, A. and Verhallen, A., 2009: In (Ed.: Brown, C.), Agronomy Guide for Field Crops: Publication 811. Toronto, Ontario.

Board, J.E., Wier, A.T., and *Boethel, D.J.,* 1997: Critical light interception during seed filling for insecticide application and optimum soybean grain yield. *Agron J. 89,* 369–374. https://doi.org/10.2134/agronj1997.00021962008900030001x

Bausch, W.C., 1993: Soil background effects on reflectance-based crop coefficients for corn. *Remote Sens Environ. 46,* 213–222. https://doi.org/10.1016/0034-4257(93)90096-G

Campos, I., Neale, C.M.U., Suyker, A.E., Arkebauer, T.J., and *Gonçalves, I.Z.,* 2017: Reflectance-based crop coefficients REDUX: For operational evapotranspiration estimates in the age of high producing hybrid varieties. *Agric. Water Manag. 187,* 140–153.

Fehr, W.R. and *Caviness, C.E.,* 1977: Stages of soybean development. Spec. Rep.80 Coop. Ext. Service. Iowa State University, Ames, Iowa.

Hsiao, T., 1990: Measurements of plant water status. In (Eds. *Stewart, B.A., Nielsen, D.R.*), Irrigation of Agricultural Crops. Agronomy Monogr. ASA, CSSA, SSSA, Madison, WI, 243–279.

Jonckheere, I., Fleck, S., Nackaerts, K., Muys, B., Coppin, P., Weiss, M., and *Baret, F*., 2004: Review of methods for in situ leaf area index determination. Part I. Theories, sensors and hemispherical photography. *Agric. For. Meteor. 121,* 19–35. https://doi.org/10.1016/j.agrformet.2003.08.027

Karintia, 2017: Vetőmag fajtakínálat (Seed varieties): https://karintia.hu/vetomagok/sigalia/; https://karintia.hu/vetomagok/sinara/ (in Hungarian)

Kross, A., Lapen, D.R., McNairn, H., Sunohara, M., Champagne, C., and *Wilkes, G.*, 2015: Satellite and in situ derived corn and soybean biomass and leaf area index: Response to controlled tile drainage under varying weather conditions. *Agric. Water Manag. 160,* 118–131. https://doi.org/10.1016/j.agwat.2015.06.007

Lessmann, J.M., Brix, H., Bauer, V., Clevering, O.A., and *Comin, F.A.,* 2001: Effect of climatic gradients on the photosynthetic responses of four *Phragmites australis* populations. *Aquatic Botany 69,* 109–126. populations. Aquatic Botany 69, 109–126. https://doi.org/10.1016/S0304-3770(01)00133-4

Malone, S., Herbert, Jr. D.A., and *Holshouser, D.L*., 2002: Relationship between leaf area index and yield in double-crop and full-season soybean systems. *J. Econ. Entom. 95,* 945–951. https://doi.org/10.1093/jee/95.5.945

Motulsky, H. and *Christopoulos, A.,* 2004: Fitting models to biological data using linear and non-linear regression. Oxford University Press, Oxford.

Montoya, F., García, C., Pintos, F., and *Otero, A*., 2017: Effects of irrigation regime on the growth and yield of irrigated soybean in temperate humid climatic conditions. *Agric. Water Manag. 193,* 30–45. https://doi.org/10.1016/j.agwat.2017.08.001

Nguy-Robertson, A., Suyker, A., and *Xiao, X.,* 2015: Modeling gross primary production of maize and soybean croplands using light quality, temperature, water stress and phenology. *Agric. For. Meteor. 213,* 160–172. https://doi.org/10.1016/j.agrformet.2015.04.008

Nielsen, D.C., 1990: Scheduling irrigations for soybeans with the crop water stress index (CWSI). *Field Crop Res. 23,* 103–116. https://doi.org/10.1016/0378-4290(90)90106-L

R Core Team, 2017. R: A language and environment for statistical computing. R Foundation for Statistical Computing, Vienna, Austria. URL: https://www.R-project.org/

Setiyono, T.D., Weiss, A., Specht, J.E., Cassman, K.G., and *Dobermann, A*., 2008: Leaf area index simulation in soybean grown under near-optimal conditions. *Field Crops Res. 108,* 82–92. https://doi.org/10.1016/j.fcr.2008.03.005

SPSS Statistics 17.0; IBM Corporation, New York, US.

Verrelst, J., Camps-Valls, G., Muñoz-Marí, J., Rivera, J.P., Veroustraete, F., Clevers, J.G.P.W., and Moreno, J., 2015: Optical remote sensing and the retrieval of terrestrial vegetation bio-geophysical properties – A review. ISPRS J. Photogrammet. Remote Sens. 108, 273–290.

Vina, A., Gitelson, A.A., Nguy-Robertson, A.L., and *Peng, Y*., 2011: Comparison of different vegetation indices for the remote assessment of green leaf area index of crops. *Remote Sens. Environ, 115.* 3468–3478. https://doi.org/10.1016/j.rse.2011.08.010

Y*ang, Y., Timlin, D.J., Fleisher, D.H., Kim, S.H., Quebedeaux, B.,* and *Reddy, V.R.*, 2009: Simulating leaf area of corn plants at contrasting water status. Agric For Meteor. 149, 1161–1167. https://doi.org/10.1016/j.agrformet.2009.02.005

IDŐJÁRÁS

Thermal seasons onset and length in Poland – a multiannual perspective on 1971–2010

Michał Kitowski[*], **Michał Marosz**, and **Mirosław Miętus**

Faculty of Oceanography and Geography, University of Gdansk,
ul. Bażyńskiego 4, 80-309, Gdańsk, Poland

[*]*Corresponding author E-mail: michal.kitowski@ug.edu.pl*

Abstract— The major aim of the research is to analyze the variability of thermal seasons characteristics (onset and length), at 7 stations in Poland during the 40-year-long period of 1971–2010. The analysis comprised the selection of the optimal method for season onset identification and the statistical analysis of the season onset and length characteristics, which was augmented with the interdecadal comparison of statistics using one-way analysis of variance (ANOVA). Also, it was investigated if the season onset type (late/normal/early) induces the season length distribution characteristics. The results show that the variability of the onset of thermal seasons is most pronounced in the case of summer and early spring. Summer also shows the tendency to occur faster, whereas autumn tends to start later. The interdecadal change of the thermal seasons length is clearly visible in the case of summer which length systematically increases and winter where the trend is reversed at most of the stations. The research also confirmed that for winter, early spring, and summer, the onset type clearly determines the distribution of the season length. Other seasons either show little variability or the differences appear only at some stations.

Key-words: thermal seasons, thermal seasons onset, thermal seasons length, air temperature, Poland

1. Introduction

A climate of an area can be described with the establishment of its seasonal structure (*Woś*, 1999). The onset, decline, and length of individual seasons are the indicators of climate's natural variability in annual cycle. Variability of the seasonal characteristics in the last century may indicate the occurring climate change (*Kwaśniewska* and *Pereyma,* 2004).

Thermal seasons identification and investigation have long been on the agenda of Polish researchers and have a history of over 100 years. As early as in 19th century, Jastrzembski attempted the recognition of climatic seasons based on thermal thresholds however, using the phenological criterion. *Romer* (1906) utilized names of the seasons which we apply until today, but it was *Merecki* (1915) who can be considered the actual pioneer of such an approach. He identified six climatic seasons: winter, early spring, spring propper, summer, autumn propper and late autumn. The utilized thermal thresholds where 0 °C, 5 °C, and 10 °C, but they referred to the multiannual monthly average temperature (*Nowosad* and *Filipiuk,* 1998). Similar approach was presented by *Bartnicki* (1948). On the other hand, *Wiszniewski* (1960) claims that the proper approach is to identify as much as eight seasons in Poland with an additional 10 °C threshold. Such method was also acknowledged by *Trybowska* (1963) and *Makowiec* (1983). Another division was proposed by *Hess* (1965), but it was restricted to mountain areas with the assumption that the onset of the specific seasons can not be mutual for varying mountain ranges at the same altitude. He also proposed to use as much as 10 seasons. *Woś* (1999) claims that the identification of climatological seasons can not be the same globally, as this should be the result of chosen methodology and geographical location. The four seasons used in Scandinavian countries can serve as an example here (*Czerneckis* and *Miętus,* 2010). A research on thermal seasons in Hornsund seems to confirm the suitability of this approach (*Kwaśniewska* and *Pereyema,* 2004). Methods utilizing daily average temperatures lead to similar results, whereas the usage of monthly means, i.e., a simplified method, does not yield robust results. Such an approach may diverge substantially from the results obtained with other methods. *Piotrowicz* (2000) points out that while defining the date of thermal threshold crossings, multiannual monthly averages are used most often. It is assumed that, the monthly average temperature is much closer to the average daily temperature of the mid-day of a month, and the changes of the temperature are linear. Analytical approach here relies on the formulas devised by *Gumiński* (1950), which were subsequently widely used by others, e.g., *Nowak* (1967), *Stopa* (1968) or *Czernecki* and *Miętus* (2010). *Stopa* (1968), mentioned that the most precise way is to draw a course of multiannual daily averages. However, this method is rarely used as it is time-consuming and laborious as well as it is hard to collect the reliable data from longer periods. *Piotrowicz* (2000) used the TERPOR software in the process which was devised by *Niedzwiedz* and *Limanówka* (1992).

Samborski and *Bednarczuk* (2009) used the division into 8 seasons in the investigation of thermal seasons in Zamość. They counted the number of days above the defined thermal thresholds. In cases when the temperature fell below the tresholds in subsequent days, the authors calculated mean value from the period in question and finally assigned to the proper season.

Czernecki and *Miętus* (2010) used the utilised formulas proposed by *Gumiński* (1948) in the initial phase of their research on the dates of the onset of

seasons in Poland. The authors compared this method with its modified version proposed by Michał Kowalewski in the Atlas of Climate of Poland by *Lorenc* (2005), mentioning that the results might be considered equal, as in the extreme cases the differences between the dates differ by one day. The applicability of Gumiński's formulas was also acknowledged by *Skowera* and *Kopec* (2008), when they used it to delimitate the economical and vegetation periods. Authors also point the cases with no thermal winter or summer. This is a problematic issue as it makes precise identification of the seasons length difficult. In such cases authors propose the approach of symmetric length of neighboring periods.

Czernecki and *Miętus* (2010) indicate that application of multiannual daily average temperatures for periods shorter than a dozen years is dubious. As they point out, this is due to the fluctuations of temperatures which can quickly oscillate of temperature ranges even three seasons. The solution proposed by the authors relies on the 7-day consecutive averages used to smooth the data. Also, they claim that the calculated indicators, which characterize the occurrence of thermal seasons, confirm their usefulness as climate change detection indicators. *Rapp* and *Schönwiese* (1994) point out that the exact date of the onset of thermal seasons and their temporal trends in Germany are assessed. Generally, a late autumn can be determined for the last 50 years, whereas spring seems to come earlier in many places. On principle, a prolongation of the warmer half of the year can be ascertained. *Jaak* and *Rein* (2000) analyzed the spatial and temporal variability of climatic seasons and phenological phases in Estonia. They used the days of onset and the duration of 8 climatic seasons and 16 spring and summer phenological phases at 23 stations in Estonia between 1946 and 1998. Using the thermal thresholds of 0 °C, 5 °C, and 13 °C. They argue that the 15 °C temperature threshold is not a suitable criterion for the summer season in Estonia, as during extremely cold summers, the daily mean air temperature does not exceed this limit for longer period of time. *Hiltunen et al.* (2014) hypothesized that the ambient temperature and the timing of thermal seasons onset might associate with the suicide rate in Finland. As climatological data, they used daily mean, minimum, and maximum temperatures from the local weather stations at the Helsinki-Vantaa, Jyväskylä, and Oulu airports, the dates for the thermal seasons for each study area for each year, and the dates for the astronomical seasons. All the data were provided by the Finnish Meteorological Institute. Authors identified 4 thermal seasons (spring, summer, winter, and autumn) and have used the thermal thresholds of 0 °C and 10 °C. Other Finnish authors (*Ruosteenoja et al.,* 2011) inferred the duration of the seasons and the growing seasons till the end of the 21st century. They are using a high-resolution observational data set covering Finland and an average of the air temperature simulated by 19 global climate models. There are four thermal seasons in Finland expected in the elevated area of northwestern Lapland. Authors predict that under the A2 scenario, thermal winter will disappear in the southwestern part of the country before the period 2070–2099.

In this paper an attempt was made to analyze the long-term (1971–2010) variability of the occurrence of the seasons (onset and length) at selected stations in Poland. The variability of characteristics was also analyzed in individual decades with the aim to identify the differences of seasons characteristics.

2. Data and methods

The analysis comprised the investigation of the general characteristics of the occurrence of the seasons, i.e., their beginning and cessation (and thus the length) with additional insight into tendencies/trends for the period 1971–2010.

The analysis concerns seven meteorological stations: Łeba, Chojnice, Toruń, Łódź, Kielce, Tarnów, and Zakopane (*Fig. 1*). The used meteorological variable is the daily average air temperature (t_d), which originates from the database of the Institute of Meteorology and Water Management – National Research Institute. The criteria for the station selection were as follows. The variability in the overall temporal structure of the occurrence and length of the seasons is the result of the different localization (in climatological context) of regions (*Lorenc,* 2005), therefore, the stations were chosen so that they cover all geographical regions, seacoasts, lakelands, lowlands, uplands, and mountain areas (*Kondracki,* 2002). The selected stations constitute a north-south transect through Poland (*Table 1*), which also reflects the variations in the incoming solar energy – a factor not to be neglected in the analysis of the thermal seasons variability.

Fig. 1. Locations of the stations in Poland.

Table 1. Coordinates and elevation (m a.s.l.) of the stations

Name	Elevation	Latitude	Longitude
ŁEBA	2	54° 45' N	17° 32' E
CHOJNICE	164	53° 42' N	17° 33' E
TORUŃ	69	53° 02' N	18° 35' E
LÓDŹ	187	51° 44' N	19° 24' E
KIELCE	260	50° 49' N	20° 42' E
TARNÓW	209	50° 02' N	20° 59' E
ZAKOPANE	855	49° 18' N	19° 57' E

Identification of the onset and end of the seasons was multistage procedure and the used thermal thresholds were common Romer-type tresholds, i.e., 0 °C, 5 °C, and 15 °C. Daily average temperature (t_d) was used (*Romer*, 1938) as a thermal indicator. Such an approach yields six seasons (*Table 2*).

Table 2. The studied thermal seasons and the air temperature thresholds utilized in the procedure of identification

Season	t_d threshold values
early spring (ESPRING)	$0.0 \,°C < t_d \leq 5.0 \,°C$
spring (SPRING)	$5.0 \,°C < t_d \leq 15.0 \,°C$
summer (SUMMER)	$t_d > 15.0 \,°C$
autumn (AUTUMN)	$5.0 \,°C < t_d \leq 15.0 \,°C$
early winter (EWINTER)	$0.0 \,°C < t_d \leq 5.0 \,°C$
winter (WINTER)	$t_d \leq 0.0 \,°C$

The selection of methodological approach is the crucial one when performing the seasons' onset identification, as differing methods yield varying results, and thus, can limit the possibility of further application.

Data originating from Institute of Meteorology and Water Management – National Research Institute (IMGW-PIB) on average daily air temperature (t_d) were checked for completeness. In the first phase of the study, an attempt was made to determine the thermal seasons based on variability of the long-term average daily air temperature. This method, although indicated in the literature

as the most thorough, proved to be too problematic due to the multiple passing of temperature across the thermal thresholds. In order to eliminate high frequency oscillations, it was decided to use a triangular filter also used for seasons' onset detection by *Nowosad* and *Filipiuk* (1998). Filters of length 3, 5, 7, 9, and 13 were used. However, the results still proved to be unsatisfactory. The frequency of the oscillation of the t_d curve in the vicinity of the threshold temperatures was still too high even for the 13-element filter (*Fig. 2*). Additionally, the use of the filter involved the loss of some data at the beginning and the end of the analyzed time series.
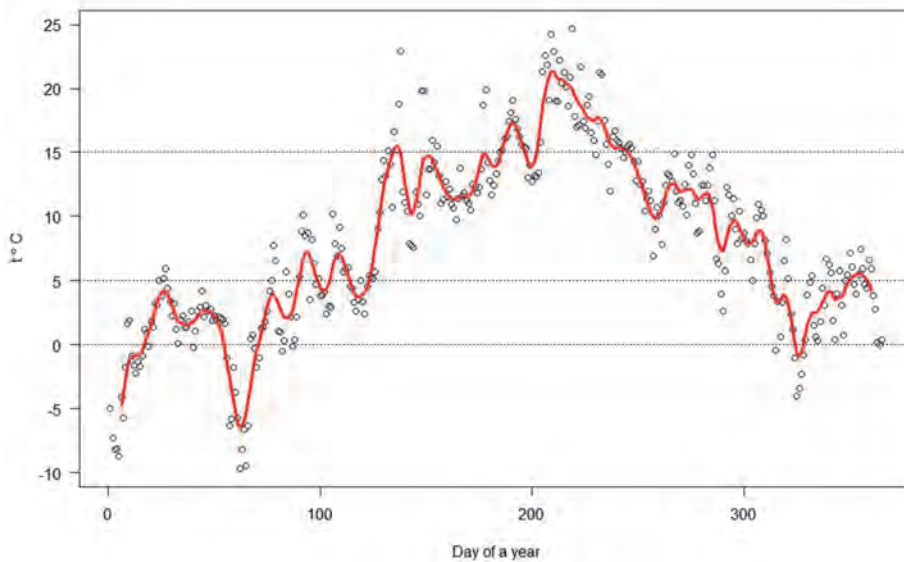
Fig. 2. Annual course of the daily average air temperature (t) with 13-element triangle filter (red line) in Łeba in 1971. Temperature thresholds (0 °C, 5 °C, and 15 °C) are marked with dotted lines.

Next, a finally satisfactory attempt comprised the utilization of 10-day (decadal) and 5-day (pentad) averages. Of course, the last decade and pentad length depend on the month. The overall assumption was that each month has 30 days, and the values of averages are assigned to the midday of the decades and pentades as 5th, 15th, and 25th and 3rd, 8th, 18th, and 28th day, respectively. Such approach allowed the detection of the date of crossing of temperature thresholds. The detection itself was automated with the usage of a linear interpolation scheme.

Dates were assigned to the onset of the seasons. Comparison of those methods (5 versus 10 days averages approach) revealed that the differences between the onset dates were not significant. Additionally, for the analysis with 5-day averages, the threshold crossing problem occurred too often. Finally, the decision was made to use the 10-day (decadal) averages in the procedure of the season onset and end identification.

The growing number of the cases of years without thermal winter or summer resulted in the impossibility to identify the length of those seasons. It was decided to use the approach proposed by *Miętus* and *Czernecki* (2010) which forces the symmetrical length of the spring and autumn (in case of no summer) and has an analogous approach in the case of early winter and early spring (in the case of no thermal winter).

To provide a more formal statistical workframe, the analysis of the decadal variability of the season's onset date and its length was further augmented with the application of ANOVA analysis (*Balicki* and *Makać,* 2007), thus allowing the identification of statistically significant differences in the season's characteristics in decades. Due to relatively small sample size in compared decades (10), it has been decided to treat $\alpha=0.1$ as a satisfactory level to acknowledge significant changes. Also, the relatively high variability of the analyzed indices within decades should be mentioned here as a potential impediment to the recognition of significant differences.

In the course of analysis of thermal seasons' onset, an additional variable was calculated indicating if the onset of the season was early, normal, or late. This was performed on the basis of the comparison of the season onset date (K) in a given year with the onset date quantiles calculated as multiannual characteristic (*Table 3*). The aim of such approach was the identification of possible links between the onset (late, normal, early) and the length of the season.

Table 3. Scheme of season onset classification

Season onset type	Criterion
early	$D < K_{0.33}$
normal	$K_{0.33} < D < K_{0.66}$
late	$D > K_{0.66}$

where D is the onset of a season, $K_{0.33}$ is the multiannual quantile 0.33 of the seasons onset, $K_{0.66}$ is the multiannual quantile 0.66 of the seasons onset, and the D and K are expressed as consecutive days in Julian year.

3. Results

3.1. Seasons' onset

In the period 1971–2010, the onset of thermal early spring occurs in February at all analyzed stations, except Zakopane. On average, at the earliest, the early spring was observed at Toruń and Tarnów stations (February 11) and at the latest at Zakopane station (March 8). Thus, the range between the onset dates of the thermal early spring amounts to 25 days (*Fig. 3*). Moreover, the earliest beginning of the early spring can be dated at December 2, 1994 in Tarnów, whereas the latest beginning of the season was on March 8, 2004 in Zakopane. During the whole analyzed period, the beginning of the early spring was noticed at the latest in Zakopane.
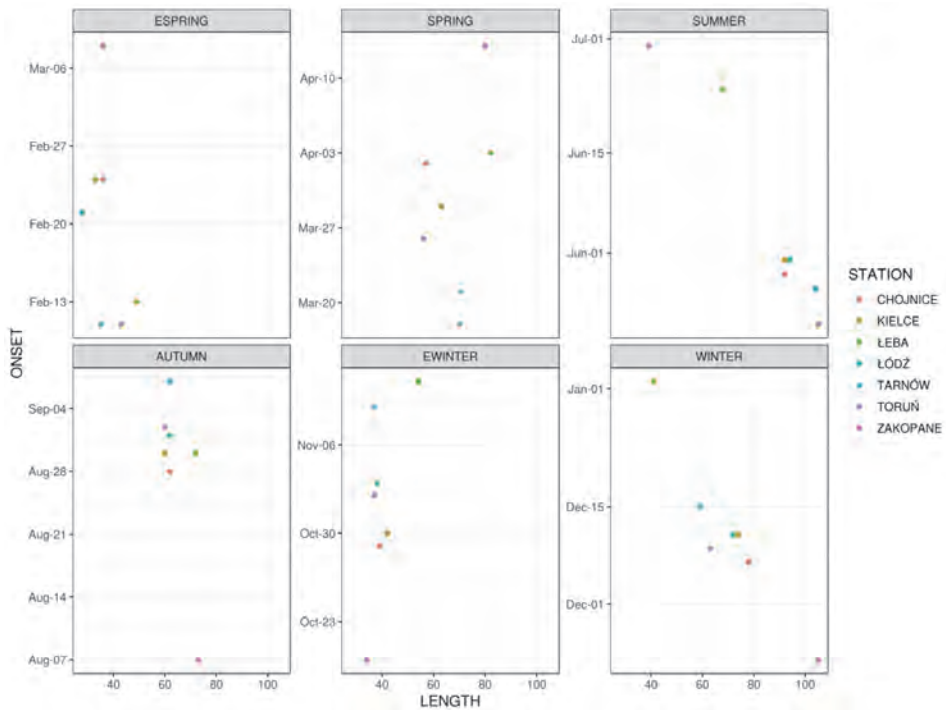
Fig. 3. Average length (days) and onset (month – day) of thermal seasons at selected stations in Poland (1971–2010).

On average, the thermal spring began at the earliest at Tarnów station (March 18), whereas at the latest its beginning could be observed at Zakopane station (April 13). Hence, the range between the beginning dates of the thermal spring builds up to nearly a month. Taking into consideration the analyzed period, the thermal spring began at the earliest at Tarnów and Łeba stations in 1990 (January 24). At the latest it was noticed at Zakopane station in 1980 (May 12). It can be also observed that the thermal spring occurs at the latest at the Zakopane station.

On average, the beginning of thermal summer can be observed at the earliest in Toruń (May 22), whereas at the latest it was noticed in Zakopane (June 30). It can be assumed that the difference between the beginning dates of the season is 39 days. In most cases the thermal summer began at the latest in Zakopane. An interesting fact, that during the analyzed period, the thermal summer did not occur at the Zakopane station (1978, 1990, 2000).

On average, the thermal autumn began at the earliest in Zakopane (August 7). At the latest, however, the thermal autumn can be noticed in Toruń (September 2) and Łódź (September 1) (*Fig. 3*). Hence, it can be calculated that the difference between the earliest and latest beginning dates of thermal autumn amounts to 30 days. Taking into consideration the whole analyzed period, the thermal autumn occurred at the earliest in Zakopane and at the latest in Tarnów. The earliest occurring of thermal autumn can be dated back to 1985 at the Łódź station (June 6). At the latest, it occurred at the Chojnice station in 1975 (September 28).

In most cases, the thermal early winter began at the earliest in Zakopane (October 20) and at the latest at the Łeba station (November 11) (*Fig. 3*). Thus, the difference between the beginning dates of thermal early winter at those two stations equals 30 days. The earliest occurring of the early winter in the analyzed period can be dated back to 1972 in Zakopane (September 24). The latest one was noticed in Łeba in 2002 (January 17). Furthermore, there is the tendency of early winter occurring later every year.

On average, the earliest beginning date of the thermal winter was noticed in Zakopane (November 23). The latest beginning date, however, was observed in Łeba (January 2). Thus, the difference between the two extreme average beginning dates of thermal winter is 52 days. At the earliest, the thermal winter occurred in Zakopane in 1973 (October 10) and at the latest in Łeba in 2000 (February 21). The thermal winter in the analyzed period can be marked by the tendency of occurring later every year. Moreover, it was noted that the thermal winter did not occur twice in the analyzed period, namely in 1974 in Łeba and in 2006 in Tarnów.

Taking into consideration the onset dates of the thermal seasons at the analyzed stations, some regularities can be observed. It can be assumed that the changes in the occurring of the thermal seasons' beginning dates are most likely

to happen at the stations located northernmost and southernmost, namely at the seaside station in Łeba and the mountain station in Zakopane.

Moreover, it can be assumed that at the Zakopane station warm thermal seasons (early spring, spring, summer) occur at the latest among all analyzed stations. However, cold thermal seasons (autumn, early winter, winter) occur in Zakopane at the earliest. Undoubtedly, it is caused by the insolation and orography of the region, as well as by the relatively long snow cover maintenance. Furthermore, the thermal spring is the season that can be marked by the tendency to occur earlier every year.

Long term variability has been described with the usage of decadal means of the thermal seasons' onset dates (*Fig. 4*). Early spring in Chojnice, Tarnów, and Zakopane exhibits small variability with about 4 days differences between the decades. Average onset date in Zakopane fall, at the first decade of March and varies only by 1–2 days. In Tarnów, the onset is in the first half of February and the inter-decadal range is 9 days. The earliest onset occurred in the decade of 1991–2000. Other stations (Łeba, Chojnice, Toruń, and Łódz) exhibit significant shift in the early spring onset date in the 1991–2000 decade. The difference is about 30 days which is accompanied with the latter return to dates observed in the first two decades of the research period. This is most visible in the case of Łeba, where the shift between the decades of 1991–2000 and 2001–2010 was nearly 30 days.
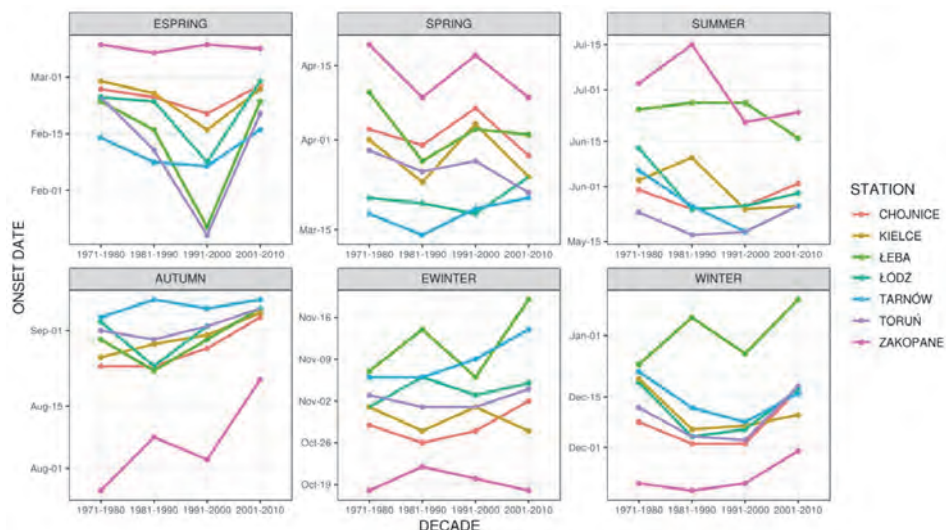
Fig. 4. Average date of the onset (month-day) of thermal seasons in decades at selected stations in Poland (1971–2010).

In case of spring, there is a visible tendency to the earlier occurrence of this season. This trend has marked fluctuations. This is most clearly presented in case of Kielce and Zakopane. The exception are Tarnów and Łódz, where the thermal spring from (March 14) occur consistently later (March 21) int he decade 1981–1990.

The thermal summer occurs earlier. This is especially visible at Zakopane, Kielce, and Łódz. The difference between the 1981–1990 and 2001–2010 decades is nearly 14 days. Also, at other stations (except Toruń), the thermal summer shows the tendency to start earlier. However, the last decade (2001–2010) shows some signs of slowing down of this trend. It may be stated that earlier occurrence of thermal summer can constitute a sign of global warming.

The thermal autumn at all analyzed stations tends to start later. At most of the stations, the overall change between decades is about 8 days. Zakopane reveals the most significant change with the shift of 25 days between the 1971–1980 and 2001–2010 decades.

The thermal early winter (especially at the Łeba and Chojnice stations) in the last decade is marked by a tendency of later occurring. Collaterally, the average time of the thermal early winter occurring in 2000–2010 at the Łódź and Chojnice stations is shorter by 30 and 20 days than in the previous decade, respectively.

The thermal early winter in Łeba is characterized by fluctuations of the onset date with the general tendency to occur later. The total difference equals 12 days. Also, in Tarnów this season reveals a consistent trend to occur later with a total change of 8 days. Other stations do not exhibit apparent tendencies, and the early winter onset falls on the break of October and November. In Zakopane early winter starts between the 18th and 22nd days of October.

The inter-decadal variability of the onset of the thermal winter can be well observed in case of Łeba, Chojnice, and Zakopane. In Łeba the onset tends to occur later with a 18 days difference between the marginal decades. The earliest starting date of the thermal winter In Zakopane in November and the overall onset shift is 11 days. At the other stations the earlier occurrence of winter is in the two middle decades of the research period: 1981–1990 and 1991–2000, and relatively rapid shift occures toward the later onset during the last decade (from 6 to 15 days). The analysis was aided with the application of the ANOVA model with decades as a factor (*Table 4*). Only in autumn, the onset dates differ significantly between decades at 3 stations: Chojnice, Łeba, and Zakopane. Zakopane exhibits significant differences in summer and Łeba in early spring. This suggests that the variability of seasons onset dates do not vary between the decades at least with respect to the average onset.

Table 4. ANOVA significance test results for the season onset types. Statistically significant differences (at alpha=0.1) are marked with "+" sign.

Station	ESPRING	SPRING	SUMMER	AUTUMN	EWINTER	WINTER
CHOJNICE				+		
KIELCE						
ŁEBA	+			+		
ŁÓDŹ						
TARNÓW						
TORUŃ						
ZAKOPANE			+	+		

3.2. Seasons' length

The average duration of thermal summer shows the tendency of elongation (*Fig. 5, Table 5*). In case of Łeba, Kielce, and Zakopane, one can observe an increasing trend. Moreover, it has been noted that in Toruń and Tarnów, thermal summer lasts the longest, when compared to all analyzed stations.

Table 5. Average length (days) of thermal seasons at selected stations in Poland 1971–2010

STATION	ESPRING	SPRING	SUMMER	AUTUMN	EWINTER	WINTER
ŁEBA	49	82	68	72	54	41
CHOJNICE	36	57	92	62	39	78
TORUŃ	43	56	105	60	37	63
ŁÓDŹ	28	71	94	62	38	72
KIELCE	33	63	92	60	42	74
TARNÓW	35	70	104	62	37	59
ZAKOPANE	36	80	39	73	34	105

According to a study of the Institute of Meteorology and Water Management (IMGW) in Kraków, Tarnów is considered to be the Polish „heat pole". The IMGW[1] (2000) study includes data from the period 1977–2006, which is concurrent with the period analyzed in the present paper. Furthermore, the findings of the present study are also coincident with those of the IMGW study. One of the findings is that the thermal summer is stated to last the longest in

---

[1] Instytut Meteorologii i Gospodarki Wodnej

Poland. The reason of the aforementioned situation might be a relatively pronounced exposure to sun in Poland (the average year insolation equals 1573 hours), the influence of the mountain foehn wind (Tatra Mountains) and the predominant west and south advection. The thermal winter shows, however, completely different tendency, when compared to the thermal summer. The most illustrative example is Łeba station, where the thermal summer is becoming longer over decades, whereas the thermal winter is shortening significantly (especially in the period of 1971–2000).
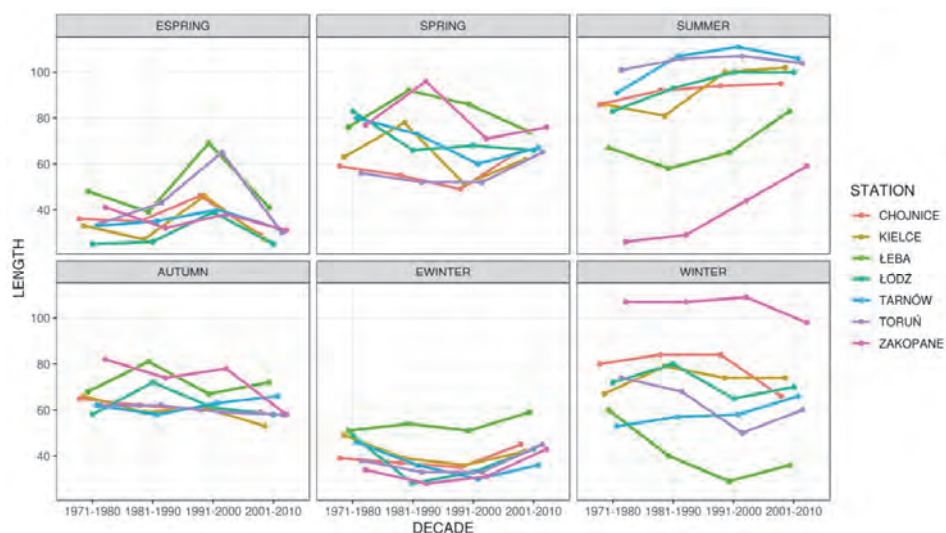
Fig. 5. Length (in days) of the thermal seasons at selected stations in Poland int he period 1971–2010.

The variability of the thermal winter is explicitly visible at the Chojnice station, where the average thermal winter duration has shortened by circa 14 days when compared to the previous decades. It can be also observed at the Zakopane station, where the thermal winter, for the first time, lasted less than 100 days in the decade from 2001 to 2010.

Furthermore, Tarnów station can be characterized by the fact that it is the only one among all the analyzed stations where thermal winter duration is successively lengthening. The ANOVA test suggests (*Table 6*) that in summer the length of this season had significant differences in mean in the different decades in Kielce, Łeba, Tarnów, and Zakopane. In spring the differences in thelength differed significantly only in Kielce and for early spring in Łeba and Toruń.

Table 6. ANOVA results for season lenght versus decade setting at selected stations in Poland in the period 1971–2010. Statistically significant differences between decades (at alpha=0.1) are marked with "+" sign

Station	ESPRING	SPRING	SUMMER	AUTUMN	EWINTER	WINTER
CHOJNICE						
KIELCE		+	+			
ŁEBA	+		+			
ŁÓDŹ						
TARNÓW			+			
TORUŃ	+					
ZAKOPANE			+			

3.3. Seasons' onset date versus duration

The onset characteristics (early/normal/late) of the season may determine the length of the season to some extent (*Fig. 6*). The general rule that can be acknowledged is the earlier the onset, the longer the season's duration. This, however, manifests itself clearly only in certain seasons and usually can be blurred by the dispersion if the data values are around the mean. In case of early spring, those differences are clearly visible at all stations There is a visible shift towards longer duration with the earlier onset. This, however, is not uniform at all the stations. It is mostly visible in the northern part of Poland (Łeba, Chojnice), where the difference in length between the late and early onset is nearly 60 days. There is no apparent (about 10 days) difference in length in case of the late/normal pair. Those differences tend to diminish southward and in Tarnów and Kielce the late/early discrepancy is about 35 days. Generally, the late onset of the season results in a very short season duration with mean values ranging from 15.6 days in Tarnów to 26.4 days in Łeba and 28.2 days in Toruń. The differences in case of the early/normal/late onset comparison are the smallest in Zakopane.

In spring, the length duration differences are much less indicated and tend to express themselves only in the northern Poland (Łeba and Chojnice) and Zakopane with means in Łeba ranging from 69.7 days (late onset) to 93.9 days (early onset). In central Poland, despite the fact the that differences in mean length values are recognisable, the flattening of the distributions makes those hardly recognizable.
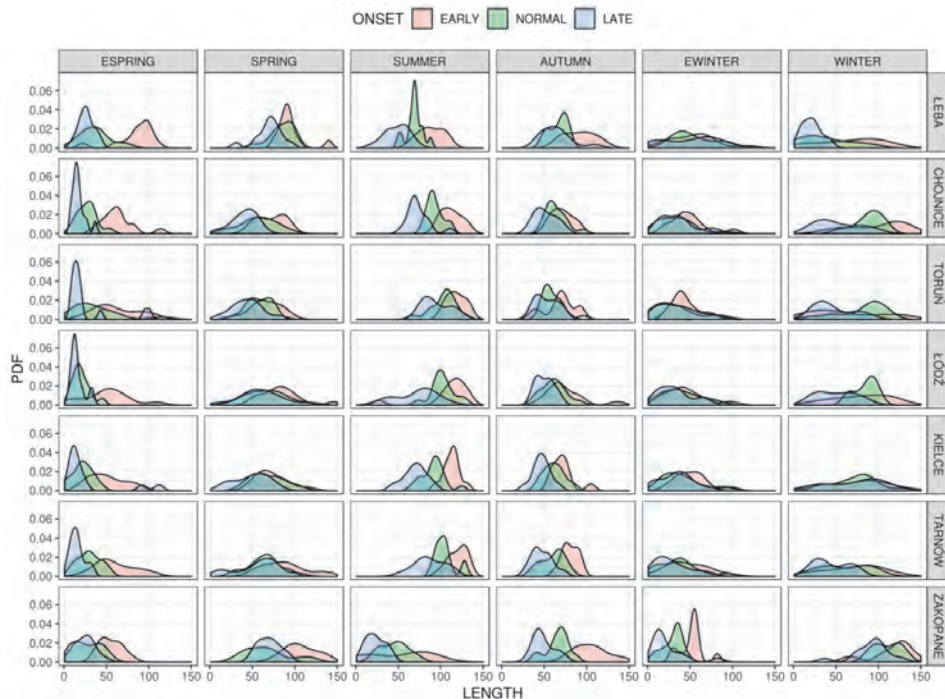
Fig. 6. Kernel density estimates for the length of the thermal seasons versus their onset characteristics at selected stations in Poland in the period 1971–2010.

Summer is another season when the onset determines the duration to a great extent. This is manifested not only in the shift of the mean season length, but also in the higher concentration of the values around the mean. The difference in length between the early/late onset is ranges from 23 in Toruń to 41 days in Łeba and 43 in Kielce.

Autumn reveals slightly smaller differences than summer. Generally, at most stations from northern and central Poland, the differences in the mean season duration between the early and late onset, only in Łeba exceed 25 days (27), while at the other stations they vary from 15 days in Toruń to 24 in Kielce. The differences exceed 30 days only in Carpathian Mountains in Tarnow and Zakopane (33 and 55 respectively).

The early winter slightly resembles the spring with small differences in mean season length especially in Łeba (5 days) and Toruń (10 days). Higher differences are recorded in Kielce and Tarnów (18 and 19 days, respectively). Also, here one can notice greater dispersions, which effectively diminishes the importance in the mean differences. This picture is somehow different only in Zakopane. Here the difference in mean length between early and late onset equals to 28 days which is

unprecedented at any other station for this season. Also, the dispersion of the season's length distribution is much less pronounced here.

In winter the differences in seasons' length are the most pronounced in northern Poland, where in Łeba and Chojnice they exceed 40 days (44 and 45 days, respectively). In Toruń, the difference is only 15 days with a visibly shifted normal onset length towards longer duration (the mean is 20 days higher than in the case of the early onset). This feature is also present in Łódz (4 days longer than for the early onset). In Kielce, there is virtually no difference between the length means (the range is 0.4 days). In Tarnow and Zakopane, the difference between the early/late onsets is quite similar and equals to 25 days.

4. Discussion and summary

The utilized method allowed unequivocal determination of the onset (and thus, duration) of the thermal seasons in Poland. The analyzed period in the aforementioned work (*Skowera* and *Kopeć*, 2008) concurs with the period studied in the present research. Comparison of the onset dates of the thermal periods at the Tarnów station show that the differences do not exceed 3 days (in spring), thus the resulting outcome may be that there is no significant difference (especially in long term analysis) between the decadal approach (utilized in the present research) and simpler methods utilizing monthly averages. Other authors used area average temperatures in the determination of the seasons onset for broader regions. To indicate the thermal seasons in the area of coast and highland, *Czernecki* and *Miętus* (2010) have used the area average obtained on the basis of the Alexanderson formula. To indicate the onset dates of the thermal seasons, the authors have used two methods, namely: the method proposed by Gumiński concerning the increase and decrease of temperature based on monthly averages, and the method utilizing weekly consecutive means. The analysis was applied to the 1951–2008 period. The authors have used the division to 6 thermal seasons, which is concordant with our research.

In case of Kielce versus Highland area, the obtained average onset dates of the thermal seasons differ by 7 days in the case of early spring, 1 day in the case of spring, 3 days in the case of summer, 4 days in the case of autumn, 8 days in the case of early winter, and 7 days in the case of winter. For Łeba station the results show similar differences. Average beginning dates of the thermal seasons differ from each other by 8 days in the case of early spring, 5 days in the case of spring, 6 days in the case of summer, 7 days in the case of autumn, 0 days in the case of early winter, and 3 days in the case of winter. Taking the differing approaches into consideration (the longer period of analysis in the study of *Czernecki* and *Miętus* (2017)), it can be stated that the findings of both works are relatively similar.

All in all, the beginning dates of the thermal seasons indicated in the present study are concurrent with those obtained by other authors. The greatest concurrence

can be found in the beginning dates of the thermal seasons for Tarnów station, which were compared with the dates indicated by *Skowera* and *Kopeć* (2008). It is worth mentioning, that all analyzed works used in the present comparison have implemented various methodologies and focused on different periods.

The analysis of seasons onset and length in 1971–2010 in Poland has allowed us to observe some regularities. In 1991–2000, the average early spring onset at all stations except Zakopane occurred earlier comparing to the 1981–1990 period. In addition, in 1991–2000, the average duration of early spring has been the longest one. The aforementioned situation coincides with the average later spring onset in 1991–2000 and its relatively short duration. The thermal summer is the season that shows visible tendencies for earlier onset and lengthening of its duration. It can be particularly well shown on the basis of the stations located in the north (Łeba) and in the south (Kielce and Zakopane). Łeba and Zakopane can be also characterized with the latest summer onset as compared with all the other stations. It can be influenced by the proximity of the Baltic Sea in the north and the altitude of Zakopane (above 900 m a.s.l.). Moreover, the thermal autumn can be characterized by a progressively later onset in the whole area of Poland. The aforementioned situation is clearly illustrated by the example of Zakopane, where the difference between the average thermal autumn onset between the decades 1971–1980 and 2001–2010 equals to 25 days. The influence on the shift of thermal autumn onset has been certainly exerted by a progressively lengthening the thermal summer duration. The length of thermal autumn does not show any noteworthy tendencies. The thermal early winter is the season that can be characterized by the averagely shortest duration when compared with the other seasons. At the Łeba, Toruń, Chojnice, Łódź, and Tarnów stations, the thermal early winter shows the tendency to occur progressively later, whereas at the Kielce and Zakopane stations, the situation is quite contrary. Variability in the thermal winter onset and length, exactly as in case of the thermal summer, can be clearly seen at the stations most distant to each other. The progressively later thermal winter onset is coincident with its progressively shorter duration at the Łeba, Chojnice, Toruń, and Zakopane stations. On average, the thermal winter begins at the latest in Łeba, and it also lasts for the shortest period (the average minimum of 20 days in 1991–2000). On average, thermal winter begins at the earliest in November at Zakopane station. Zakopane is also the station, where the thermal winter lasts for the longest period (over 100 days).

References

Balicki, A. and *Makać, W.*, 2007: Metody wnioskowania statystycznego, Wydawnictwo Uniwersytetu Gdańskiego. (In Polish)
Bartnicki, L., 1948: O porach roku i o osobliwościach klimatu Polski, Gazeta Obserwatora Państwowego Instytutu Hydrologiczno-Meteorologicznego, Warszawa, I, 4, 1–6. (In Polish)

Czernecki, B. and *Miętus, M.,* 2010: Wstępna analiza występowania i zmienności termicznych pór roku w wybranych regionach Polski na przykładzie Pasa Pobrzeży Południowobałtyckich i Wyżyn Polskich, Klimat Polski na tle Klimatu. Warunki termiczne i opadowe. *Bogucki Wydawnictwo Naukowe. 15*,. 9–26. (In Polish)

Czernecki, B. and *Miętus, M.,* 2017: The thermal seasons variability in Poland, 1951–2010. *Theor. Appl. Climatol. 127*, 481–493. https://doi.org/10.1007/s00704-015-1647-z

Gumiński, R., 1948: Próba wydzielenia dzielnic rolniczo-klimatycznych w Polsce. *Prz. Met. Hydr. 1,* 7–20. (In Polish)

Gumiński, R., 1950: Ważniejsze elementy klimatu rolniczego Polski południowo-wschodniej. W*iadomości Służby Hydrologicznej i Meteorologicznej, 3*, 57–113. (In Polish)

Hess, M., 1965: Piętra klimatyczne w Polskich Karpatach Zachodnich, Zesz. *Nauk. UJ. Prace Geogr., 11.* (In Polish)

Hiltunen, L., Haukka, J., Ruuhela, R., Suominen, K., and *Partonen, T.,* 2014: Local daily temperatures, thermal seasons, and suicide rates in Finland from 1974 to 2010. *Environ. Health. Prevent. Medic. 19,* 286–294. https://doi.org/10.1007/s12199-014-0391-9

IMGW, 2000: Charakterystyka wybranych elementów klimatu Tarnowa, IMGW- Kraków. (In Polish)

Jaak, J., and *Rein, A.*, 2000: Space-time variations of climatic seasons and their correlation with the phenological development of nature in Estonia. *Climate Res. 15,* 207–219. https://doi.org/10.3354/cr015207

Kondracki J., 2002: Geografia regionalna Polski, PWN, Warszawa. (In Polish)

Kwaśniewska, E. and *Pereyma J.,* 2004: Termiczne Pory roku w Hondurasie (SW Spitsbergen), *Problemy Klimatologii Polarnej 14*, 157–169. (In Polish)

Lorenc, H. (ed.), 2005: Atlas klimatu Polski. IMGW, Warszawa. (In Polish)

Makowiec, M., 1983: Wyznaczanie termicznych pór roku. *Pr. Geofizyc. 28,* 209–220.(In Polish)

Merecki, M., 1915: Klimatologia ziem Polskich, Księgarnia Gebethnera i Wolffa, Warszawa. (In Polish)

Niedźwiedź, T., and *Limanówka, D.,* 1992: Termiczne pory roku w Polsce. Zesz. Nauk. Uniw. Jagiell. *Pr. Geogr. 90.*, 53–69. (In Polish)

Nowak, M., 1967: Termiczne pory roku na obszarze województwa olsztyńskiego, Zesz. Geogr. WSP w G*dańsku, R. 9*, 257–266. (In Polish)

Nowosad, M. and *Filipiuk, E.,* 1998: Zmiany czasu trwania termicznych pór roku w Lublinie w latach 1951–1995, Acta Universittatica Lodziensis. Folia Geographica Physica 3. (In Polish)

Piotrowicz, K., 2000: Zróżnicowanie termicznych pór roku w Krakowie, Prace Geograficzne., *UJ Kraków, z. 105*, 112–122. (In Polish)

Rapp, J. and *Schönwiese, C.D.,* 1994: "Thermishe jahreszeiten" als anschauliche Charakteristik klimatischer Trends. *Meteorol. Z. 3,* 91–94. (In German)

Romer, E., 1906: Zimia. Geografia fizyczna ziem polskich. In]Polska Obrazy i Opisy, t. 1, Wydawnictwo Macierzy Polskiej. (In Polish)

Romer, E., 1938: Pogląd na klimat Polski. Czas. Geogr., t. 16, 193-224, also Wybór prac, t. III PTG/ PWN, Warszawa 1962, 389–361. (In Polish)

Ruosteenoja, K., Räisänen, J., and *Pirinen, P.*, 2011: Projected changes in thermalseasons and the growing season in Finland. *Int. J. Climatol. 31*, 1473–1487. https://doi.org/10.1002/joc.2171

Samborski, A. and *Bednarczuk, J.*, 2009: Termiczne pory roku w okolicach Zamościa w latach 2001– 2008. *Acta Agrophysica 14*, 187–194. (In Polish)

Skowera, B. and *Kopeć,* 2008: Okresy termiczne w Polsce Południowo-Wschodniej (1971-2000). *Acta Agrophysica 12*, 517–526. (In Polish)

Stopa, M., 1968: Temperatura powietrza w Polsce, *Dokumentacja Geograficzna 2*, PAN, Warszawa. (In Polish)

Trybowska, E., 1963: Klimatologiczne pory roku w Rabce Zdroju, *Przegl. Geofiz., R. 8*, 151–154. (In Polish)

Woś, A., 1999: Klimat Polski, PWN, Warszawa. (In Polish)

Wiszniewski W., 1960: Kilka uwag o meteorologicznych porach roku w Polsce w świetle średnich wieloletnich wartości temperatury, *Prz. Geofizycz. 5,* 31–39. (In Polish)

IDŐJÁRÁS

Predicting future shift of drought tolerance zones of ornamental plants in Hungary

Ákos Bede-Fazekas[1,2,*] and **Krisztina Szabó**[3]

[1]*MTA Centre for Ecological Research,*
Institute of Ecology and Botany,
H-2163 Vácrátót, Alkomány u. 2-4., Hungary

[2]*MTA Centre for Ecological Research,*
GINOP Sustainable Ecosystems Group,
H-8237 Tihany, Klebelsberg Kuno u. 3., Hungary

[3]*Szent István University,*
Faculty of Landscape Architecture and Urbanism;
H-1118 Budapest, Villányi út 29-43., Hungary

* *Corresponding author E-mail: bede-fazekas.akos@okologia.mta.hu*

Abstract— Climate of Hungary, Central Europe, is predicted to undergo substantial aridification by 2100 due to the decrease of precipitation in the summer season. Dendrology and ornamental plant application require adaptation to these climatic changes. This paper aims at giving guidance for landscape architects, dendrologist, and horticulturists by providing spatial predictions on both drought tolerance zones of ornamental plants and the amount of needed irrigation (i.e., precipitation deficit). Future climate of two prediction periods (2025–2050, 2071–2100) are compared to that of the reference period (1961–1990), based on regional climate model RegCM3 driven by IPCC SRES scenario A1B. Three drought tolerance zones are studied that are found to shift northward in the future. It is predicted that, by the end of the 21st century, the less drought tolerant ornamental plants applied countrywide nowadays will lose the chance to survive without considerable irrigation efforts in Baranya, Bács-Kiskun, and Csongrád counties (southern Hungary). Since nursery production is now located in those regions that may be mostly affected by aridification, it needs planning adaptation measures.

Key-words: climate change, drought tolerance, dendrology, predictive ecological model

1. Introduction

Hungary's ornamental plant production is noteworthy: the number of cultivated species and cultivars exceeds 4000. The predicted future warming of the Hungarian climate and the increasing aridity will affect ornamental plant production (*Schmidt*, 2006) and plant application as well (*Bede-Fazekas*, 2017). Changing climate forces us not only to apply new species, cultivars, and even cultivation methods (e.g., plant protection against new pests and diseases, economical irrigation, etc.) but also to eliminate those species and genera from the list of recommended plants that prefer humid and wet environment (e.g., *Chamaecyparis, Hydrangea, Hypericum, Magnolia; Szabó* and *Bede-Fazekas,* 2012). The direct negative impacts of aridity on horticultural plants include the unfavorable shift in phenology (the time and length of flowering, fruiting, defoliation, etc.), in pollination, problems in nutrients intake, decrease of lifespan, or even the death of plants (*Soltész et al.,* 2011; *Bede-Fazekas et al.,* 2015, *Bede-Fazekas,* 2017). In Hungary, selection of stress tolerant ornamental plants has started in the 1950's with taxa *Sorbus*, *Tilia*, *Fraxinus*, *Cornus*, and *Juniperus*. The continuation of this research on cultivar selection, and especially that of the drought tolerant cultivars, may get even more importance during the struggle against aridity and seems to became essential in the future (*Szabó* and *Bede-Fazekas,* 2012). Besides using native species, the newly introduced alien taxa might also enrich the assortment.

Climatic perspectives are important from the point of view of landscape architecture, horticulture, and maintenance as well. The application of drought-tolerant plant species can help decreasing the frequency and quantity of required irrigation. Thus, total cost of afforestation or planting may be reduced. Only 27% of the easily obtainable ornamental plant species of Hungary are drought-tolerant ones (*Szabó* and *Bede-Fazekas,* 2012).

Hungary is located in the temperate zone, on the border of different climatic subzones. A Mediterranean-like climate is predominant in the south and southwestern parts, while the continental climate features are dominant in the eastern parts, and atlantic climate features influence the western counties. The southern and southeastern parts are rich in submediterranean species. Due to the geographic position of the Carpathian Basin, the mean temperature of Hungary is slightly higher than that of the areas on the same latitude. Topography of Hungary is relatively uniform: on a large scale, there is no significant difference in the climate of the regions (*Bacsó*, 1966).

The sum and distribution of precipitation is a limiting factor that may become more important for the future plant application than for nowadays. The dry areas of Hungary are situated in central territories of the Pannonian Plain, where average annual rainfall is under 500 mm and the number of summer days is outstanding (85) (*Steinhauser,* 1970; *Pálfai,* 2002). Approximately 90% of the territory of Hungary is endangered with aridity, and only the western parts of Hungary are free from aridity (*Vermes et al.*, 2000). The aridity problem will grow in the future,

which one has to think about, and prepare for, in terms of plant application. These findings are in accordance with current aridity maps (*Steinhauser*, 1970; *Pálfai*, 2002) and predictions (*Bartholy* and *Pongrácz,* 2005; *Sheffield* and *Wood*, 2008; *Lakatos et al.*, 2011; *Bartholy et al.,* 2013; *Pongrácz et al.,* 2014).

Future climate change is predicted to greatly affect Hungary. Although the increase of the annual and seasonal temperature is predicted by global and regional models in great agreement, the change in precipitation sum and monthly precipitation distribution is highly uncertain (*Torma*, 2011; *Van Oldenborgh et al.*, 2013; *Pongrácz et al.,* 2014). The country is located between the northern and southern parts of Europe, where annual precipitation sum is predicted to increase and decrease, respectively (*Van Oldenborgh et al.*, 2013). According to the model ensemble of the FORESEE database (*Dobor et al.*, 2015), precipitation sum of Central Europe might decrease by 3% by the end of the 21st century. The frequency of extreme drought events in Hungary is predicted to increase, mainly in summer and spring, according to an ensemble of 11 models (*Pongrácz et al.*, 2014).

According to RegCM and Aladin regional climate models, annual mean temperature of Hungary may increase by 1–2 °C and 3–5 °C by the periods 2021–2050 and 2071–2100, respectively (*Sábitz et al*., 2015). RegCM predicts moderate warming (<1 °C) in summer and fall for the near future period, but, in agreement with Aladin model, increase of the temperature of these seasons is more pronounced by the end of the century (*Torma*, 2011; *Sábitz et al.,* 2015). For annual precipitation, RegCM is much more pessimistic than Aladin for the period 2021–2050, while their order change if period 2071–2100 is studied (*Sábitz et al.,* 2015). According to RegCM, while most part of the country, and most of all the southern parts, will suffer from precipitation decrease in the near future period, almost one third of Hungary will undergo increase of precipitation (*Torma* 2011; *Sábitz et al.,* 2015).

Similarly to the findings of *Bartholy et al* (2008) on a model ensemble, RegCM predicts the decrease of monthly variability of the precipitation: summer, which is now the wettest season, will undergo an aridification, while the driest winter may get more precipitation in the future (*Torma* 2011; *Sábitz et al.,* 2015). Expected temperature and precipitation changes are confirmed by the prediction of *Belda et al.* (2015).

Climate of Hungary in the period of 2011–2040 is predicted to be similar to the past (i.e., 1961–1990) climate of South Romania, North Bulgaria, North Greece, Serbia, and Macedonia. In the period of 2071–2100 it is expected to be analogous with the North Africa region (*Horváth,* 2008).

In this paper we aimed to locate drought-tolerance zones that relate to the three drought-tolerance categories specified in our previous study (*Szabó* and *Bede-Fazekas*, 2012) and to predict future shift of these zones. Moreover, we aimed to support maintenance planning with maps of predicted water deficit (needed amount of irrigation water).

2. Materials and methods

2.1. Definition of drought tolerance zones

Drought tolerance categories were defined in a way that enables them to serve as proxies for the 3-class classification of the plant material of the most important Hungarian nurseries according to *Szabó* and *Bede-Fazekas* (2012). Aggregated species list of the category 'drought tolerant' of *Szabó* and *Bede-Fazekas* (2012) and the related categories '1-1', '1-2', '1-3', and '1-4' of climate-species matrix defined by *Roloff et al.* (2009) are available from the Supplementary Material S1. Suitability of the listed species for dry habitats were checked against finding in other sources (e.g., *Krüssmann*, 1977; *Retkes* and *Tóth*, 2004, 2015; *Tóth* 2012; *Schmidt et al.*, 2013).

Calculation of the three drought tolerant zones is based on indicator functions, Eqs. (1–3), that result in 1 (true value) if the mean of maximum temperature of summer months and the precipitation sum of the vegetation period are larger/smaller than certain values. These values (24.0 °C, 25.5 °C, and 290 mm, 330 mm) were selected to fulfill our secondary aim, that was the separation of the territory of Hungary in a way, that results in three subterritories comparable to each other in terms of their area.

$$I_1^p = \left(\frac{\sum_{m \in [6,8]} Tmax_m^p}{3} > 25.5\,°C \right) \wedge \left(\sum_{m \in [4,9]} P_m^p < 290\,mm \right) \qquad (1)$$

$$I_2^p = \left(\frac{\sum_{m \in [6,8]} Tmax_m^p}{3} > 24.0\,°C \right) \wedge \left(\sum_{m \in [4,9]} P_m^p < 330\,mm \right) \wedge \neg I_1^p \qquad (2)$$

$$I_3^p = \neg I_1^p \wedge \neg I_2^p \qquad (3)$$

In Eqs. (1–3), I_n^p is the indicator function of drought tolerant zone n ($n \in [1,3]$) in the period p ($p \in [1961-1990, 2021-2050, 2071-2100]$). $Tmax_m^p$ and P_m^p mean are the maximum temperature and precipitation, respectively, of month m averaged in the period p.

2.2. Data and software

Climatic data from the reference period (1961–1990) and the prediction periods (2025–2050, 2071–2100) were derived from the downscaled RegCM3 regional climate model (*Torma et al.,* 2008, 2011), one of the high-resolution RCMs of the project Central and Eastern Europe Climate Change Impact and Vulnerability Assessment (CECILIA). RegCM is based on the IPCC SRES scenario A1B (*Nakićenović* and *Swart*, 2000). Daily maximum ground temperature and daily precipitation were obtained from the grid with horizontal

resolution of 10 km, and monthly means of maximum temperature and sums of precipitation were calculated and then averaged in the three studied periods. Instead of observed climatic data, modeled data were used in case of the reference period, and no bias correction of the modeled future data were done, since the aim of this study was a comparison of drought tolerance zones and the detection of future change, rather than analysis of future climate. Hence, our results are not comparable to those of studies based on observed climatic data and bias corrected model results.

Modeling and displaying of the results were done by ESRI ArcGIS 10.0 geoinformation software, and statistics were calculated by R statistical environment (R Core Team, 2014). Data Management and Spatial Analyst extensions of ArcGIS, and packages sp (*Pebesma* and *Bivand*, 2005; *Bivand et al.,* 2013), rgdal (*Bivand et al.*, 2014), raster (*Hijmans,* 2015), and maptools (*Bivand* and *Lewin-Koh*, 2015) of R were used.

2.3. *Modeling the shift and precipitation deficit of drought tolerance zones*

Modeling the shift of drought tolerance zones was started by calculating the mean of summer maximum temperature and sum of precipitation of the vegetation period in case of all the grid points and the three studied periods. It was done by creating two new columns of float number format and calculating the values using a Python script. The new values were interpolated with inverse distance weighted (IDW) method, using cell size 0.01 decimal degrees (of WGS-84 geographic system), 2nd power and 12 neighbor variables. The drought tolerance zones were identified by the Raster Calculator tool.

Modeling the precipitation deficit of drought tolerance zones was based on the previously calculated and interpolated precipitation sum of the vegetation period. The values were displayed with manually set categorization according to the difference between the limiting value of the drought tolerance category and the modeled values. Temperature and precipitation limits were displayed based on the Contour tool of the Spatial Analyst extension.

2.4. *Statistics on precipitation and the ratio of zones*

Calculation of statistics was started by setting up the geoinformation environment in R (loading packages, opening data, transforming data in order to their projection math each other). Then masking of the raster of the drought tolerance zones and the precipitation sum of the vegetation period by the polygons of counties was done. Minimum, maximum, mean, and standard deviation of precipitation, and area ratio of the three drought tolerance zones within the counties were calculated in iterative way. Results were exported to shape files in order to display them in ArcGIS.
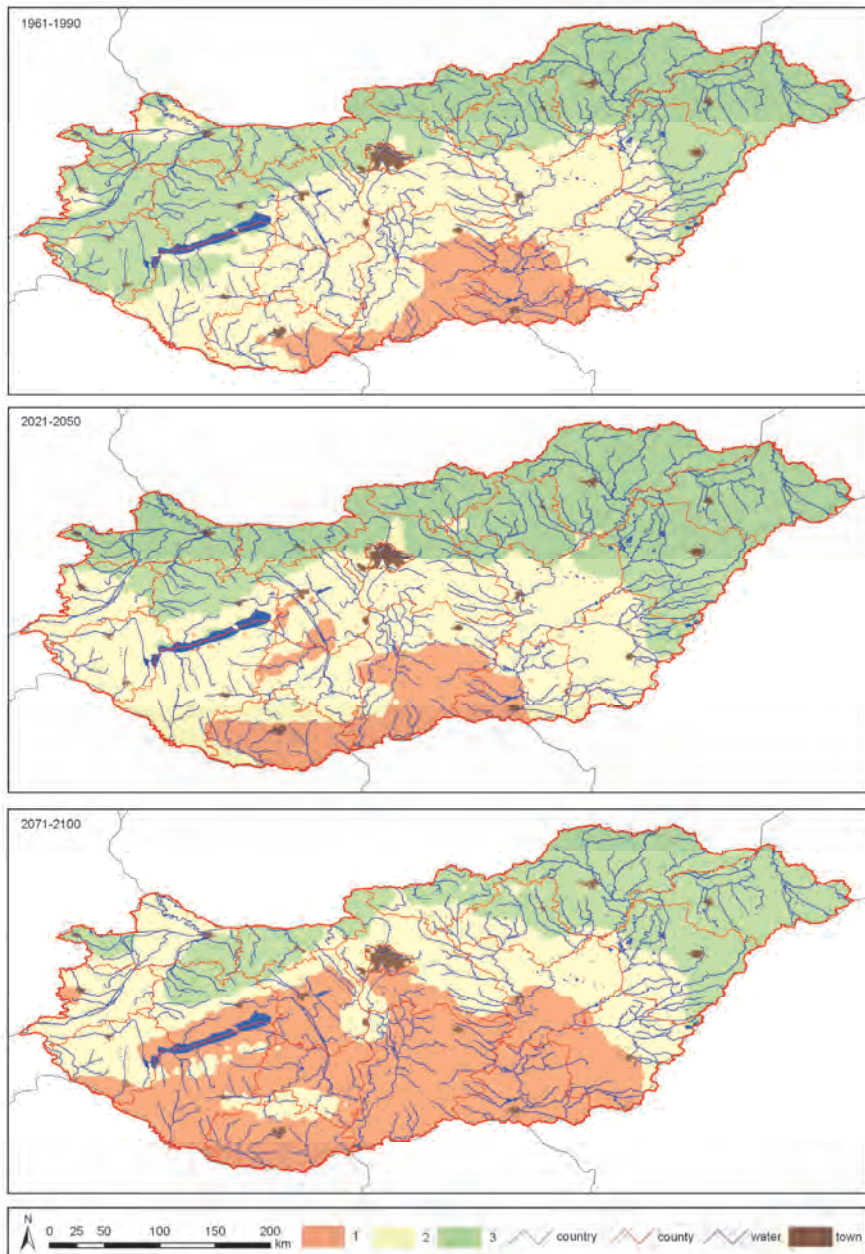
3. Results

3.1. Shift of drought tolerance zones

Drought tolerance zones are predicted to shift northward during the 21st century in accordance with the global and regional climate predictions. The extension and situation of the zones (*Fig. 1*) are found to change much more by the far future (2071–2100) period than by the near future (2021–2050). Zone 1 is found in the southern part of Hungary in the reference period, and is predicted to become fragmented but not undergo expansion by the near future period. By the end of the century, it is predicted to double its area by incorporating almost the entire territory of Somogy, Baranya, Tolna, Bács-Kiskun, and Csongrád counties, embracing the lake Balaton and reaching Budapest from south. The most noteworthy northward expansion of zone 1 is predicted to occur in the western part of the country (Dunántúl) by reaching Szombathely (Vas County) in the far future period.

Drought tolerance zone 2 is delimited from the zone of least tolerant ornamental plants (i.e., zone 3) by the lake Balaton, Budapest, and Hortobágy (Hajdú-Bihar County) in the reference period. An isolated part is found in the northwestern corner of the country, which is predicted to become wetter in 2021–2050 (i.e., will belong to zone 3). In the near future period, while remarkably northward shift of zone 2 can be observed in Vas and Zala counties (western Dunántúl), its seems to stand in its place in the eastern parts. In the far future period, zone 2 may reach the north border of Hungary. Some territories, e.g., Mecsek Mountains (Baranya and Tolna counties) and the touch of Fejér and Bács-Kiskun counties (south to Budapest), are predicted to consistently belong to zone 2 from 1961 to 2100.

Zone 3, the zone of the least drought tolerant species, covers the northern parts of the country in the reference period, and gradually moves back to the northeastern region by abandoning Zala, Vas, and the half of Győr-Moson-Sopron counties in the future periods. Zone 3 is not predicted to change substantially in the eastern region (Tiszántúl). While in the reference period, the zone includes most parts of Hungary of high altitudes, Dunántúli Mountains seems to suffer a considerable aridification: zone 2 will reach it in the near future, and zone 1 in the far future period. Northern Mountains are predicted to be much less affected.

Fig. 1. Drought categories 1, 2, and 3 (see detailed in Section 2) in the reference period (1961–1990, top) and the two prediction periods (2021–2050, center; 2071–2100, bottom).

3.2. Precipitation deficit of drought tolerance zones

Results on precipitation deficit foreshadow that in case of the zone of the less drought tolerant ornamental plants, i.e., zone 2 and zone 3, the needed irrigation water quantity will gradually grow by the end of the 21st century. Although the precipitation deficit shows southward increase throughout the country, this zonality is most easily observed in the eastern part of Hungary.

By studying precipitation deficit relative to zone 3 (*Fig. 2*), one can estimate the impact of future climate change on the irrigation needs of the least drought tolerant ornamental species. While in the reference period, precipitation deficit is under 50 mm almost everywhere in the country, southern regions and the surroundings of the lake Balaton are predicted to suffer greater deficiency both in the near and the far future prediction periods. The most precipitation deficient areas, i.e., where more than 70 mm irrigation will be needed, occur in limited parts of Bács-Kiskun and Baranya counties in 2021–2050, while they are predicted to expand substantially by the period 2071–2100 and contain half of Csongrád County. Precipitation deficit in the near future period may reach 60 mm in the region which belongs to zone 3 in the reference period. This sudden change will affect the western part of Hungary, most of all the surroundings of the lake Balaton. In most of the other deficient regions, substantial change between the reference and near future periods is not predicted. Areas of the contraction of zone 3 between the two future periods, i.e. mostly northwestern Hungary, will suffer much less deficit (0–20 mm) in 2071–2100. Not considering the border of zone 3, the least aridification is predicted to occur in Mecsek Mountains (Baranya and Tolna counties). Results imply that despite the slow and minor changes by 2021–2050 in great part of the country, Baranya and Veszprém counties will undergo a substantial and rapid aridification. Change in Baranya County is contradictory: the smallest and largest deficit occur within 50 km distance from each other. By the end of the century, the aridification may become more expanded and more considerable in most of those parts of Hungary that does not belong to zone 3.

While precipitation deficit relative to zone 2 (*Fig. 3*) is less than 20 mm everywhere in the reference period, it can exceed 30 mm in one southern county (Baranya) in the near future prediction period, and two more counties (Bács-Kiskun and Csongrád) in the far future period. Surroundings of the lake Balaton is predicted to suffer even more than 30 mm deficit in 2071–2100. 0–20 mm deficit is predicted in the period 2021–2050 for those regions that are abandoned by zone 2 (Fejér, Tolna, Baranya, and Bács-Kiskun counties). Those areas that belong to zone 2 in the near future period but are classified as zone 1 in the far future period, will suffer greater aridification up to 30 mm precipitation deficit, or more.

Figs. 2 and *3* show temperature and precipitation limits of the zones separately. The results indicate that both of zone 3 and zone 2 are limited mainly by precipitation in their southern (i.e., arid) border. Those isotherms that limits zone 3 and zone 2 by definition (24 and 25.5 °C, respectively) run near the related isohyets (330 and 290 mm, respectively) in the reference period. In the near future period, the isotherms detach more from the isohyets and have minimal impact on the location of the zones. In the far future period, the isotherms run mainly north to the northern border of Hungary, and does not affect the expansion of the zones.

3.3. *Statistics on precipitation and the ratio of zones*

County-level descriptive statistics on the precipitation of the vegetation period (*Table 1* – mean and standard deviation, *Table 2* – minimum and maximum) confirm our previous findings. Although almost all the countries (except *SSB*) will suffer more or less aridification by the end of the 21st century, the tendency is not monotonic in case of *Bar*, *BAZ*, *Bek*, *GMS*, *HB*, *Hev*, *JNS*, *KE*, *Nog*, *Pes,* and *SSB*. Gradual aridification is predicted to occur mainly in the counties of Dunántúl (western Hungary). The mean of the precipitation sum of the vegetation period is between 282.51–371.09 mm, 284.43–412.99 mm, and 257.89–378.24 mm in the periods 1961–1990, 2021–2050, and 2071–2100, respectively. Since the statistical range of the mean precipitation is predicted to be larger in the future periods than in the reference period, climate of Hungary may be tolerable by more ornamental species. The overall tendency shows, however, aridification in most parts of the country. Driest counties are *Cso*, *BK*, and *Bar*. *SSB* is found to be consequently the wettest county in all the three studied periods (with no observable aridification), while *Baz*, *KE,* and Nog are also among the wettest counties.

Standard deviations vary between 4.64–33.67 mm, 6.4–49.92 mm, and 6.41–37.82 mm in the periods 1961–1990, 2021–2050, and 2071–2100, respectively. Substantial standard deviations are found in *Bar*, *BAZ*, *GMS*, *Pes*, *SSB* and *Ves*. The latter shows outstanding deviations in all the three periods (maximum is reached in the near future prediction period), which indicates that great spatial variations might occur within the county.

The smallest difference of the minimum and maximum values of precipitation sum of the vegetation period was found in *Tol* in the reference period, and it is predicted to occur in *Bud* in the two prediction periods. In accordance with the findings on the standard deviation, the greatest differences are presented in *Ves* not only in the reference but also in the two prediction periods.
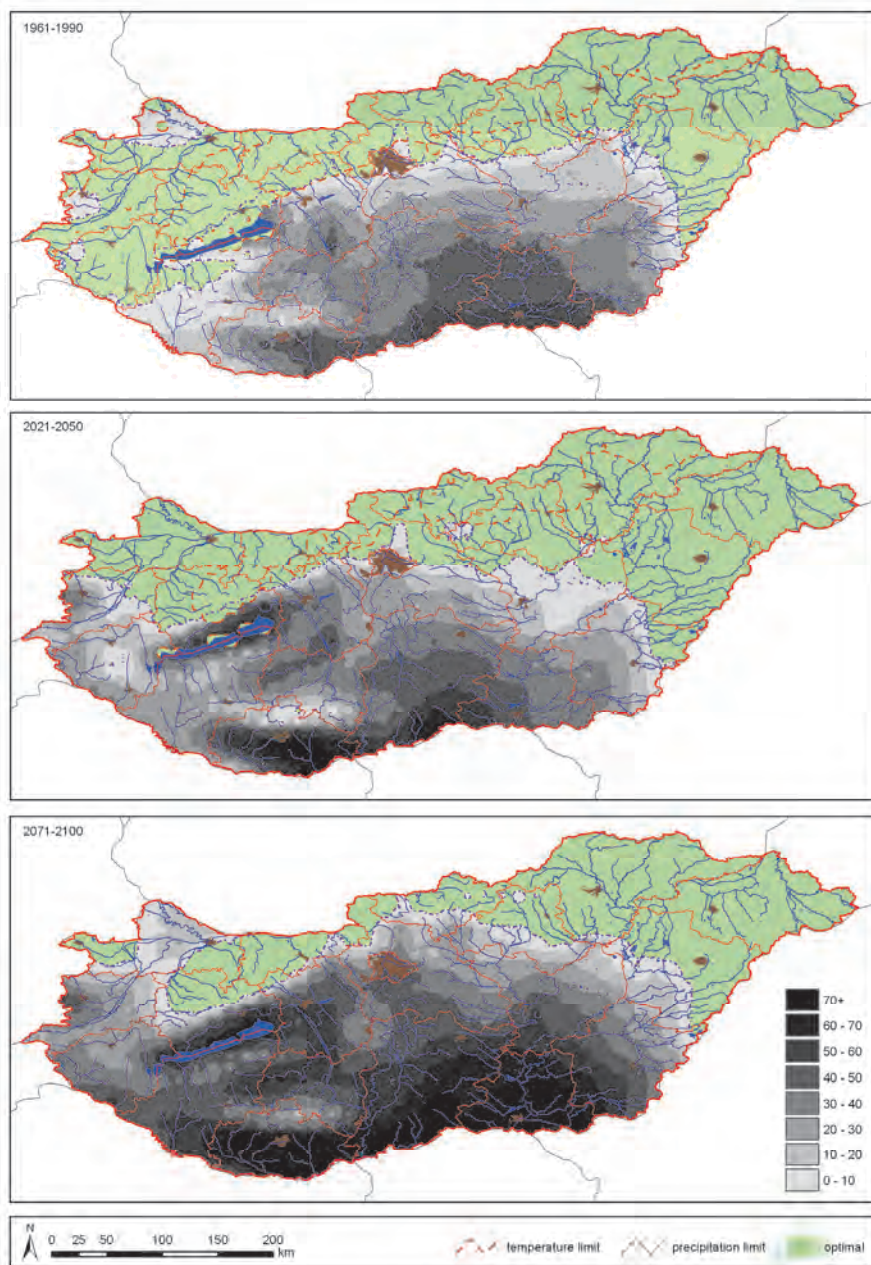
Fig. 2. Deficit of precipitation sum during the vegetation period (mm; see greyscale legend on the bottom right corner) in the suboptimal territories of drought category 3 (see detailed in Section 2) in the reference period (1961–1990, top) and the two prediction periods (2021–2050, center; 2071–2100, bottom). Temperature (orange dashed line) and precipitation (purple dashed-dot line) limits of the drought category are also drawn.
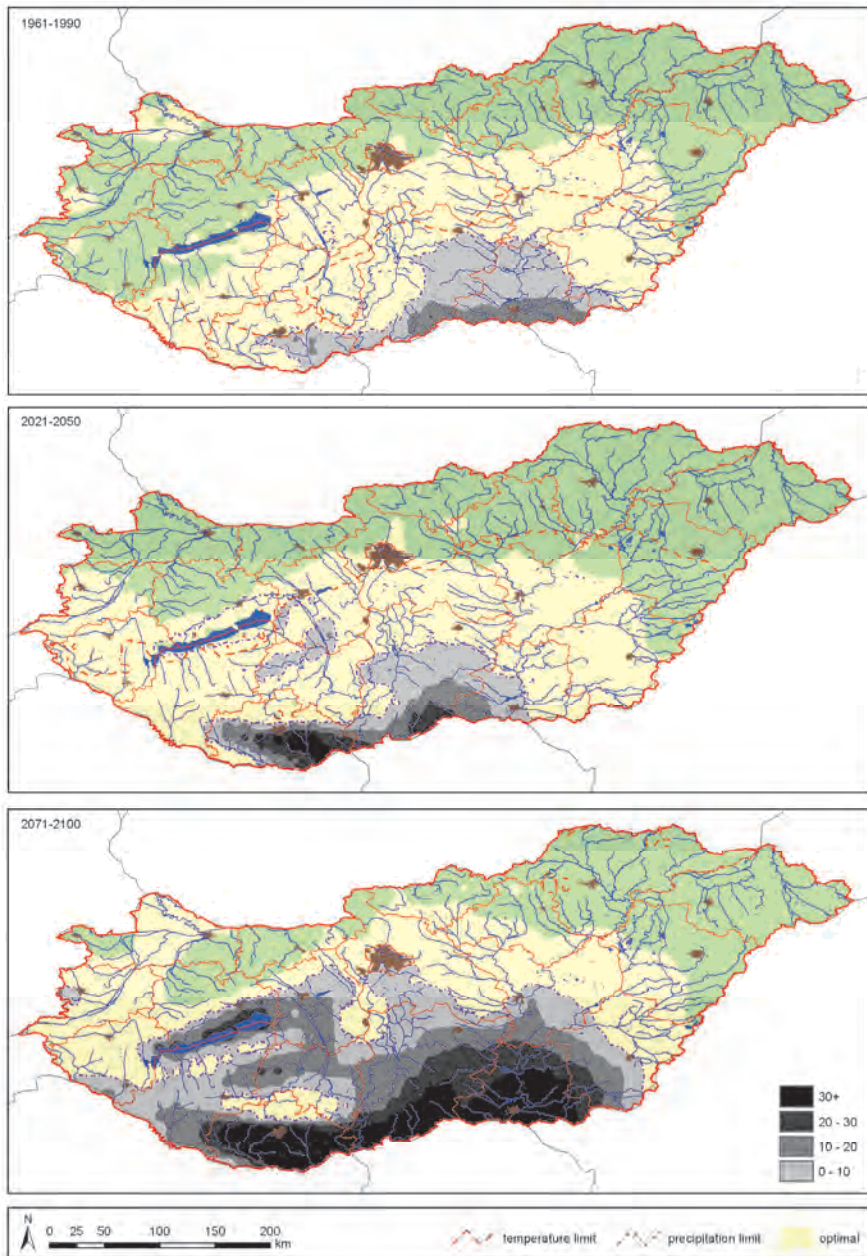
Fig. 3. Deficit of precipitation sum during the vegetation period (mm; see greyscale legend on the bottom right corner) in the suboptimal territories of drought category 2 (see detailed in Section 2) in the reference period (1961–1990, top) and the two prediction periods (2021–2050, center; 2071–2100, bottom). Temperature (orange dashed line) and precipitation (purple dashed-dot line) limits of the drought category are also drawn.

Table 1. Mean and standard deviation (in the form of 'mean ±sd') of precipitation sum during the vegetation period (mm) found within the 19 counties and the capital (Budapest) of Hungary in the reference period (1961–1990) and the two prediction periods (2021–2050, 2071–2100)

ID	County name	1961–1990	2021–2050	2071–2100
Bar	Baranya	299.71 ±12.15	284.43 ±21.04	263.01 ±19.32
BAZ	Borsod–Abaúj–Zemplén	368.19 ±21.3	396.57 ±25.69	367.78 ±18.33
Bek	Békés	302.84 ±12.38	315.89 ±16.21	290.23 ±16.02
BK	Bács–Kiskun	291.27 ±6.8	288.04 ±10.05	269.76 ±12.56
Bud	Budapest (capital)	327.61 ±7.27	317.72 ±6.4	292.3 ±6.41
Cso	Csongrád	282.51 ±5.29	290.46 ±7.08	257.89 ±6.43
Fej	Fejér	315.83 ±19.49	305.73 ±21.33	290 ±15.67
GMS	Győr–Moson–Sopron	340.46 ±18.81	363.51 ±22.85	333.22 ±19.71
HB	Hajdú–Bihar	341.85 ±15.54	365.25 ±17.53	336.37 ±13.77
Hev	Heves	348.33 ±16.36	349.68 ±15.88	327.9 ±14.24
JNS	Jász–Nagykun–Szolnok	311.88 ±10.14	325.2 ±9.01	296.49 ±13.43
KE	Komárom–Esztergom	369.84 ±10.67	384.86 ±16.58	345.31 ±16.42
Nog	Nógrád	363.55 ±11.6	364.08 ±14.61	332.35 ±10.8
Pes	Pest	325.65 ±23.1	326.13 ±22.94	301.19 ±16.26
Som	Somogy	321.17 ±11.06	301.37 ±10.45	282.23 ±7.57
SSB	Szabolcs–Szatmár–Bereg	371.09 ±23.73	412.99 ±19.44	378.24 ±20.71
Tol	Tolna	300.26 ±4.64	299.07 ±9.39	282.68 ±7.65
Vas	Vas	335.79 ±5.84	320.11 ±12.99	304.97 ±8.81
Ves	Veszprém	349.89 ±33.67	335.68 ±49.92	314.84 ±37.82
Zal	Zala	340.15 ±8.55	311.05 ±9.36	294.25 ±8.35

Table 2. Minimum and maximum (in the form of 'min–max') of precipitation sum during the vegetation period (mm) found within the 19 counties and the capital (Budapest) of Hungary in the reference period (1961–1990) and the two prediction periods (2021–2050, 2071–2100)

| ID	County name	1961–1990	2021–2050	2071–2100
Bar	Baranya	277.63–328.34	247.75–335.38	230.31–314.41
BAZ	Borsod–Abaúj–Zemplén	293.69–446.04	305.65–459.64	301.67–425.08
Bek	Békés	283.13–368.56	291.88–380.37	255.65–352.94
BK	Bács–Kiskun	269.55–309.78	263.86–317.34	241.28–297.43
Bud	Budapest (capital)	314.75–352.63	309.06–342.61	281.07–313.35
Cso	Csongrád	269.11–294.61	270.89–305.74	243.53–273.69
Fej	Fejér	284.18–379.44	276.54–398.86	269.57–366.6
GMS	Győr–Moson–Sopron	319.24–419.58	336.91–462.77	308.18–416.53
HB	Hajdú–Bihar	307.76–383.04	326.53–401.62	306.68–369.99
Hev	Heves	293.74–389.09	305.72–417.84	300.91–387.37
JNS	Jász–Nagykun–Szolnok	285.49–343.97	294.75–352.2	266.05–325.65
KE	Komárom–Esztergom	338.83–403.21	343.12–436.78	309.06–395.09
Nog	Nógrád	331.27–403.07	317.6–405.36	299.94–360.61
Pes	Pest	293.13–418.32	298.12–420.3	281.68–373.81
Som	Somogy	258.83–346.28	248.83–323.73	248.61–304.98
SSB	Szabolcs–Szatmár–Bereg	339.74–469.33	375.25–494.64	345.51–456.38
Tol	Tolna	287.2–319.16	282.8–331.86	261.66–311.25
Vas	Vas	319.19–357.27	281.34–350.43	270.56–328.59
Ves	Veszprém	268.18–426.12	247.08–458.55	247.3–403.91
Zal	Zala	293.51–363.85	259.89–333.71	253.04–315.37

County-level distribution of the three drought tolerance categories (*Table 3, Fig. 4*) shows inconsistencies. While in the reference period, homogeneously wet (i.e., entirely belonging to zone 3) counties are *KE*, *Nog,* and *SSB*, some other counties (*GMS*, *BAZ,* and *HB*) join this group in the near future period, which indicates the opposite tendency of aridification. However, in the far future period, only *SSB* remain homogeneously wet. Southeastern counties, such as *Cso*, *JNS*, *HB,* and *Bek* are also predicted to become wetter by 2021–2050. Some counties of Dunántúl (*Fej*, *Ves*, *Vas*, *Zal*, *Som*, *Tol,* and *Bar*) and *BK* show clear aridification by 2021–2050, as well. This contradiction confirms our findings on the country-wide range of mean precipitation sum. However, aridity is gradually increasing in terms of the number of the counties not containing area of drought category 1: 15, 13, and 7, in the periods 1961–1990, 2021–2050, and 2071–2100, respectively.

The far future period is consistently drier than the near future period. *Cso* is found to be homogeneously dry (i.e., entirely belonging to zone 1), but other counties show the same tendency of aridification. Some counties (e.g., *Vas* and *Zal*) that are dominated by category 3 in the reference period are predicted to become significantly drier by the end of the century, since they will not accommodate drought category 3 anymore.

Table 3. Spatial ratio of the drought categories 1, 2, and 3 (in the form of '1–2–3%'; see detailed in the Section 2) within the 19 counties and the capital (Budapest) of Hungary in the reference period (1961–1990) and the two prediction periods (2021–2050, 2071–2100)

ID	County name	1961–1990	2021–2050	2071–2100
Bar	Baranya	27.05–72.95–0%	65.72–33.75–0.52%	84.51–15.49–0%
BAZ	Borsod–Abaúj–Zemplén	0–2.01–97.99%	0–0.4–99.6%	0–2.24–97.76%
Bek	Békés	5.81–89.88–4.3%	0–82.41–17.59%	51.83–46.66–1.51%
BK	Bács–Kiskun	42.36–57.64–0%	58.22–41.78–0%	96.1–3.9–0%
Bud	Budapest (capital)	0–70.49–29.51%	0–95.22–4.78%	40.83–59.17–0%
Cso	Csongrád	95.36–4.64–0%	36.13–63.87–0%	100–0–0%
Fej	Fejér	0–75.46–24.54%	13.52–74.03–12.45%	64.3–31.43–4.27%
GMS	Győr–Moson–Sopron	0–26.92–73.08%	0–0–100%	0–60.44–39.56%
HB	Hajdú–Bihar	0–26.1–73.9%	0–0.36–99.64%	0–35.97–64.03%
Hev	Heves	0–12.75–87.25%	0–5.13–94.87%	0–53.48–46.52%
JNS	Jász–Nagykun–Szolnok	2.29–90.9–6.81%	0–71.53–28.47%	34.71–65.29–0%
KE	Komárom–Esztergom	0–0–100%	0–0–100%	0–14.03–85.97%
Nog	Nógrád	0–0–100%	0–1.8–98.2%	0–33.99–66.01%
Pes	Pest	0–65.11–34.89%	0–66.43–33.57%	24.79–67.49–7.73%
Som	Somogy	0–76.52–23.48%	2.02–95.23–2.75%	86.09–13.91–0%
SSB	Szabolcs–Szatmár–Bereg	0–0–100%	0–0–100%	0–0–100%
Tol	Tolna	0.46–99.54–0%	16.5–83.43–0.07%	84.1–15.9–0%
Vas	Vas	0–12.9–87.1%	0–73.52–26.48%	5.78–94.22–0%
Ves	Veszprém	0–8.04–91.96%	0.94–35.04–64.02%	34.32–31.58–34.1%
Zal	Zala	0–7.13–92.87%	0–97.28–2.72%	25.22–74.78–0%
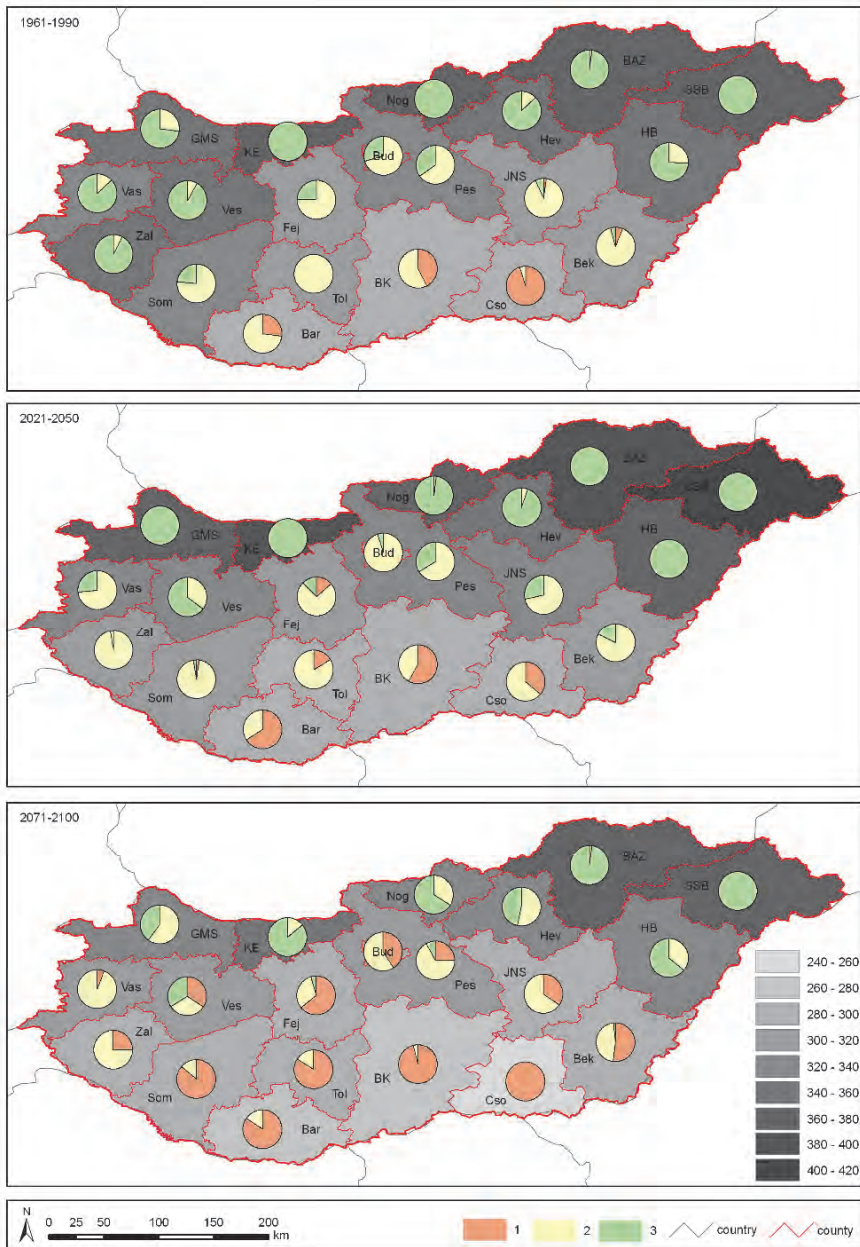
Fig. 4. Spatial ratio of the drought categories 1, 2, and 3 (red, yellow, and green, respectively; see detailed in Section 2) and the mean of precipitation sum during the vegetation period (mm; see greyscale legend on the bottom right corner) found within the 19 counties and the capital (Budapest) of Hungary in the reference period (1961–1990, top) and the two prediction periods (2021–2050, center; 2071–2100, bottom)

121

4. Discussion

During the 21st century, the drought hazard in Hungary is likely to increase in a spatially heterogeneous manner due to climate change. Comparing our prediction with another assessments showed little difference. Future changes based on De Martonne index, PAI index, and SAI index show that the highest drought level is located in the Pannonian Plain, and it decreases toward the north and west (*Blanka et al.*, 2013). According to the drought map of the current state (*Pálfai*, 2004), the highest values (extremely high rate of exposure) are found in the central and southern part of the Pannonian Plain, and the lowest values are in the higher elevations of Alpokalja region (Vas County) and on the higher hills of Northern Mountains. According to our results, the higher hills of Northern Mountains, the northeastern part of the country, plain of Upper Tisza, and northern parts of Nyírség, Hajdúság, Marcal Basin, Komárom Plain, and Dunántúli Mountains remain relatively wet. The drought hazardous areas stretch out from the Pannonian Plain toward the western landscape units as far as the longitude of the lake Balaton. The aridity can cause problem, and needs adaptation, almost everywhere in Hungary in the 2071–2100 period. Budapest, the capital of Hungary, where plant application is limited by urban heat island, air pollution, and other disadvantages of being a metropolis, is predicted to be reached by the boundary of drought tolerance zone 1 in the far future period, that might make plant application more difficult.

More substantial changes are predicted to occur in the western region, while aridity of Tiszántúl seems to be relatively constant. Zonal distribution (*Fig. 1*) of the near future period is more similar to that of the reference period than to that of the far future period, even though the former is closer to it in term of time. This result implies that the progression of aridification will accelerate during the 21st century. In the far future period, zone 2 is predicted shrink and provide a narrower buffer from zone 1 and zone 3, which indicates less balanced zonality and, therefore, less resistance to extreme drought events. Our predictions can not reject the hypothesis on climate extrapolation, i.e., the future strengthening of the continental effects on the east and the increase of dominance of Mediterranean effects of the south, which effects define now the climate of Hungary together with the Atlantic effects. Our results prove that the future climate of western part of Hungary may be more Mediterranean-like than it was in the reference period.

The results on the limiting isotherms and isohyets imply that more substantial warming (i.e., increase of maximum temperature) than decrease of precipitation of the vegetation period will occur in Hungary. Hence, future climatic conditions are predicted to have no precedent in the reference climate (1961–1990) of Hungary, which might complicate the adaptation.

Nursery production, that is now located partly in the Pannonian Plain and in western Hungary, may need to plan adaptation measures. Nowadays Vas and

Zala counties are considered to be the wettest territories of Hungary providing excellent areas for developing of ornamental trees, shrubs, and specially, evergreens. According to our results, in the second prediction period, both these counties and those of the Pannonian Plain will suffer significant aridification that may hinder cost-effective nursery production. Production of some cultures (e.g., rose, bulb) will be possible under controlled and irrigated circumstances in the future (*Soltész et al.,* 2011). Our research emphasizes the need of research on drought tolerance and drought tolerant plant selection, which has little literature in Hungary yet (e.g., *Schmidt* and *Sütöriné Diószegi*; 2010, *Szabó* and *Gerzson*, 2011; *Maráczi* and *Baracsi*, 2012).

The results are in line with the findings on the impact of future climate change on forests (*Mátyás,* 1994; *Szentkirályi et al.,* 1998; *Mátyás* and *Czimber*, 2000) and on other seminatural vegetation types (*Bede-Fazekas,* 2017; *Somodi et al.,* 2017; *Bede-Fazekas et at.*, 2017). Our results emphasize that we have to pay more attention on ecological aspects and sustainability in the future. The desire for informed sustainable, ecological, and regenerative design is increasing everywhere, and is enhanced by the urgent need for adaptation to the warmer and more arid climate (*Hunter,* 2011; *Beck*, 2013; *Bede-Fazekas*, 2017). Substantial aridity, which we predicted in the far future period, threatens the structure and function of ecological communities in urban areas including public and private gardens (*Hunter,* 2011).

Since climate predictions show great uncertainty if precipitation change is studied in Central Europe (*Torma*, 2011; *Van Oldenborgh et al.,* 2013; *Pongrácz et al.*, 2014), selection of one regional climate model seems to be accidental. Therefore, our results seek for confirmation by model ensemble. This need is emphasized also by the fact that the selected model, RegCM, shows considerable differences to other regional climate models of the Carpathian Basin in terms of the relative similarity of the near future climate to the reference period (*Sábitz et al.*, 2015; *Bede-Fazekas*, 2017). Our predictions are able to serve as quick overview of the possible impacts of future climate change on ornamental plant application, but can not substitute for ecological niche models. Therefore, instead of being interpretable in species or location level, our predictions provide guidance for landscape architects, dendrologists, and horticulturists to plan adaptation measures by making the spatial and temporal aspects of aridification tendencies available for studying them.

References

Bacsó, N., 1966: Bevezetés az agrometeorológiába. Mezőgazdasági Könyv- és Folyóiratkiadó Vállalat, Budapest, Hungary.

Bartholy, J., Pongrácz, R., Gelybó, Gy., and *Szabó, P.,* 2008: Analysis of expected climate change in the Carpathian Basin using the PRUDENCE results. *Időjárás 112,* 249–264.

Bartholy, J. and *Pongrácz, R.,* 2005: Tendencies of extreme climate indices based on daily precipitation in the Carpathian Basin for the 20th century. *Időjárás 109,* 1–20.

Bartholy, J., Pongrácz, R., and *Hollósi, B.,* 2013: Analysis of projected drought hazards for Hungary. *Adv. Geoscie. 35,* 61–66. https://doi.org/10.5194/adgeo-35-61-2013

Beck, T., 2013: Principles of Ecological Landscape Design. Island Press, Washington, DC, USA. https://doi.org/10.5822/978-1-61091-199-3

Bede-Fazekas, Á., Trásy, K., and *Csóka, Gy.,* 2015: Changing visual value of deciduous species in the climate change. In (Eds.: *Wolf, J., Nečasová, J., Nečas, T.*): Proceedings of the international conference "Horticulture in quality and culture of life". Mendel University in Brno, Faculty of Horticulture in Lednice, Lednice, Czech Republic.

Bede-Fazekas, Á. 2017: Fás szárú dísznövények potenciális telepíthetőségi területének előrejelzése természetközeli élőhelyekre készített modellek alapján. PhD dissertation. Szent István Egyetem, Gödöllő, Hungary. (In Hungarian)

Bede-Fazekas, Á., Czúcz, B., and *Somodi, I.,* 2017: Vulnerability of natural landscapes to climate change – a case study of Hungary. *Időjárás 121*, 393–414.

Belda, M., Skalák, P., Farda, A., Halenka, T., Déqué, M., Csima, G., Bartholy, J., Torma, C., Boroneant, C., Caian, M., and Spiridonov, V., 2015: CECILIA regional climate simulations for future climate: Analysis of climate change signal. Adv. Meteorol. 2015(1), 354727.

Bivand, R., Keitt, T., and *Rowlinson, B.,* 2014: rgdal: Bindings for the Geospatial Data Abstraction Library. R package version 0.8-16.
URL: https://cran.r-project.org/web/packages/rgdal/index.html

Bivand, R. and *Lewin-Koh, N.* 2015: maptools: Tools for Reading and Handling Spatial Objects. R package version 0.8-34. URL: https://cran.r-project.org/web/packages/maptools/index.html

Bivand. R.S., Pebesma, E., and *Gomez-Rubio, V.,* 2013: Applied spatial data analysis with R. Springer, New York, NY, USA. https://doi.org/10.1007/978-1-4614-7618-4

Blanka, V., Mezősi, G., and *Meyer, B.,* 2013: Projected changes in the drought hazard in Hungary due to climate change. *Időjárás 117,* 219–237.

Dobor, L., Barcza, Z., Hlásny, T., Havasi, Á., Horváth, F., Ittzés, P., and Bartholy, J. 2015: Bridging the gap between climate models and impact studies: the FORESEE Database. Geoscie. Data J 2, 1–11. https://doi.org/10.1002/gdj3.22

Hijmans, R.J., 2015: raster: Geographic Data Analysis and Modeling. R package version 2.3-40. URL: https://cran.r-project.org/web/packages/raster/index.html

Horváth, L. 2008: Földrajzi analógia alkalmazása klímaszcenáriók elemzésében és értékelésében. PhD dissertation. Corvinus Egyetem of Budapest, Faculty of Horticultural Science, Budapest, Hungary. (In Hungarian)

Hunter, M., 2011: Using Ecological Theory to Guide Urban Planting Design: An adaptation strategy for climate change. *Landscape J. 30,* 173–193. https://doi.org/10.3368/lj.30.2.173

Krüssmann, G., 1977: Manual of cultivated broad-leaved trees and shrubs. American Horticultural Society, Alexandria, VA, USA and Timber Press, Portland, OR, USA.

Lakatos, M., Szentimrey, T., and *Bihari, Z.,* (2011): Application of gridded daily data series for calculation of extreme temperature and precipitation indices in Hungary. *Időjárás 115*, 99–109.

Maráczi, K.H. and *Baracsi, É.,* 2012: Melegigényes díszcserjék télállósági vizsgálatai. In (Ed. Pannon Egyetem Georgikon Kar) LIV. Georgikon Napok. A mezőgazdaságtól a vidékgazda(g)ságig – 54th Georgikon Scientific Conference. Pannon Egyetem Georgikon Kar, Keszthely, Hungary. (In Hungarian)

Mátyás, Cs., 1994: Modelling climate change effects with provenance test data. *Tree Physiol. 14*, 797–804. https://doi.org/10.1093/treephys/14.7-8-9.797

Mátyás, Cs. and *Czimber, K.,* 2000: Zonális erdőtakaró mezoklíma szintű modellezése: lehetőségek a klímaváltozás hatásainak előrejelzésére. In: (Ed. *Tar, K.*) III. Erdő és Klíma Konferencia Debrecen, DE–TTK Meteorológia Tanszék, Debrecen, Hungary. (In Hungarian)

Nakićenović, N. and *Swart, R,.* (eds.) 2000: Emissions Scenarios. Cambridge University Press, Cambridge, UK.

Pálfai, I. 2002: Magyarország aszályossági zónái. *Vízügyi Közlemények 84,* 323–357. (In Hungarian)

Pálfai, I. 2004: Belvizek és aszályok Magyarországon. Hidrológiai tanulmányok. *Vízügyi Közlemények 86,* 318–320.

Pebesma, E.J. and *Bivand, R.S.,* 2005: Classes and methods for spatial data in R. *R News 5(2).*

Pongrácz, R., Bartholy, .J, and *Kis, A.,* 2014: Estimation of future precipitation conditions for Hungary with special focus on dry periods. *Időjárás 118,* 305–321.

R Core Team, 2014: R: A language and environment for statistical computing. R Foundation for Statistical Computing, Vienna, Austria. URL: https://www.r-project.org/

Retkes, J. and *Tóth, I.,* 2015: Lombos fák, cserjék. Nyugat-dunántúli Díszfaiskolások Egyesülete, Szombathely, Hungary. (In Hungarian)

Retkes, J. and *Tóth, I.,* 2004: Lombos fák, cserjék. Mezőgazda Kiadó, Budapest, Hungary. (In Hungarian)

Roloff, A., Korn, S., and *Gillner, S.,* 2009: The Climate-Species-Matrix to select tree species for urban habitats considering climate change. *Urban Forest. Urban Green. 8,* 295–308. https://doi.org/10.1016/j.ufug.2009.08.002

Sábitz, J., Szépszó, G., Zsebeházi, G., Szabó, P., Illy, T., Bartholy, J., Pieczka, I., and *Pongrácz, R.,* 2015: A klímamodellekből levezethető indikátorok alkalmazási lehetőségei. NATéR EEA-C11-1 beszámoló.
URL: www.met.hu/downloads.php?fn=/RCMTeR/doc/reports/C11-1_indikatorok_tanulmany.pdf

Schmidt, G., 2006: Klíma- és időjárás-változás és a fás szárú dísznövények. In: Csete L, Nyéki J (eds.): Klímaváltozás és a magyarországi kertgazdaság. AGRO-21 Kutatási Programiroda, Budapest, Hungary. (In Hungarian)

Schmidt, G. and *Sütöriné Diószegi, M.,* 2010: Testing urban climate with heat-tolerant woody plants in the Buda Arboretum. In: Proc. Int. Symp. Plants in Urban Areas and Landscape. Slovak University of Agriculture in Nitra, Nitra, Slovakia.

Schmidt, G., Tóth, I., and *Sütöriné Diószegi, M.,* 2013: Dendrológia (tanulmányi segédlet). Budapesti Corvinus Egyetem, Kertészettudományi Kar, Dísznövénytermesztési és Dendrológiai Tanszék, Budapest, Hungary. (In Hungarian)

Sheffield, J. and *Wood, E.F.,* 2008: Global trends and variability in soil moisture and drought characteristics, 1950-2000, from observation-driven simulations of the terrestrial hydrologic cycle. *J. Climate 21*, 432–458. https://doi.org/10.1175/2007JCLI1822.1

Soltész, M., Nyéki, J., and *Lévai, P.,* 2011: Az aszály és szárazodás elleni küzdelem a kertészeti termelésben. *"Klíma-21" Füzetek 64,* 5–11.

Somodi, I., Molnár, Zs., Czúcz, B., Bede-Fazekas, Á., Bölöni, J., Pásztor, L., Laborczi, A., and *Zimmermann, N.E.*, 2017: Implementation and application of Multiple Potential Natural Vegetation models – a case study of Hungary. J. Vegetat. Sci. 28, 1260–1269. https://doi.org/10.1111/jvs.12564

Steinhauser, F. 1970: Climatic atlas of Europe I. Maps of mean temperature and precipitation. WMO Unesco Cartographia Hungary, Budapest, Hungary.

Szabó, K. and *Bede-Fazekas, Á.,* 2012: A forgalomban lévő fásszárú dísznövénytaxonok szárazságtűrésének értékelése a klímaváltozás tükrében. *Kertgazdaság 44(4)*, 62–73. (In Hungarian)

Szabó, K. and *Gerzson, L.,* 2011: Evaluation of the Winter-hardy Yucca taxa among extreme conditions in landscape applications. *Acta Universitatis Sapientiae Agriculture and Environment 3(Suppl.)*, 122–131.

Szentkirályi, F., Leskó, K. and*, Kádár, F.,* 1998: Aszályos évek hatása a rovarpopulációk hosszú távú fluktuációs mintázatára. In (Eds. *Tar, K., Szilágyi, K.*) II. Erdő és Klíma Konferencia, Sopron, 1997. június 4–6. Kossuth Egyetemi Kiadó, Debrecen, Hungary. (In Hungarian)

Torma, Cs. 2011: Átlagos és szélsőséges hőmérsékleti és csapadék viszonyok modellezése a Kárpát-medencére a XXI. századra a RegCM regionális klímamodell alkalmazásával. PhD dissertation. Eötvös Loránd University, Budapest, Hungary. (In Hingarian)

Torma, Cs., Bartholy, J., Pongrácz, R., Barcza, Z., Coppola, E., and Giorgi, F., 2008: Adaptation of the RegCM3 climate model for the Carpathian Basin. Időjárás 112, 233–247.

Torma, Cs., Coppola, E., Giorgi, F., Bartholy, J., and *Pongrácz, R.* 2011: Validation of a High-Resolution Version of the Regional Climate Model RegCM3 over the Carpathian Basin. *J. Hydrometeorol. 12*, 84–100. https://doi.org/10.1175/2010JHM1234.1

Tóth, I., 2012: Lomblevelű díszfák, díszcserjék kézikönyve. Tarkavirág Kereskedelmi és Szolgáltató Kft, Budapest, Hungary. (In Hungarian)

Van Oldenborgh, G.J., Collins, M., Arblaster, J., Christensen, J.H., Marotzke, J., Power, S.B., Rummukainen, M., and *Zhou, T.*, 2013: Annex I: Atlas of Global and Regional Climate Projections Supplementary Material RCP8.5. In (Eds. *Stocker, T.F., Qin, D., Plattner, G.-K., Tignor, M., Allen, S.K., Boschung, J., Nauels, A., Xia, Y., Bex, V., Midgley, P.M.*) Climate Change 2013: The Physical Science Basis Contribution of Working Group I to the Fifth Assessment Report of the Intergovernmental Panel on Climate Change.
URL: https://www.ipcc.ch/pdf/assessment-report/ar5/wg1/WG1AR5_AnnexI_FINAL.pdf

Vermes, L., Fésűs, I., Nemes, C., Pálfai, I., and *Szalai, S.* 2000: Status and progress of the national drought mitigation strategy in Hungary. In (Eds. *Vermes, L., Szemessy, Á.*): Proceedings of the Central and Eastern European Workshop on Drought Mitigation. RePRINTStudio, Budapest, Hungary.

IDŐJÁRÁS

Comparison of regression models of PM$_{10}$ particulate concentration in relation to selected meteorological elements based on the example of Sosnowiec, Poland

Adam Adamek and **Agnieszka Ziernicka-Wojtaszek***

Department of Ecology, Climatology and Air Protection,
Faculty of Environmental Engineering and Land Surveying,
University of Agriculture in Kraków,
al. Mickiewicza 24/28, 30-059 Krakow, Poland

*Corresponding author E-mail: a.ziernicka-wojtaszek@ur.krakow.pl

Abstract— The aim of the study was to construct linear regression and multiple regression models, describing the dependence of PM$_{10}$ particulate concentration in the city of Sosnowiec on selected meteorological elements: air temperature, precipitation and wind speed. Three multiple regression models were constructed: a generic variant without regard to the barometric situation, and two models separately for high-pressure and low-pressure situations. The data used in the study were the average daily concentrations of PM$_{10}$ registered during the 2013–2015 heating seasons at the Sosnowiec station on Lubelska Street, belonging to the Air Quality Monitoring System operated by the Voivodeship Environmental Protection Inspectorate in Katowice.

Key-words: air quality, particulate matter, regression model, heating season

1. Introduction

Poland is one of the countries with the worst air quality in Europe, with PM$_{10}$ levels very often exceeding acceptable levels (*European Environment Agency,* 2016). Excessively high PM$_{10}$ concentrations are noted during the heating season in nearly the entire country. Smog, i.e., extremely high concentrations of suspended particulates, is a common phenomenon that is harmful to human health. An association is observed between PM$_{10}$ concentrations and emissions

of pollutants from industry, transport, and home furnaces. However, the concentration of air pollutants is also influenced by local meteorological elements, such as air temperature, wind speed, precipitation, and the type of atmospheric circulation (*Majewski*, 2005*; Czarnecka* and *Kalbarczyk,* 2008*; Leśniok and Caputa,* 2009; *Niedźwiedź* and *Małarzewski*, 2016). This study deals with the concentration of PM_{10} particulates registered in the city of Sosnowiec in the central part of the Silesian Voivodeship.

Analyses of the dependence of concentrations of air pollutants on meteorological elements are frequently carried out using statistical methods. A common solution is to construct models based on linear regression or multiple regression analysis.

The aim of the study was to compare the accuracy of linear regression models and multiple regression models constructed in generic, anticyclone, and cyclone variants.

2. Materials and methods

The input data for the study were average daily PM_{10} concentrations recorded at the Air Quality Monitoring System station, managed by the Voivodeship Environmental Protection Inspectorate and located on Lubelska Street in Sosnowiec, as well as meteorological data for nearby Katowice, obtained from the Institute of Meteorology and Water Management. Data pertaining to PM_{10} concentrations and meteorological elements were considered in conjunction with data on the type of pressure system, determined according to the calendar of circulation types by *Niedźwiedź* (*Niedźwiedź*, 1981; *Leśniok, et al.*, 2010). The analytical method chosen was the construction of linear regression models describing how the PM_{10} concentration depends on air temperature, wind speed, and precipitation, and multiple models that take into account all of these elements at the same time. Three multiple models were constructed: a generic model taking into account all situations, regardless of the type of pressure system, and separate models for both high and low pressure systems. The first stage of the study was the construction of linear regression models between PM_{10} concentration and each of the above-mentioned meteorological elements. The R^2 coefficients obtained were compared to the R^2 coefficient for multiple regression. Then, using only multiple regression, which produced more accurate results, anticyclone and cyclone situations were compared. It is widely accepted that changes in concentrations of air pollutants are seasonal (*Majewski,* 2007*; Czarnecka* and *Nidzgorska-Lencewicz,* 2010). Norms are very frequently exceeded during the heating season, when low-quality fuels are burned in home boilers, which are often outdated. Taking into account the variability of PM_{10} concentrations during the year, the months of the heating season (January, February, March, April, October, November, and December) in 2013–2015 were selected for the study period.

3. Results

For all recorded PM_{10} concentrations in the heating season, the mean value was 50.9 µg/m^3 with a standard deviation of 29.6 µg/m^3. The coefficient of variation was 58.1%. During the study period, anticyclone situations accounted for 54.7%. The mean PM_{10} concentration in anticyclone situations was 55.3 µg/m^3, with minimum and maximum concentrations of 16.0 and 235.0 µg/m^3, respectively. The standard deviation of the anticyclone population was 32.0 µg/m^3, and the coefficient of variation was 56.3%. Cyclone situations accounted for 45.3%, with mean, minimum, and maximum PM_{10} concentrations of 45.2, 10.0, and 177.0 µg/m^3, respectively. Taking into account the standard deviation of the population of cyclone situations of 25.0 µg/m^3, the coefficient of variation was 55.3%. PM10 concentrations in the 2013–2015 heating seasons were characterized by a relatively high degree of variability, showing slightly greater variation during cyclone situations. Acceptable levels were exceeded on 40.0% of days. The 24-hour permissible limit of PM_{10} is 50.0 μg/m^3 (Regulation of the Minister of the Environment of 24 August 2012 on the levels of certain substances in the air (Journal of Laws of 2012 item 1031)). In all months of the study, the maximum value exceeded the permissible limit. *Table 1* presents the minimum, average, and maximum PM_{10} concentrations during the research period.

Table 1. Selected characteristics of mean daily PM10 concentrations in each month of the heating season in Sosnowiec (2013-2015)

| | PM10 concentration, µg/m^3 | | | | | | | | |
| | 2013 | | | 2014 | | | 2015 | | |
	min.	average	max.	min.	average	max.	min.	average	max.
January	10.0	73.2	225.0	14.0	52.2	116.0	14.0	38.5	91.0
February	22.0	58.9	103.0	33.0	71.1	148.0	22.0	60.5	136.0
March	20.0	54.3	95.0	13.0	47.0	126.0	10.0	51.5	115.0
April	20.0	49.2	84.0	13.0	33.8	68.0	10.0	27.9	59.0
October	19.0	51.5	95.0	17.0	46.0	123.0	24.0	47.1	117.0
November	16.0	51.9	152.0	27.0	48.9	105.0	12.0	60.7	235.0
December	13.0	50.8	126.0	13.0	52.6	139.0	16.0	45.2	92.0

Linear regression with respect to individual meteorological elements, i.e., air temperature, precipitation, and wind velocity, shows statistical significance at α=0.05 in all cases, but the coefficients of determination R^2 are low: 8.0%, 3.4%, and 24.6%, respectively (*Fig. 1*). The fit at this level is unsatisfactory.
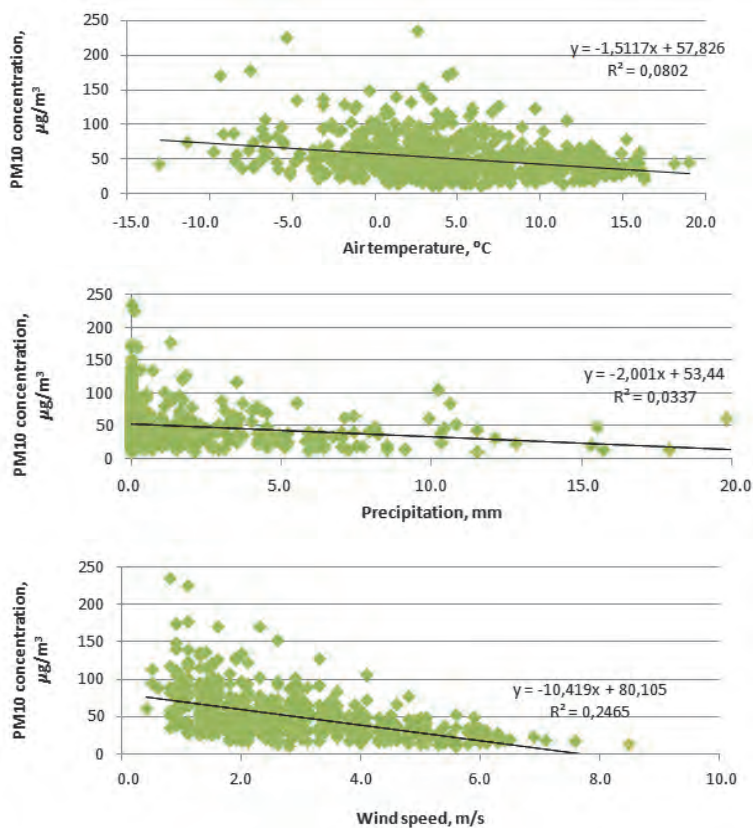
Fig. 1. Regression relationships between PM₁₀ concentration and air temperature, precipitation and wind speed in each month of the heating season (January, February, March, April, October, November, and December) in Sosnowiec, in 2013–2015.

In order to obtain a better fit, a regression model was constructed according to dependency 1 at significance level α = 0.05:

$$y = T \cdot x_1 + P \cdot x_2 + V \cdot x_3 + x_4, \qquad (1)$$

where:

y	–	PM₁₀ concentration, μg/m³,
T	–	air temperature, °C,
P	–	precipitation, mm,
V	–	wind velocity, m/s, and
$x_{1...4}$	–	multiple regression coefficient.

Multiple analysis taking into account all three meteorological elements resulted in an R^2 coefficient of 33.8%, which is still a relatively low value, but much higher than in the previous cases. In addition, air temperature, precipitation, and wind speed all proved to be statistically significant in the model. Analogous regression models were constructed separately for low and high pressure systems. The results are presented in *Table 2*.

Table 2. Results of regression models for dependency of PM_{10} concentration on air temperature, precipitation, and wind speed

		Multiple regression coefficients		
		Generic variant	High-pressure systems	Low-pressure systems
Air temperature	x_1	−1.5	−1.5	−1.4
Precipitation	x_2	−1.0	−1.3	−0.7
Wind speed	x_3	−10.0	−11.6	−8.0
Constant term	x_4	89.9	93.0	77.5
	R^2	33.8%	30.2%	35.9%

The models for high- and low-pressure systems produced similar values for the coefficient of determination R^2, at a level of 30.2% for high systems and 35.9% for low systems. These values do not differ significantly from the generic model. It is worth noting, however, that in the case of the low-pressure model, the rainfall parameter was statistically non-significant. This may be due to the fairly small data population in comparison with the other regression models. It can be concluded that construction of a general model is sufficient for analysis of the relationship between PM_{10} concentration and meteorological elements. Breakdown into high- and low-pressure systems does not lead to either a significant decrease or increase in accuracy, but requires more labour.

4. Discussion and conclusions

In Sosnowiec, during the 2013–2015 heating seasons, permissible PM_{10} levels were exceeded on 40.0% of days. Similar results were obtained for this city in other studies (*Cembrzyńska et al.*, 2015). In all months of the study, the maximum value exceeded the 24-hour permissible limit of PM10, which is 50 μg/m^3 (Regulation of the Minister of the Environment of 24 August 2012 on the levels of certain substances in the air (Journal of Laws of 2012 item 1031)). The main objective of the analysis was to compare several variants of models based

on regression analysis. The analysis showed that a multiple regression model is more accurate than a linear regression model. Among the variables tested, wind speed had the greatest influence on the level of PM_{10} concentration. PM_{10} concentration has been found to be most strongly correlated with wind speed in other parts of the country as well (*Czarnecka* and *Nidzgorska-Lencewicz*, 2008). The multiple regression model taking into account air temperature, wind speed, and precipitation in the 2013–2015 heating seasons resulted in a coefficient of determination of 33.8% on average. Comparable values have been obtained in studies on other areas of Poland (*Czarnecka* and *Nidzgorska-Lencewicz*, 2008). The accuracy of the model can be improved by increasing the number of elements taken into account. The literature describes regression models that also include visibility, atmospheric equilibrium, and relative humidity (*Ćwiek* and *Majewski*, 2015). The inclusion of more variables in the model could lead to higher coefficients of determination. Irrespective of the approach and the method, determination of patterns in the dependence of concentrations of pollutants on the complex of weather elements and types of synoptic situations can be used in particular to predict high and excessive concentrations on the basis of weather forecasts (*Niedźwiedź* and *Ustrnul*, 1989; *Niedźwiedź* and *Olecki*, 1994; *Ośródka*, 1996).

To sum up, the following conclusions can be drawn from the research:

1) Higher accuracy described by the coefficient of determination R^2 is achieved using multiple regression models than for linear regression models. On average, the R^2 coefficient was 33.8% for multiple regression and 8.0%, 3.4% and 24.6% for linear regression, in the case of air temperature, precipitation, and wind speed, respectively.

2) The optimal solution was to construct a generic multiple regression model ($R^2 = 33.8\%$) based on the entire data set from the 2013–2015 heating seasons. The R^2 coefficients from models, constructed separately for high-pressure systems ($R^2 = 30.2\%$) and low-pressure systems ($R^2 = 35.9\%$), did not differ significantly from the coefficient obtained for the general model. The accuracy of the model could be improved by expanding the population of input data and by incorporating additional variables in the model, such as visibility or atmospheric equilibrium.

3) During the 2013–2015 heating seasons, the most significant meteorological element affecting the PM_{10} concentration in Sosnowiec was wind speed, which had the highest statistical significance in the model. Precipitation proved to be the least significant.

4) The relationships demonstrated can be used to predict concentrations and exceedances of permissible PM_{10} levels based on the forecast of meteorological elements.

References

Cembrzyńska, J., Krakowiak, E., and *Brewczyński, P.Z.,* 2015: Sezonowa zmienność stężenia pyłu zawieszonego oraz jakości powietrza na terenie miasta Sosnowiec, Medycyna Środowiskowa – *Environmental Medicine 18(4)* 27–35. (in Polish)

Czarnecka, M. and *Kalbarczyk, R.* 2008: Warunki meteorologiczne kształtujące zmienność stężenia pyłu zawieszonego na Pomorzu. *Acta Agrophysica 11*, 357–636. (in Polish)

Czarnecka, M. and *Nidzgorska-Lencewicz, J.* 2008: Warunki meteorologiczne kształtujące jakość powietrza w Szczecinie w styczniu i lipcu w roku 2006. *Acta Agrophysica 12*, 55–72. (in Polish)

Czarnecka, M. and *Nidzgorska-Lencewicz, J.* 2010: The influence of precipitation conditions on the concentration of suspended particulates PM10. *Meteorol. Climatol. Res..* red. J. Leśny. Acta Agrophysica. Rozprawy i Monografie *184,* 132–147.

Ćwiek, K. and *Majewski, G.* 2015: Wpływ elementów meteorologicznych na kształtowanie się stężeń zanieczyszczeń powietrza na przykładzie Krakowa. Przegląd Naukowy – Inżynieria i *Kształtowanie Środowiska 67,* 54–66. (in Polish)

European Environment Agency, 2016: Air quality in Europe — 2016 report.

Journal of Laws of 2012 item 1031, Rozporządzenie Ministra Środowiska z dnia 24 sierpnia 2012 r. w sprawie poziomów niektórych substancji w powietrzu. (in Polish)

Leśniok, M. and *Caputa, Z.* 2009: The role of atmospheric circulation in air pollution distribution in Upper Silesia (Southern Poland). *Int. J. Environ. Waste Manage. 4*, 62–74. https://doi.org/10.1504/IJEWM.2009.026884

Leśniok, M., Małarzewski, Ł., and *Niedźwiedź, T.* 2010: Classification of circulation types for Southern Poland with an application to air pollution concentration in Upper Silesia. *Phys. Chem. Earth 35*, 516–522. https://doi.org/10.1016/j.pce.2009.11.006

Majewski, G. 2005: Zanieczyszczenie powietrza pyłem zawieszonym PM10 na Ursynowie i jego związek z warunkami meteorologicznymi. Przegląd Naukowy Inżynieria i Kształtowanie Środowiska 14, 1(31) Wydawnictwo SGGW, 210–223. (in Polish)

Majewski, G. 2007: Wpływ warunków meteorologicznych na zanieczyszczenie powietrza pyłem zawieszonym w rejonie aglomeracji warszawskiej. Praca doktorska. Wydział Inżynierii i Kształtowania Środowiska SGGW. (in Polish)

Niedźwiedź, T. 1981: Sytuacje synoptyczne i ich wpływ na zróżnicowanie przestrzenne wybranych elementów klimatu w dorzeczu górnej Wisły, Rozprawy Habilitacyjne UJ 58. (in Polish)

Niedźwiedź, T., Ustrnul Z. 1989: Wpływ sytuacji synoptycznej na występowanie nad Górnośląskim Okręgiem Przemysłowym typów pogody sprzyjających koncentracji lub rozpraszaniu zanieczyszczeń powietrza (Influence of synoptic situations on the occurrence of weather types favorable to concentration or dispersion of air pollution above the Upper Silesia Industrial Region), *Wiadomości IMGW XII (XXXIII)*, 31–39. (in Polish)

Niedźwiedź, T., Olecki Z. 1994: Wpływ sytuacji synoptycznych na zanieczyszczenie powietrza w Krakowie (The influence of synoptic situations on air pollution in Cracow), Zeszyty Naukowe UJ, *Prace Geograficzne 96,* 55–67. (in Polish)

Niedźwiedź, T., Małarzewski, Ł. 2016: Klimat Sosnowca [in:] Sosnowiec. Obraz miasta i jego dzieje, Tom I, red. Barciak A., Jankowski A.T.: Część pierwsza: Środowisko geograficzno-przyrodnicze. Rozwój przestrzenny. Muzeum w Sosnowcu, Sosnowiec, 74–85. (in Polish)

Ośródka, L. 1996: Development of smog warning system in large industrial metropolises based on the example of Upper Silesian Industrial Region. In (Eds. *Allegrini I., de Santis F.*) Urban Air Pollution. NATO ASI Series, Springer Verlag, 367–375. https://doi.org/10.1007/978-3-642-61120-9_29

INSTRUCTIONS TO AUTHORS OF *IDŐJÁRÁS*

The purpose of the journal is to publish papers in any field of meteorology and atmosphere related scientific areas. These may be

- research papers on new results of scientific investigations,
- critical review articles summarizing the current state of art of a certain topic,
- short contributions dealing with a particular question.

Some issues contain "News" and "Book review", therefore, such contributions are also welcome. The papers must be in American English and should be checked by a native speaker if necessary.

Authors are requested to send their manuscripts to

including all illustrations. MS Word format is preferred in electronic submission. Papers will then be reviewed normally by two independent referees, who remain unidentified for the author(s). The Editor-in-Chief will inform the author(s) whether or not the paper is acceptable for publication, and what modifications, if any, are necessary.

Please, follow the order given below when typing manuscripts.

Title page should consist of the title, the name(s) of the author(s), their affiliation(s) including full postal and e-mail address(es). In case of more than one author, the corresponding author must be identified.

Abstract: should contain the purpose, the applied data and methods as well as the basic conclusion(s) of the paper.

Key-words: must be included (from 5 to 10) to help to classify the topic.

Text: has to be typed in single spacing on an A4 size paper using 14 pt Times New Roman font if possible. Use of S.I.

units are expected, and the use of negative exponent is preferred to fractional sign. Mathematical formulae are expected to be as simple as possible and numbered in parentheses at the right margin.

All publications cited in the text should be presented in the *list of references*, arranged in alphabetical order. For an article: name(s) of author(s) in Italics, year, title of article, name of journal, volume, number (the latter two in Italics) and pages. E.g., *Nathan, K.K.,* 1986: A note on the relationship between photo-synthetically active radiation and cloud amount. *Időjárás 90,* 10–13. For a book: name(s) of author(s), year, title of the book (all in Italics except the year), publisher and place of publication. E.g., *Junge, C.E.,* 1963: *Air Chemistry and Radioactivity.* Academic Press, New York and London. Reference in the text should contain the name(s) of the author(s) in Italics and year of publication. E.g., in the case of one author: *Miller* (1989); in the case of two authors: *Gamov* and *Cleveland* (1973); and if there are more than two authors: *Smith et al.* (1990). If the name of the author cannot be fitted into the text: *(Miller,* 1989); etc. When referring papers published in the same year by the same author, letters a, b, c, etc. should follow the year of publication. DOI numbers of references should be provided if applicable.

Tables should be marked by Arabic numbers and printed in separate sheets with their numbers and legends given below them. Avoid too lengthy or complicated tables, or tables duplicating results given in other form in the manuscript (e.g., graphs). *Figures* should also be marked with Arabic numbers and printed in black and white or color (under special arrangement) in separate sheets with their numbers and captions given below them. JPG, TIF, GIF, BMP or PNG formats should be used for electronic artwork submission.

More information for authors is available: journal.idojaras@met.hu